MODELLING OF ICE THROW AND NOISE FROM WIND TURBINES

SUMITA BISWAS

A DISSERTATION SUBMITTED TO THE FACULTY OF GRADUATE STUDIES IN PARTIAL FULFILLMENT OF THE REQUIREMENTS

FOR THE DEGREE OF

DOCTOR OF PHILOSOPHY

GRADUATE PROGRAMME IN EARTH AND SPACE SCIENCE

YORK UNIVERSITY

TORONTO, ONTARIO

July 2021

Abstract

To assess the impact of the issues related to ice throw and noise from the wind turbine two independent mathematical models were developed. A model of the trajectories of ice fragments thrown from a rotating wind turbine blade is used to estimate the ground impact locations that could occur under different scenarios. Wind speed, ejection position on the blade and turbine rotation rate play a role in determining the impact point, as well as mass, density and drag coefficient of the ice fragment. For 'compact' ice fragments, the trajectory depends on the combination C_DA/M where C_D is the drag coefficient, A is the frontal area and M the mass of the ice fragment. Sensitivity tests show that ice fragments can travel further laterally for low C_D and further downwind for high C_D. For plate-like fragments, aerodynamic lift can increase the distance travelled if the plate maintains an orientation to maximize lift. Although this may be a relatively rare event, but result from the simulation shows a case, where a 1 kg plate-like fragment could travel up to 350 m from the base of the turbine. Another model based on the ray theory is developed to simulate propagation of sound from a point source. The model incorporates propagation loss, loss due to refraction, ground interaction and atmospheric absorption. Sound pressure level at a specific distance from the sound source can be calculated using the model. Variation in the terrain feature is included to investigate its impact on the ray trajectory.

I dedicate this thesis to my parents Babul Chandra Biswas and Purabi Chowdhury, who have been my inspiration since childhood.

Acknowledgments

I would like to thank my supervisor Professor Peter A. Taylor for his guidance, support, and enormous patience throughout the course of my PhD program. I will always remain grateful to him.

I would also like to thank my thesis supervisory committee, Dr. Jim Salmon and Dr. Costas Armenakis for their valuable advice, graduate program director, Dr. Mark Gordon, chair of the examining committee Dr. Yongsheng Chen and Marcia Gaynor (Graduate program assistant) for their support that made the completion of this degree possible.

My thanks are also extended to my husband Sanjoy Mallick for his continuous encouragement during this long program, my children (Aditri and Aarav), my brother (Sudip Biswas) for his guidance in programming.

Table of Contents

List of Figures

List of Tables

List of abbreviations

ASL	Ambient Sound Level
BSL	Basic Sound Level
CSL	Cumulative Sound Level
dB	Decibel
dBA	A-weighted Decibel
ISO	International Organization for standardization
MOECP	Ministry of the Environment, Conservation and Parks
SPL	Sound pressure level
SWL	Sound Power level
PSL	Permissible sound level

List of symbols

C_D	Drag coefficient
C_L	Lift coefficient
L	Lift force
D	Drag force
ω	Angular speed
M	Mass
ρ	Density of air
g	Gravity
Θ	Angle
c	Speed of sound
R	Ideal gas constant
T	Temperature
P	Pressure
P_{ref}	Reference Pressure
L_p	Sound pressure level
L_w	Sound power level
I	Intensity
W	Power
W_{ref}	Reference sound power
r	Distance
k	Wave number
t	Time
f	Frequency
U	Wind speed
γ	Specific heat ratio
c_p	Specific heat capacity at constant pressure

c_v	Specific heat capacity at constant volume
z_0	Surface roughness length
Z_{ground}	Ground impedance
θ_i	Angle of incidence
Q	Spherical wave reflection coefficient
z	Vertical distance (height)
ΔL	Relative sound pressure level

Chapter One
Introduction

The energy generation from wind turbines has some issues requiring proper assessment and mitigation, including ice throw, shadow flicker, noise, death of birds, bats, impact on fish from offshore turbines. In this dissertation, ice throw and the propagation of sound emitted from a wind turbine will be discussed.

1.1 Ice throw issue

Wind turbines in cold climates face challenges arising from icing. In a cold climate, a glaze of ice can build up on both stationary and operating wind turbine blades, towers and nacelles under specific temperature and humidity conditions. During ice storms, if liquid precipitation strikes a turbine blade below the freezing point glaze ice can form.

Ice formation mostly occurs on wind turbines located in mountain sites at an elevation higher than about 600m in low clouds. Exposure of turbine blade surfaces to the cloud can lead to deposition of frost on the turbine blade because of the presence of super-cooled water droplets in the cloud (Lacroix & Manwell, 2000). In the Canadian context, freezing rain is the leading cause of ice build-up on turbine blades in southern Ontario.

Further, ice throw from the wind turbines is an issue in a cold climate. There are several problems associated with ice accretion on the blade. Ice buildup on the blade can lead to total shutdown of operation from a couple of hours to several days or longer. The ice accumulation can cause the overloading of the blade and other structure. This phenomenon reduces the lifespan of the gearbox and bearings.

When the wind turbine is not operating, ice can fall from the turbine blade and could potentially strike maintenance personnel working under or downwind of the turbine. The extent of damage from a sudden strike by falling ice can be significant from an operating wind turbine. In case of wind turbines located near a residential area, industry or highway, ice can be thrown away from the blade and could strike the pedestrians, vehicles, or houses nearby. Whether the impact of ice fragments can cause damage to the property depends on the location of the turbine and how far the ice fragment can travel in the worst-case situation.

Warmer air temperatures and radiation may loosen the grip of ice on the blades and free the ice. In addition, several techniques are currently available to mitigate the situation arising due to icing. For example, de-icing and anti-icing technologies are available to install on the turbine. Some wind turbine manufacturers (*e.g.,* Enercon) use warm-air circulation within the structure of the turbine to melt the ice while some companies use electro-thermal heating foils on the blade surface to act as an anti-icing tool (Tammelin, 2000).

One problem with turbine icing is that the size and shape of the ice that falls or is thrown from the blades are unpredictable. As ice fall and ice throw presents itself as safety issues for individuals working near the turbine as well as for other people and property in the vicinity, there is a necessity of using a risk assessment model to ensure the safety of the public.

In a risk assessment model, modelled ice slabs of various sizes and shapes can be thrown from the turbine blade to simulate their final landing positions. The model can include a range of conditions to simulate the real atmosphere and a variety of ice fragment sizes. The results can be used to establish a safe setback from the wind turbine.

The Ice throw model described in Chapter 2 was developed in 2009/2010 in response to a need for Zephyr North Ltd (https://zephyrnorth.com/) to provide site specific risk assessments for wind farm developers, mostly in southern Ontario. Some early, generic, studies had been undertaken by Garrad-Hassan based on the model proposed by Morgan *et al* (1996) but did not take account of wind speed variation with height and adopted a Monte Carlo approach to determining ice fragment positions on the blades. The model in Chapter 2 can, and has been, extended and used in conjunction with site specific wind and turbine information by Zephyr North Ltd to provide risk assessments for several wind farm projects.

Szász *et al* (2019) cites the ice throw paper by Biswas *et al* (2011) and computes the ice throw trajectory. They further extend the computation to include the ice fragments that rotate during the flight. Computational fluid dynamics (CFD) is used to calculate the aerodynamic force acting on the ice fragment during its flight until it reaches the ground. Lennie *et al* (2019) uses the ice throw model (described in Chapter 2) as a basis of their model named "QBlade". They also validated the model results with some experimental data. A recent International Energy Agency set of International Recommendations by Krenn *et al* (2018) cites and summarizes the paper based on the material in Chapter 2, as their example of a suitable trajectory model for use in international risk assessment. It is worth mentioning that there are not many developed trajectory models to assess the risk from ice throw. The purpose of the recommendations is to provide a uniform approach to be adopted by the wind farm developers. According to the guideline, the first step

assessment is the use of a model to compute the trajectory of ice fragments. A standard model should include the following parameters,

1. A representation of area/mass distribution which can be either fixed or derived from size and density of several ice fragments and drag co-efficient.
2. Site specific environmental data (*e.g.*, vertical wind speed profile, air density).
3. Wind turbine characteristics (the hub height, rotor diameter, position of the ice fragment on the blade).

The model should include information on the amount of the ice and the properties of ice. The amount of ice data for the site of interest (N_{site}) can be calculated from the amount of ice data from a historical observation site (N_{obs}) by using appropriate scaling factors. The equation for the amount of ice for the site of interest is,

$$N_{site} = sf_{ice} \cdot sf_{rotor} \cdot sf_{op} \cdot N_{obs} \qquad (1.1)$$

Here sf_{ice} is the scaling factor for site icing conditions, sf_{rotor} is the scaling factor for rotor dimensions, and sf_{op} is the scaling factor for operational mode.

Risk assessment can be performed using the DIN ISO 12100 method. According to this method, the first step of risk assessment is identification of the source of hazards and their associated risk level (Krenn, et al., 2018). If the level of risk is acceptable then no action is required. But if the risk is beyond the acceptable limit, proper mitigation techniques need to be implemented. These risk reduction methods can include performing sensitivity analyses, using simulation software and quantifying the effects of a conservative approach. If these solutions are not enough, some physical measures should be carried out. These can include the installation of safety barriers on the site, design modifications and restriction of operations. It is vital to accurately measure the risk to

determine the necessity of implementation of mitigation techniques. The analysis of risk can be done using the following formula,

Risk= Likelihood (probability of occurrence) *Consequence (Impact of occurrence)

If the likelihood of getting hit by an ice fragment is high, the consequence must be low to keep the risk manageable.

To determine the probability of occurrence it is necessary to perform an ice fall analysis in the vicinity of the wind turbine to determine the impact locations on the ground. This simulation should be combined with realistic number of ice fragments. Using these data, the individual or societal risk can be calculated.

The consequence can be determined using the "Probit function' method. The "Probit function" can be calculated from the velocity and mass of the ice fragment. Krenn *et al* (2018) show a table containing values of "Probit function" for a range of mass (0.1-4.5kg) with their corresponding values of mortality rate. The higher the value of "Probit function", the greater the mortality rate.

If there is any potential of risk found after the risk assessment, some mitigation steps are recommended. A term 'Risk Reduction Factor'(RRF) is used to quantify the effectiveness of these measures (Krenn, et al., 2018). For example, if the wind farm is located at a remote location, putting a warning sign may be adequate as the roads near the turbine will be rarely used. The RRF for this action is 10 which means this could reduce the risk by a factor of 10. For the roads that are close to the turbine and frequently used, a physical barrier would reduce the risk by a factor of 100. If these measures do not work, then additional steps such as reducing the hub height or relocating the wind turbine or taking a different route around the turbine should be considered.

1.2 Noise

The sound emitted from a wind turbine can be the subject of complaint if it causes public annoyance. People express concern over disruption with sleep patterns, headache, visual blurring, nausea tied with wind turbine noise. In Goderich, Ontario, a family filed a case in court to stop the construction of a wind farm close to their residence in 2014 (https://globalnews.ca/news/3490234/ontario-wind-turbines-family-complaints/). One couple from the same community in Ontario mentioned that wind turbines had made life a 'nightmare' (https://globalnews.ca/news/3490234/ontario-wind-turbines-family-complaints/). Similar stories on opposition can be found in other provinces of Canada and internationally. In Germany, where 37.5% of electricity supply comes from clean energy, people are fighting against the wind farms close to their homes (https://www.dw.com/en/the-germans-fighting-wind-farms-close-to-their-homes/a-51417653). The Dutch health institute has recently announced investigating the health implications of wind turbine noise in response to growing opposition among the residences near proposed wind farms (https://www.dutchnews.nl/news/2021/06/rivm-investigates-effects-of-noisy-wind-turbines-on-health-amid-growing-protests/). Health Canada convened an expert panel to research the effect of wind turbine noise on human health. It found inconclusive evidence of noise affecting health (The expert panel on Wind Turbine, 2015). These events paint a picture of people's attitude towards wind turbines, especially when they are planned near their dwellings.

To address this concern, it is necessary to make sure that wind turbines are planned far enough from residential areas so that the sound cannot significantly impact the regular life of the residents.

Specific rules have been developed to protect the interest of the public from the effects of noise. The proponent of a wind farm needs to acquire a list of approvals from different government

organizations. Each province in Canada has established a set of rules for the permissible sound level. Wind farm owners need to submit a noise impact assessment (NIA) report to show that the proposed farm will not exceed the relevant noise limits. A step in the preparation of a NIA report is the use of a standard sound propagation model. The output from the model is used to predict the sound level from the proposed wind farm at relevant noise receptors. It can be argued that the standard sound propagation method (*e.g.*, ISO-9613 (ISO/DIS 9613-2: Attenuation of sound during propagation outdoors- Part 2: General method of calculation, 1996)) provides constant sound pressure level at receptor points in every direction (Søndergaard & Plovsing, 2009) and that research on a more detailed model should lead to more accurate results.

Salomons (2001) reviews several approaches to the numerical solution of the governing equations for sound propagation. Two contenders for computationally efficient and effective solutions in cases with point monopole sources within the atmospheric boundary layer are ray models and parabolic equation (PE) models. Ray models can separate and illustrate the different factors associated with sound propagation, including the changes in sound pressure level with distance along a ray caused by geometrical attenuation, refraction effects, atmospheric absorption, and reflection from the ground. The PE method, usually based on a narrow angle, is a two-dimensional approximation to the Helmholtz equation for the complex pressure amplitude. The 2-D (r,z) idealization excludes refraction effects caused by cross ray (y) variations in sound speed or wind speed which may play a role in sound propagation over complex terrain. Also, rays reflected from a surface with a normal not lying in the r-z plane are difficult to deal with.

The Danish Technical University (DTU) sound propagation model presented by Zhu *et al* (2017) is based on the 2-D PE model proposed by Sack and West (1995) but can also allow for complex terrain effects as described in the ATMOS model developed by CSTB (Centre Scientifique et

Technique du Bâtiment) in France (Aballea & Defrance, 2006). Bolin *et al* (2014) also uses a PE method.

The approach in thesis has been to further explore the ray model developed in 2D by Lamancusa *et al* (1993) and extend it to 3D.

1.3 Contributions

The objectives of the studies contained in this thesis are to investigate two wind energy related issues, ice throw and sound propagation from wind turbines. Risks associated with ice throw and effects of noise are discussed. Two separate models have been developed to address the risks originating from ice throw and to evaluate the sound level at receivers from wind turbine. The work on ice throw was done early in the PhD program and completed. The sound propagation model is developed recently and still continuing in terms of submitting papers for journal publication. The results from the ice throw model can be applied to assess the potential risk of injury caused by ice throw. The output from the noise model is useful in the noise impact assessment generally required to get approval for wind farms.

The ice throw model developed in this thesis is an extension of a model (Morgan, 1998; Morgan & Bossanyi, 1996) developed as part of the WECO project (Tammelin, 2000). The previous model considered the motion of ice thrown from the turbine in two dimensions. A crosswind direction is added in the current model to allow the ice fragment to travel in all directions and upgrade it to a 3-D model. A logarithmic wind profile is added to the simulation replacing the constant wind speed with height in the original model. An illustration of the impact of lift force is added to the existing drag force to show the potential combined effect on the ice fragment trajectory and final position.

Sensitivity tests are done to examine the impact of the following parameters: i) mass and shape of the ice fragment, ii) the position of the ice fragment on the blade, iii) the drag coefficient, iv) rotor speed, and v) wind speed.

The results from the model can be significant to find the possible distribution of the ice impact locations on the ground. Trajectory model results, coupled with wind speed and direction statistics, can then lead to a map of potential impact probabilities in the area surrounding the wind turbine in order to assess the spatial distribution of the risk of ice fragments hitting the ground. Zephyr North Ltd, a consulting company in Ontario uses software based on the model. They assess the risk of ice throw from the wind turbine as a part of the planning and approval process for developers in Canada and USA.

In this thesis, an alternate approach to simulate sound propagation from an elevated source is proposed. Other published research has been mainly focused on application and continuous improvement in estimating sound level by the Parabolic equation method, which can be computationally time-consuming. However, the author believes that sound level measurement by tracing sound rays from the source has its advantages and hence is studied here. The ray model developed in this dissertation is based on a model developed by Lamancusa *et al* (1993) in two dimensions. In this study, that model is extended by incorporating sound propagation in three-dimensional space. The model includes wind speed, temperature, and sound speed variation with height. It also incorporates terrain variation and has been validated against the ISO 9613 (ISO/DIS 9613-2: Attenuation of sound during propagation outdoors- Part 2: General method of calculation, 1996) method, the recommended approach by the Ontario regulatory authority and other provinces to compute sound propagation in the atmosphere.

The widely accepted International Standard ISO 9613 is a common method for the calculation of sound propagation in the atmosphere. However, in this approach sound pressure is calculated only in the downwind direction from the source. It also does not clearly explain how the model incorporates refraction in the atmosphere. In the ray model, the receiver location can be in any direction. The refraction in the atmosphere can be considered by varying the wind and sound speed profiles in three dimensions. A receptor point can receive multiple rays which can occur due to refraction and reflection from the ground.

1.4 Organization of the Dissertation

This dissertation is divided into two parts. The first part contains a single chapter (Chapter Two) which describes the ice throw model and results from the model. The second part of the thesis has five chapters that discusses sound propagation in the atmosphere, development of the ray model and results. The noise issue and the research conducted to find its effect on public health are discussed in Chapter Three. The current regulations that are in practice to protect the public interest are also included. The fourth chapter includes a general discussion about sound propagation, sound pressure levels, intensity, and frequency through a medium. Human perception of sound over a range of frequencies and sound pressure levels are also discussed. In Chapter Five, the equation for a simple source is derived. Several numerical methods developed by other authors to estimate sound pressure levels are also presented in the same chapter. Chapter Six gives an overview of the ray theory method and how the model is set up in relation to the source, medium and characteristics of the terrain. The results from the ray model are presented in Chapter Seven. Chapter Eight concludes with a summary of all the results for both the ice trajectory and noise models.

Chapter 2
Ice throw model

2.1 Introduction

The objective of this section is to describe a simple trajectory model for ice thrown from a wind turbine and to study the model's sensitivity to input parameters. Most of the results will be for "compact" ice fragments in the terminology of windborne debris but some consideration of the effect of lift forces on plate-like fragments will also be included. The model was run for a range of values of different parameters that can affect the trajectory. The results from the model coupled with site specific wind information will be helpful to find the possible distribution of the ice impact locations on the ground.

A paper by Biswas *et al* (2011) was published based on the findings of the Ice throw model during the early years of a much extended (by two maternity leaves) PhD program. This chapter is essentially that paper. The work was done as a part of this PhD research project. The co-authors (Peter Taylor and Jim Salmon) initially suggested the task and helped with editing the paper but most of the work was done by the candidate. The model developed was subsequently reprogrammed with additional output for commercial use by Zephyr North Ltd. and is currently

used for risk assessment studies. As noted later, a recent International Energy Agency set of International Recommendations by Krenn *et al* (2018) cites and summarizes that paper (Biswas, Taylor, & Salmon, 2011) as their example of a suitable trajectory model.

2.2 Garrad Hassan model

An ice throw model (Morgan, 1998; Morgan & Bossanyi, 1996) developed as part of the WECO project (Tammelin, 2000) is described in the GHP report (Leblanc, 2007) on ice throw risk assessment for Ontario, Canada. The model is used to estimate the probability of ice strikes per square meter per ice day as a function of distance from the turbine base. In the model, the initial position of the fragment is determined by its position on the blade and the blade angle. The ice fragment is assumed to be thrown from random locations on a rotating turbine blade. After the ice fragment is detached from the blade, gravity and aerodynamic drag forces work on the fragment and bring it to the ground. The trajectory of the ice fragment is calculated based on the equations of motion. The model has also been used to calculate trajectories with an additional 'sling shot' effect in which the ice fragment slides all the way to the tip of the blade and an additional radial velocity is added to the tangential velocity of the blade (Morgan, Bossanyi, & Seifert, Assessment of safety risks arising from wind turbine icing, 1998). LeBlanc (2007) assumed standard values for some parameters. The wind turbine was chosen with an 80 m hub height and the radius of the rotor was 40 m. The rotor speed ω, was 15 rpm. The mass of the ice fragment (M) was 1 kg with a frontal area (A) of 0.01 m^2. This would correspond to an ice fragment of dimensions 0.1 m x 0.1 m x 0.111 m with a density of 900 kgm^{-3}. For a 1 kg sphere of ice with density 900 kg m^{-3} the frontal area would be approximately 0.013 m^2. The drag coefficient, C_D, was 1.0, aerodynamic lift

was not included, and the assumed wind speed distribution was independent of height and had a value of 8 ms^{-1}. Some of these assumptions warrant further examination.

When the trajectory was calculated without a sling shot effect the greatest distance that the ice fragment could travel under these conditions was about 200 m. This distance was achieved when the fragment was thrown upwards from the tip of the blade at an angle of 45^0 from the horizontal. The landing speed was also calculated. The maximum speed that the ice fragments had when hitting the ground was 60 ms^{-1}. With the sling shot effect, the maximum range increased to 250 m. To assess the risk of an individual or building being hit by a piece of ice, a Monte Carlo analysis was used with 100,000 ice fragments shed from the turbine. The result the Monte Carlo analysis is the probability of any ice fragment landing in one square meter of ground area as a function of distance from the turbine base. When this probability of ice strike per square meter was multiplied by the number of days when icing occurs in a year, it gives an estimate of ice strikes per square meter per year.

Seifert *et al* (2003) have presented sample calculations to illustrate possible uses for specific sites while Battisti *et al* (2006) used the model to investigate the area under risk around an offshore wind turbine. The main concern there was whether ice thrown from one turbine could strike another in an offshore wind farm. In these calculations the major strike probability area was within 200 m around the turbine and the maximum distance travelled by an ice fragment was 250 m from the base of turbine.

2.3 Windborne debris studies

Modelling and wind tunnel studies of windborne debris have been conducted since the 1980s, especially by Professor Masao Tachikawa from Kagoshima University in Japan (Holmes, Baker, & Tamura, 2006). Three classes of debris are generally considered; "compact" debris where lift forces are not considered, plate or sheet debris and rod debris. Most studies relate to debris picked up from rest by a uniform wind and many, such as Holmes *et al* (2006) are limited to two dimensional investigations but include lift and pitching moments as aerodynamic forces on the debris. In 2D a plate-like object has 3 degrees of freedom (x,z,θ) where x and z define the position of the center of mass and θ defines the angle of the plate relative to the horizontal. In 3D there are six degrees of freedom (Richards, 2008) for a plate-like object and specification of the forces and pitching moments, via a center of pressure, become more complex and less certain. In either a 2D or a 3D formulation the plates can rotate, and lift forces associated with the Magnus effect are often important (Holmes & Letchford, Investigations of plate-type windborne debris-Part II: Computed trajectories, 2006). Effects of turbulence can also be considered, although Baker (2007) claims that uniform flow calculations may be adequate for most purposes.

For ice fragments thrown across the wind from a rotating wind turbine the situation is immediately three dimensional. The shape and size of the ice fragment may be highly variable but both compact and plate-like ice fragments are possible. The initial model will deal only with compact ice fragment debris, with no lift force involved. This can be used to investigate the effects of a range of parameters which impact the trajectories. Full six degree of freedom calculations have not been attempted here because of the wide range of possible cases that arise. However, some calculations with lift forces are included to illustrate the impact of lift on plate-like fragments.

2.4 Model description

In order to investigate issues related to compact fragment (*i.e.*, no lift) ice throw and to test the sensitivity of trajectories to various parameters, a simple ice throw model has been developed to calculate the three-dimensional trajectory of a single ice fragment thrown from a wind turbine. The basic assumptions and equations are essentially the same as those used in the GH model (Morgan & Bossanyi, 1996; Seifert, 2003) but are given in detail here.

When a piece of ice is thrown from the turbine the initial velocity is assumed to be the same as the velocity of turbine blade at the position and time of release. Aerodynamic drag and gravity then determine the trajectory of the ice fragment until it reaches the ground. The initial position of the ice fragment is specified by its radial position on the turbine blade (r), the angle of the blade relative to the horizontal (θ), and the azimuth (φ) and tilt angles of the normal to the rotor plane relative to the wind direction and the horizontal. The tilt angle was set to zero in the subsequent calculations but can easily be included. If x, y and z are taken as along wind, lateral and vertical positions of the ice fragment, relative to a coordinate system with its origin at the base of the turbine tower, equations to calculate trajectories for a compact ice fragment of known mass and size can be written as

$$M\frac{d^2x}{dt^2} = -\frac{1}{2}\rho C_D A\left(\frac{dx}{dt} - U\right)|V| \qquad (2.1)$$

$$M\frac{d^2y}{dt^2} = -\frac{1}{2}\rho C_D A\left(\frac{dy}{dt}\right)|V| \qquad (2.2)$$

$$M\frac{d^2z}{dt^2} = -Mg - \frac{1}{2}\rho C_D A\left(\frac{dz}{dt}\right)|V| \qquad (2.3)$$

Here, M = mass of ice fragment

A = effective frontal area of ice fragment

C_D = drag coefficient

$U(z)$ = wind speed

Relative wind speed,

$$|V| = \sqrt{\left(\frac{dx}{dt} - U\right)^2 + \left(\frac{dy}{dt}\right)^2 + \left(\frac{dz}{dt}\right)^2} \qquad (2.4)$$

g = gravitational acceleration

ρ = air density

These equations have not included a lift force and assume that drag, opposite in direction to the fragment's velocity relative to the air, is the only aerodynamic force component. Lift can certainly occur for non-spherical ice fragments and may be substantial for plate-like pieces of ice. However, one problem is that the lift direction could be anywhere in the plane perpendicular to the air-relative velocity of the ice fragment and could be changing randomly as the ice fragment spins around. Some cases with lift will be considered later in Section 5.

The wind profile in the lower part of an atmospheric boundary layer is assumed to be

$$U(z) = \frac{u_*}{k} ln \frac{(z + z_0)}{z_0} \qquad (2.5)$$

Where z is the height above the local terrain, u_* is the friction velocity, z_0 is the roughness length and k, the von Karman constant is taken as 0.4. Wind profiles are not always of this form due to thermal stratification, complex terrain, or roughness variations but it is considered more appropriate than the constant, height-independent assumption of in earlier models (Morgan, 1998; Morgan & Bossanyi, 1996).

The initial position (x, y, z) and velocity (dx/dt, dy/dt, dz/dt) of the ice fragment at t = 0 are (0,

r cosθ, h + r sinθ) and (0, -rω sinθ, rωcosθ) with θ measured positive from the horizontal position with the blade rising. Please note the tilt angle is set to zero while defining the initial position of the fragment. Position on the blade is given by r and ω (radians per second) is the angular velocity of the rotating blade. Here, x is in the downwind direction. The blade rotates counterclockwise from the horizontal position.

Computations have been made with the 4th order Runge-Kutta (RK) method for solving Ordinary Differential Equations (Press, 2007). Calculations have been carried out using the base set of parameters listed in Table 2.1, variations to explore sensitivity.

As far as the trajectory equations are concerned, it is the combined ice fragment parameter C_DA/M that matters. For the base case, $C_DA/M = 0.02$ m^{2}kg^{-1}. If a velocity scale is used such as $U_h = U(h)$, g and air density, ρ, a dimensionless parameter could be formed, $K^* = 0.5\rho C_D A U_h^2/Mg$, similar to the Tachikawa number proposed by Holmes *et al* (2006) but including C_D. C_D depends on the shape and orientation of the ice fragment and for a bluff body (*e.g.*, cylinders and spheres) of the type of the values would normally be of order 1 (Batchelor, 1967). Lower values are possible for streamlined objects. A smooth sphere at a Reynolds number of 4 x 10^5 drops to 0.06 but a value around 0.4 is more typical at high Reynolds number or with a rough surface. Ice density, ρ_i, could vary from about 500 kgm^{-3} to 900 kgm^{-3} depending on the formation mechanism (riming or freezing rain). The C_DA/M combination (0.02 m^{2}kg^{-1}) can be thought of as a 1 kg, rectangular block of ice, 0.1 m x 0.2 m in frontal area and with a thickness which could range from 0.055 m to 0.1 m as ice density decreases. In the model the hub height of the turbine is taken as 100 m and the length of the blade is 45 m. The wind speed (*U*) is taken from the logarithmic wind profile at the consecutive heights of the ice fragment during its travel through the air until it hits the ground.

The trajectory of a single ice fragment in three dimensions is using Table 2.1 parameters shown in Figure 2.1.

Table 2.1: Base set of parameters used for the calculations.

Hub height	100 m
Blade length	45 m
Rotor speed (tilt angle=0º)	14.5 rpm = 1.518 radians s^{-1}
Ice fragment mass, M	1 kg
Ice fragment frontal area, A	0.02 m^2
Drag coefficient, C_D	1.0
Ground roughness length, z_0	0.01 m
Friction velocity	0.6514 ms^{-1}
Hub height wind speed, U_h	15 ms^{-1}
Air density, ρ	1.225 kg/m^3

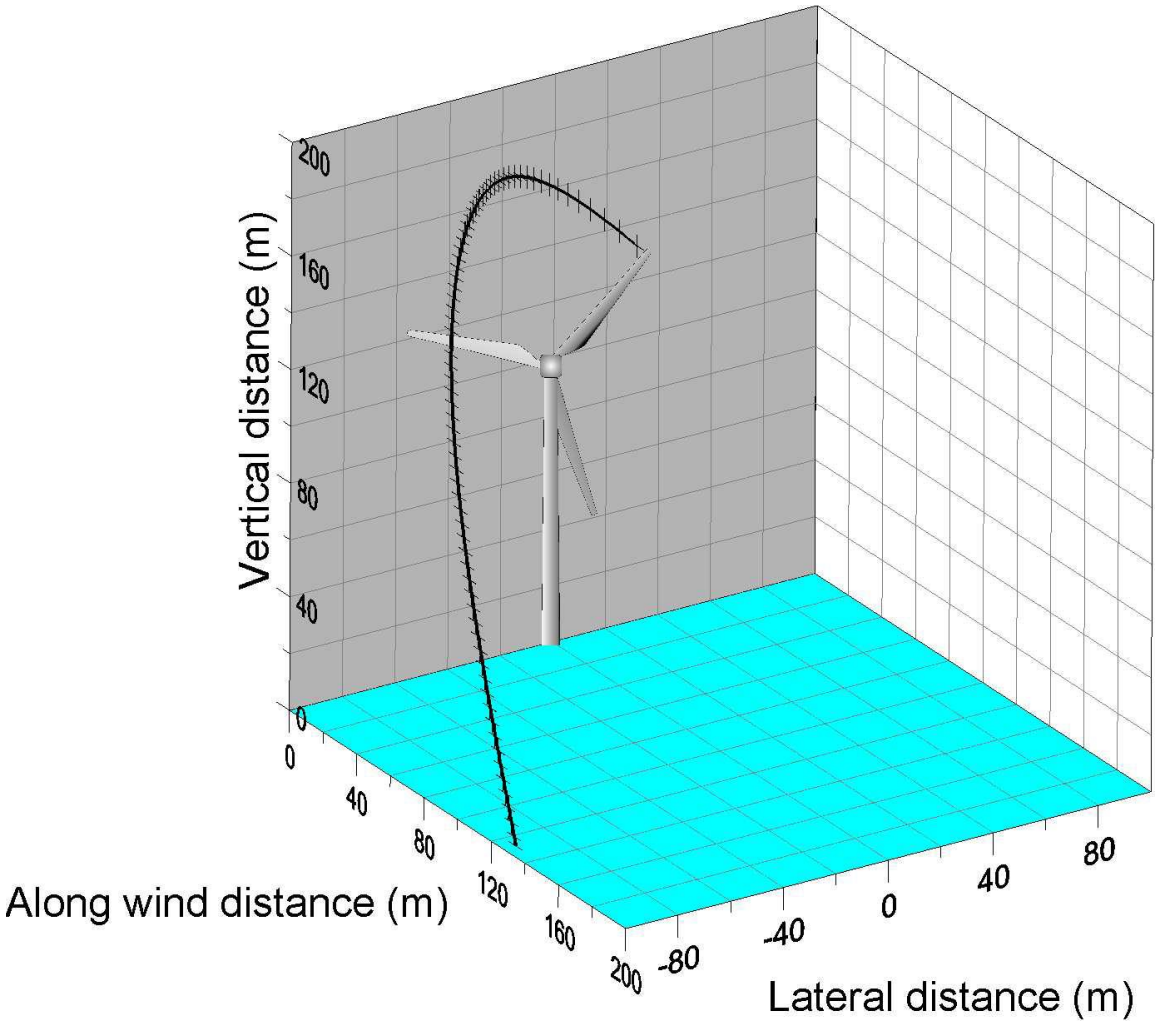

Figure 2.1: Trajectory (x, y, z) of a single, 1 kg ice fragment released at angle, $\Theta=45^0$. Rotor speed, ω =14.5 rpm, r = 45 m, C_DA/M = 0.02 m^2kg^{-1}, U_h = 15 ms^{-1}.

Specifically, an ice fragment of 1 kg was ejected from the tip of the blade (r = 45 m) with a blade angle of 45^0. The ice fragment travelled 127 m along the wind and 95 m in the lateral direction and hit the ground 158 m away from the base of the turbine.

2.5 Sensitivity tests of the model

The trajectory of an ice fragment varies with a number of parameters which will change its final location on the ground. The parameters can be categorized in four groups. First, the properties of the ice fragment itself. The mass, frontal area, shape, and density of the fragment are all significant but as noted earlier, the combination C_DA/M or the dimensionless number K* is what controls the dynamics. Second are the specification parameters of the turbine *i.e.*, hub height, length of the rotor blade, and speed of rotation (ω). Third are the initial position of the ice fragment (*i.e.*, radial position on the blade (r) and the angle of the blade relative to the horizontal (θ)). The fourth group includes the wind speed profile parameters (u_*, z_0) as well as the topography of the site (although in the calculations presented here a simple, horizontal terrain will be assumed). All these parameters together affect the total distance the ice fragment will travel and the final position of the ice fragment on the ground.

2.5.1 Ice fragment launch positions.

The radial position of the ice fragment (r) was varied as it was ejected but, for studies of the maximum downwind distance travelled, the blade angle (θ) was fixed at 45º with the blade moving upwards in that position. Figure 2.2 shows the height and downwind position of the ice fragment, which is released initially from r = 0 to 45 m. The wind speed parameters are $u_* = 0.6514$ ms^{-1} and $z_0 = 0.01$ m, so that hub height wind speed is 15 ms^{-1}. The radial distance of the ice fragment is incremented and finally from r=0 until the ice is ejected from the tip of the blade (r = 45 m).

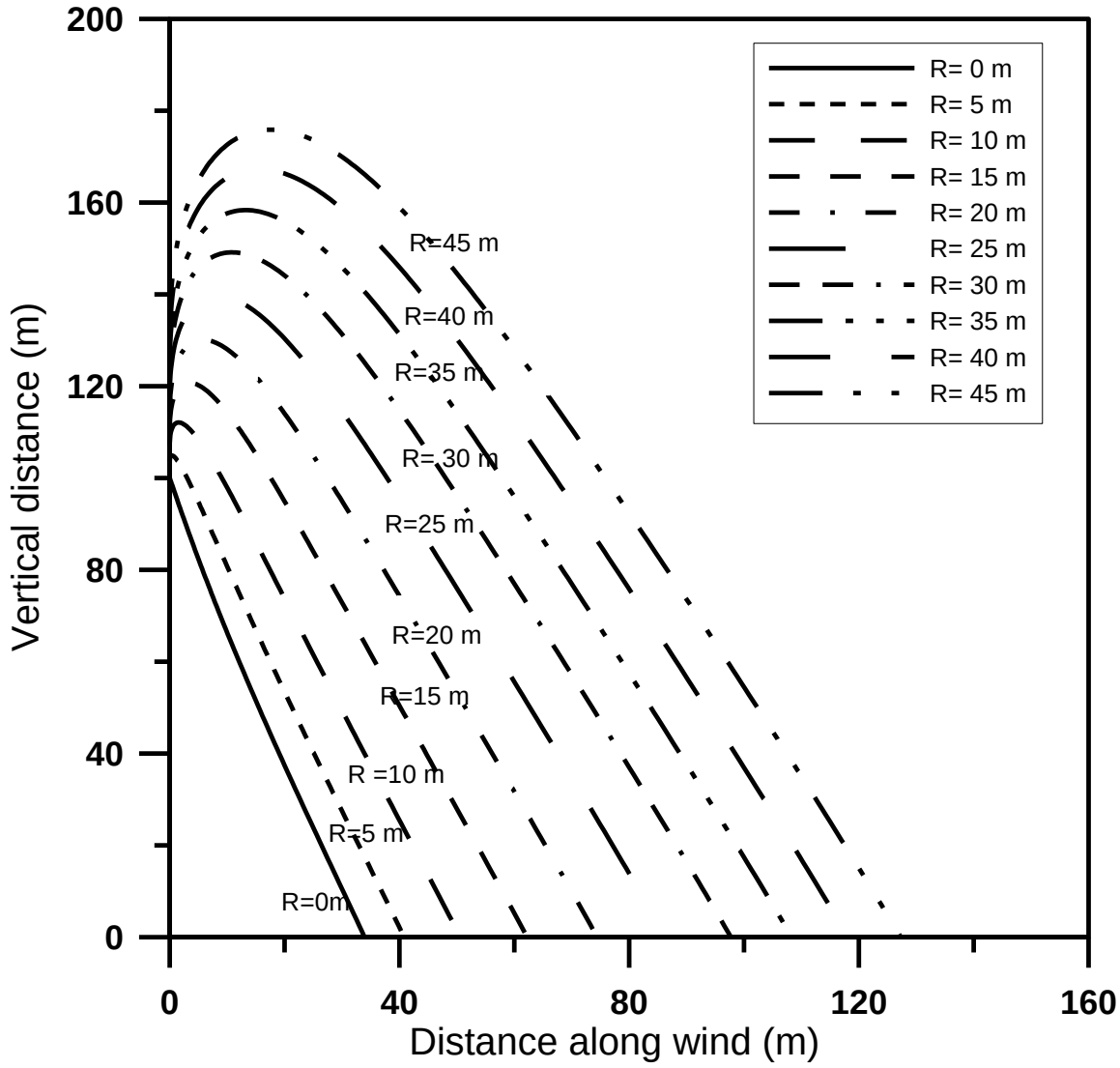

Figure 2.2: Trajectories (z, x) of a single ice fragment released at various radial distances (0-45 m in increments of 5m). $\theta = 45^{o}$ is measured relative to the positive y axis in the reference plane (x = 0). In these cases, $C_D A/M = 0.02$ $m^2 kg^{-1}$, $\omega = 14.5$ rpm and $u_* = 0.6514$ ms^{-1}.

The ice fragment thrown from the tip of the blade travels 127 m downwind. The coordinates of the locations where ice fragments reach the ground have also been calculated. Ice fragments were ejected from various radial distances and θ was also varied from 0º-360º. The impact locations on

the ground are shown in Figure 2.3. It is seen that the fragments ejected from the tip of the blade travel a maximum of 134 m along wind and 157 m in the lateral direction. The throwing angle for which an ice fragment travels the maximum distance laterally is 300^o for r = 45 m. It is also seen that changing the radial position from 0 m to 45 m changes its downwind range from about 34 m to 144 m.

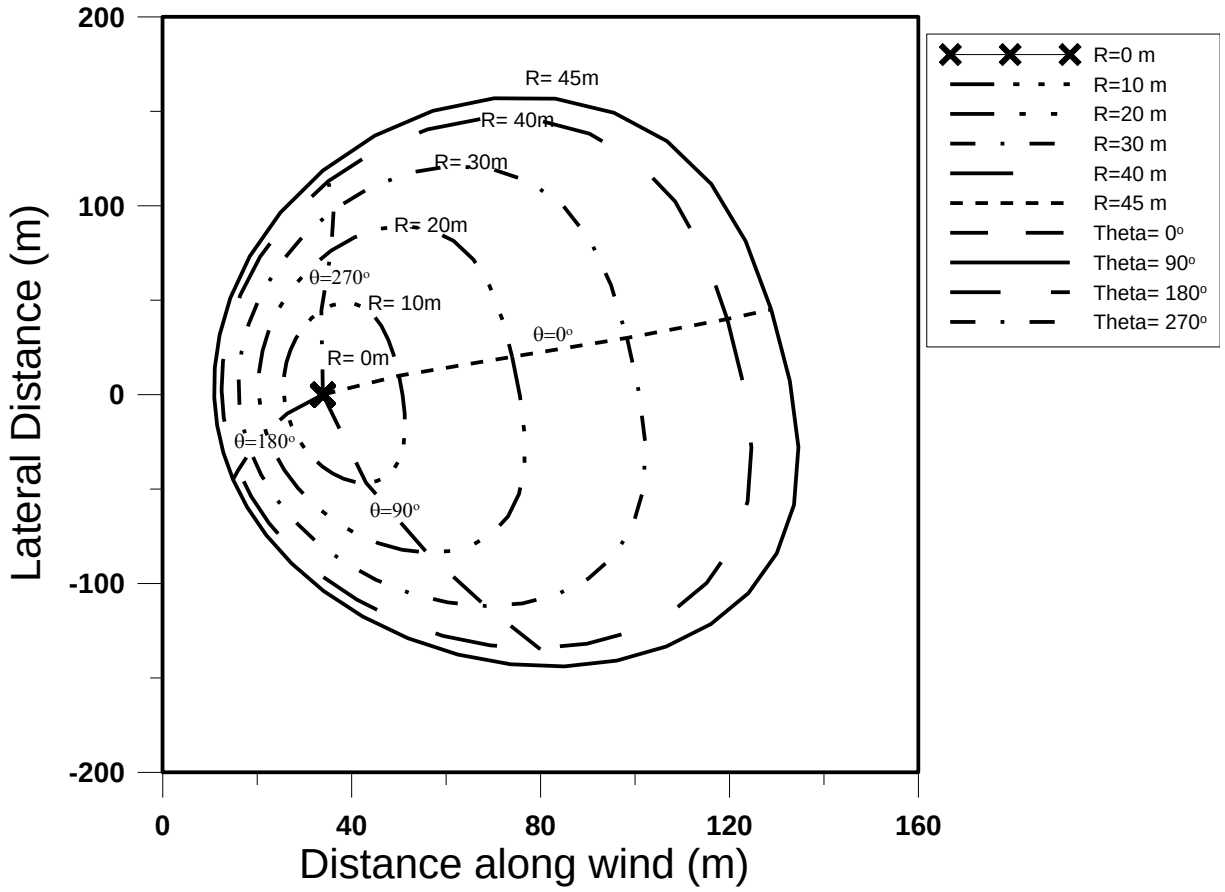

Figure 2.3: Impact locations for ice fragments released at different radial locations on the blade and varying θ. C_DA/M = 0.02 m^2kg^{-1}, ω = 14.5 rpm, z_0 = 0.01 m, and $u_* = 0.6514\ ms^{-1}$.

The trajectories can also be viewed in the y-z plane. Varying θ from 0º-360º with r = 45 m gives the trajectories shown in Figure 2.4. The angle for which the ice fragment travels the maximum distance in the positive lateral direction is 300º. For the opposite side of the y axis the maximum distance is achieved by throwing the fragment at 90º.

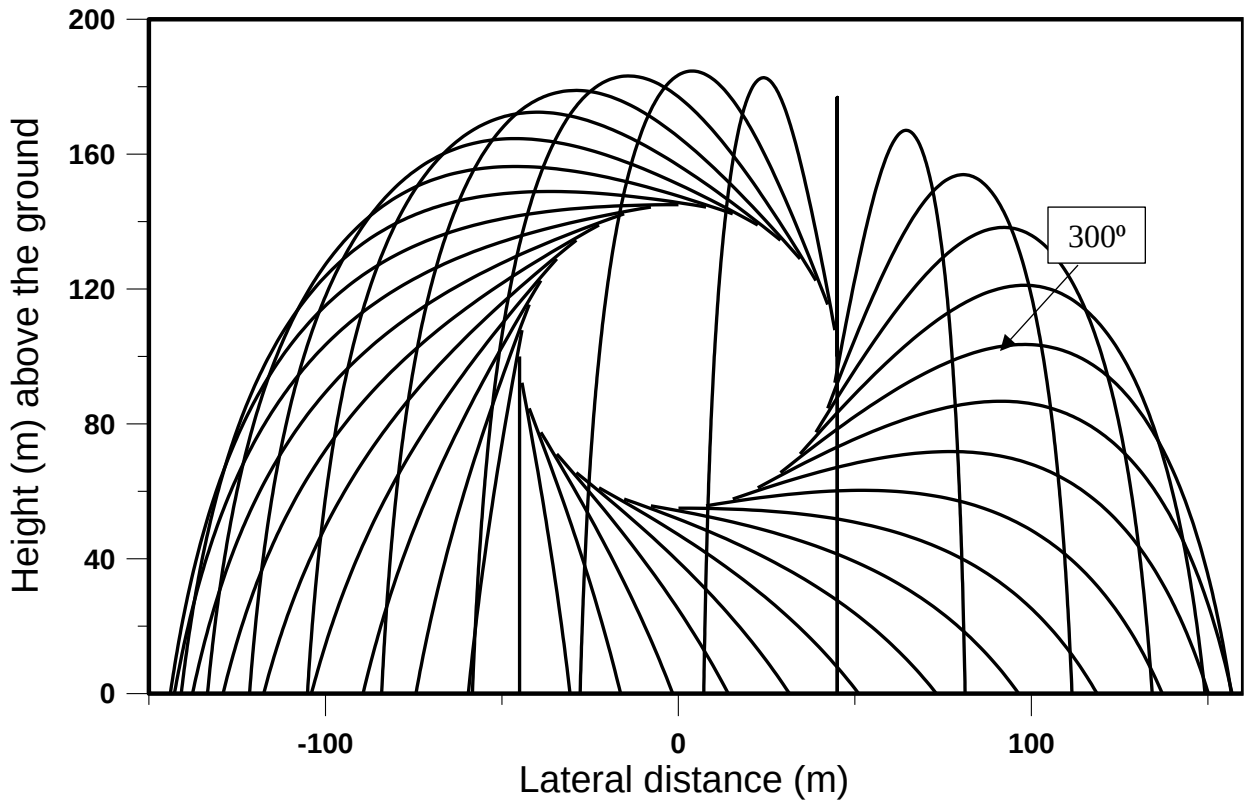

Figure 2.4: Trajectories (y, z) of ice fragments launched at various angles, (Θ=0-360), ω = 14.5 rpm, r = 45 m, C_DA/M = 0.02 m^2kg^{-1}, z_0 = 0.01 m and $u_* = 0.6514\ ms^{-1}$.

2.5.2 Ice fragment drag coefficient.

The drag force is an important parameter in this model. Ice fragments traveling under a higher drag force fall closer laterally to the turbine but can travel further downwind. Ice fragments go further laterally when the drag force is lower. The value of the drag coefficient depends on the shape of the ice fragment in this trajectory calculation. The field studies reported by Cattin *et al* (2007) of ice throw from a relatively small wind turbine (600 kW) investigated the size of ice fragments found on the ground. During their study period in winters 2005/6 and 2006/7 the maximum length of the ice fragments was more than 100 cm and the mass varied up to 1.8 kg. Ice density was not reported but the photographs appear to show relatively clear ice which would have a density close to 900 kgm^{-3}. They also note occasions with rime ice fragments and with wet snow thrown from the blades. It might be noted that long ice fragments are expected to break into pieces during their flight or as soon as they hit the ground. The value of drag coefficient was assumed to be unity in most of the calculations. In Figure 2.5 we illustrate the impact location of ice fragments for various drag coefficients. In the figure the smallest area covered is by the $C_D = 4$ curve for those ice fragments falling under the highest drag force. It is noticeable that for low C_D values the ice fragment often goes farther laterally than it goes in the along-wind direction. When there is no drag force applied, the ice only travels laterally.

The drag force is related to the mass, area, and shape of the ice fragment. In this model the standard mass of the ice fragment was taken to be 1 kg and frontal area was taken as 0.02 m^2. In the field study conducted by Cattin *et al* (2007) around 50% of the ice fragments found on the ground were less than 50 g and only 4% of them were more than 500 g. The maximum weight of an ice fragment was 1.8 kg. Note that it is the combined factor C_DA/M that controls the trajectory calculations.

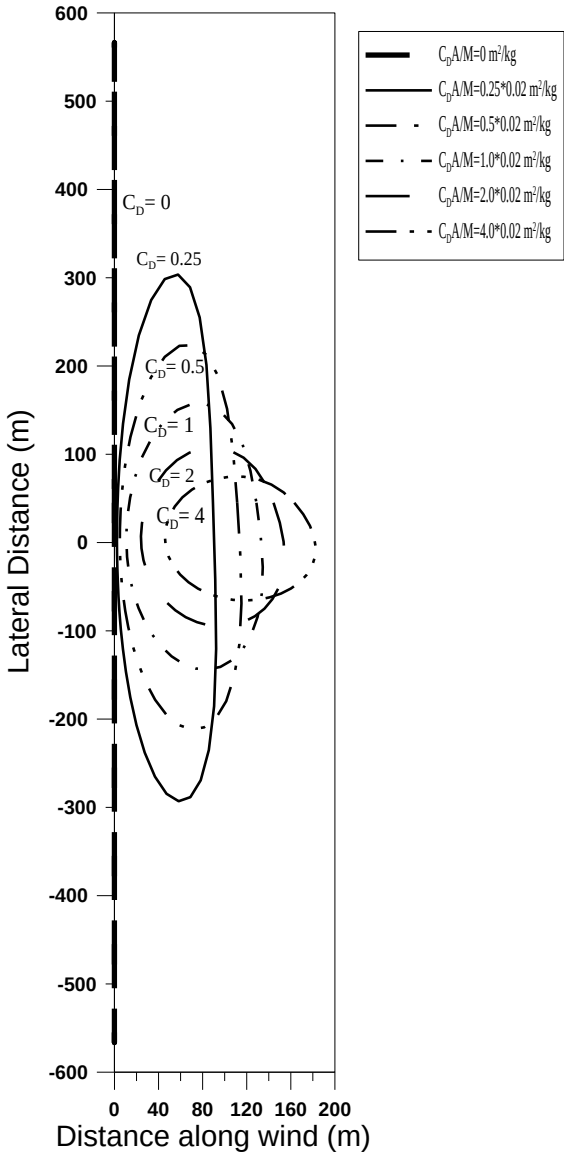

Figure 2.5: Effects of variation in the ratio C_DA/M. Co-ordinates of ice fragment impact locations on the ground (z = 0 m) after being thrown from a wind turbine. Different points on the curves correspond to different release points (θ), Results are for r = 45 m, ω = 14.5 rpm, z_0 = 0.01 m and $u_* = 0.6514\ ms^{-1}$. Results can be interpreted as applying to different drag coefficients (0-4) with m = 1 kg and A = 0.02 m^2 but can also be regarded as differing ice fragment frontal area and mass corresponding to variations in size, shape, and density.

For the same ice density and shape, M is proportional to $A^{3/2}$ so that A/M increases as the ice fragment gets smaller. As a consequence, an ice fragment of mass 0.125 kg and A = 0.005 m^2 with C_D = 1 would have the same trajectory as the A = 0.02 m^2, 1 kg fragment with C_D = 2, and a fragment of mass 0.0156 kg with A = 0.00125 m^2 and C_D = 1 would have the same trajectory as a 1 kg fragment of the same shape and density with A = 0.02 m^2 and C_D = 4.

If a somewhat extreme case of a 1 kg sphere of ice with A = 0.013 m^2 and a drag coefficient of 0.4 (the minimum likely value though golf balls get lower) is considered, it gives $C_DA/M \approx 0.005$ (=0.25 x 0.02) and the maximum lateral distance thrown is about 303 m.

2.5.3 Blade rotation speed

The rotation speed, ω, is another important parameter in this model. Higher rotation speed provides greater initial velocity to the ice fragments. As a result, the lateral range of the ice fragments impact positions increases. Ice fragments can also be projected to greater heights and maximum downwind distances also increase. Most large wind turbines have ω in the 6- 20 rpm range. Results for this range are shown in Figure 2.6.

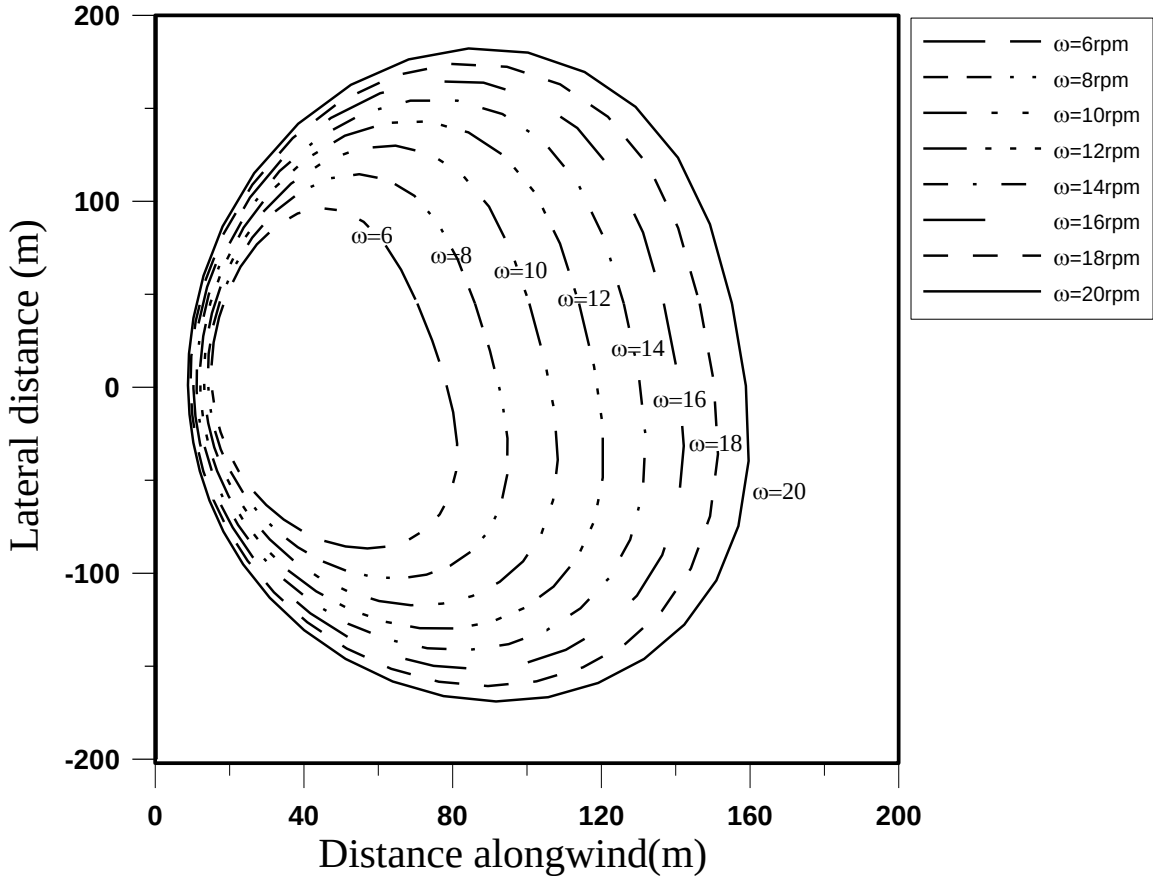

Figure 2.6: Final positions of ice fragments for different rotor speeds. Computations have been made for $C_DA/M = 0.02\ m^2kg^{-1}$, hub height wind speed = 15 ms^{-1}, $z_0 = 0.01$ m and r = 45 m.

2.5.4 Wind speed

The wind speed also plays a significant role in the model. As a typical example the cut-in hub height wind speed is taken as 4 ms^{-1} and the cut-out wind speed is 25 ms^{-1}. In Figure 2.7 the effect of wind speed is shown. It is seen from the figure that as the wind speed increases ice fragments

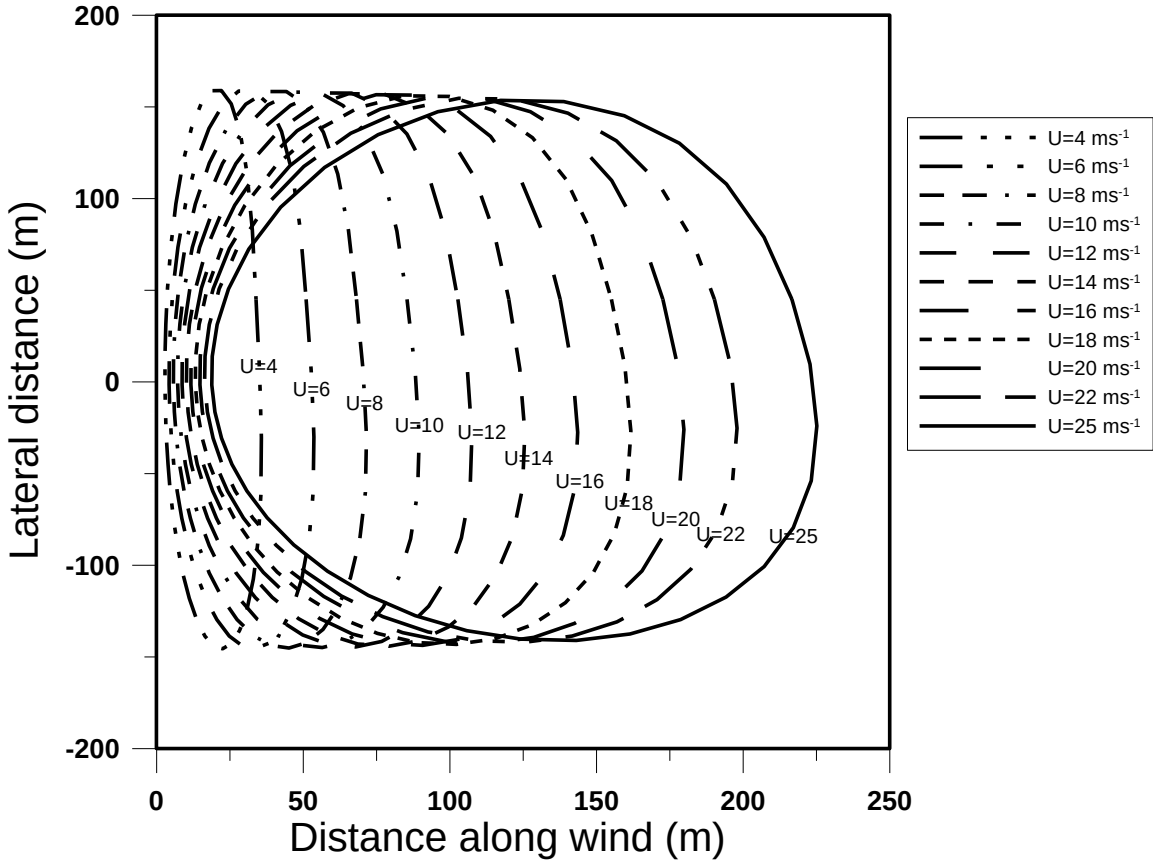

Figure 2.7: Co-ordinates (x,y) of ice fragment landing points for different hub height (100 m) wind speeds. Computations for rotor speed = 14.5 rpm, r=45 m, C_D=1, z_0=0.01 m.

travel further in the along wind direction and slightly less laterally. The range along wind reaches about 225 m downwind when the wind speed goes up to 25 ms^{-1}. These calculations were all with a fixed ω, but similar calculations could be made with variable rotation rate and a fixed tip speed ratio.

At high wind speeds and in severe icing conditions turbines should normally be shut down. However, ice fragments could still become detached from the blades and be carried down-wind of

the turbine. Figure 2.8 shows landing points for this case with winds up to 30 ms^{-1}. Ice fragments are unlikely to travel more than 200 m from the turbine even at 30 ms^{-1}.

In the field study done by Cattin *et al* (2007) throwing distance was judged to be independent of the fragment mass but there was a good correlation between the range of ice fragment landing location and the wind speed. In the GH model (Morgan & Bossanyi, 1996; Leblanc, 2007) it was seen that the distance traveled by ice fragments depends more on the tip speed than on the mass of the fragment. The results from the model show that wind speed and the rotor speed had the highest impact on the range of the ice fragment but variations in mass or density would have an impact.

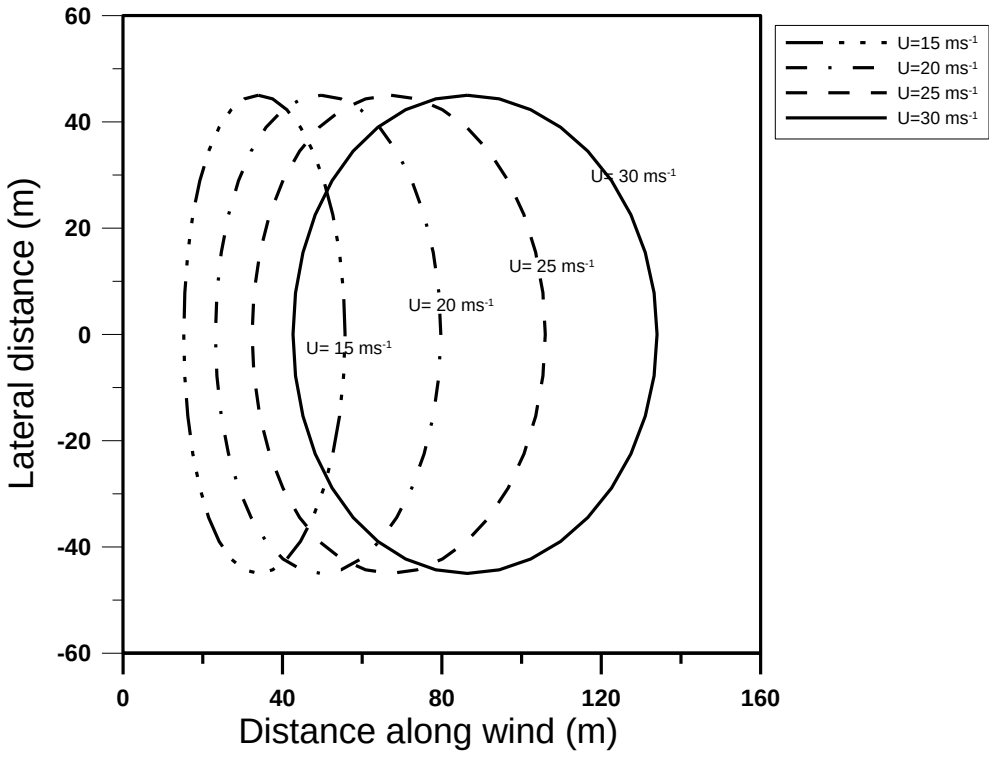

Figure 2.8: Co-ordinates (x,y) of ice fragment landing points for different hub height (100 m) wind speeds from stationary wind turbine. Computations for rotor speed ω = 0 rpm, r = 45 m, C_DA/M = 0.02 m^2kg^{-1}, z_0 = 0.01 m.

2.6 Cases with Lift

As noted in Section 3 the basic model ignores lift forces, in part because the initial studies assumed relatively isotropic ice fragments, 0.1 m x 0.2 m x 0.1 m blocks and ice spheres for which drag would dominate. Also, the direction of the lift force would be unpredictable and would probably change randomly during the flight of the ice fragment. It is however quite conceivable that for flatter, more sheet-like ice fragments, the lift could be as great as the drag and these fragments could possibly maintain a relatively stable orientation. The situation is complicated by switches in the direction of the relative wind at different points along the trajectory. These are illustrated in Figure 2.9 below. For simplicity it will be assumed that the plate like fragment has its normal in the plane defined by **u**-**U** and the vertical. Consider an ice fragment which has been released from an upward moving blade with u = 0. In this case, w > 0 and u-U < 0 as illustrated in case (a). For an ice fragment orientation of 45º relative to **u**-**U** the lift would act to increase both u and w while drag would increase u and decrease w. If lift and drag are in a vertical plane, they will both act to reduce v. In case (b) the ice fragment is falling towards the ground, but it still has U > u. In this situation with the same 45º orientation the lift and drag could both act to reduce the fall speed (-w), drag would act to increase u while lift could reduce u. Both lift and drag would again act to reduce |v|. In general, U > u is expected, but in the final stage close to the ground the ice fragment can be travelling faster than the wind as wind speed reduces close to the surface. This is illustrated in part (c). With the same 45º angle of attack lift is now assisting the drag in slowing the rate of descent and is also acting to increase the u component velocity while drag will oppose u. Drag will also oppose v while lift can act to amplify v.

Suppose that a 1 kg ice fragment is a plate of thickness 0.02m and area 0.1m x 0.6m. Density and thickness could, for example, be quite plausible values of 625 kg m^{-3} and 0.02 m or 900kg m^{-3} and 0.014 m. As in the compact ice fragment cases the trajectories are controlled by the quantity C_DA/M, plus, in this case C_LA/M so reducing the area and the mass in proportion would give the same result, provided that C_L was not changed by the change in shape of the object. The frontal area would depend upon the orientation (0.06 sin θ) where θ is the angle between the plane of the plate and the relative wind vector **u**-**U**, i.e., the angle of attack. However, for a flat plate at an angle to the wind it is customary to take the reference area for lift and drag coefficients as the total area of the plate rather than a frontal area. With this convention the drag coefficient on a long flat plate has a maximum of about 2 at normal incidence and both lift and drag coefficients are approximately 1 at an angle of attack of 45º (Holmes & Letchford, 2006). This orientation provides approximately the maximum lift.

With lift forces included and the worst-case scenario described above the Equations (1)-(3) have been modified and explicitly include the elevation angle χ of the vector u-U relative to the coordinate system. The equations can then be written,

$$M\frac{d^2x}{dt^2} = L(|u-U|/U_H)sin|\chi| - D((u-U)/U_H)cos\chi \qquad (2.5)$$

$$M\frac{d^2y}{dt^2} = L(v/U_H)sin|\chi| - D(v/U_H)cos\chi \qquad (2.6)$$

$$M\frac{d^2z}{dt^2} = -Mg + L\,cos\chi - Dsin\chi \qquad (2.7)$$

Where

$U_H^2 = (u\text{-}U)^2 + v^2$, $D=½\rho C_D A|V|^2$, $L=½\rho C_L A|V|^2$ and $|V|$ is as defined in Equation (2.4).

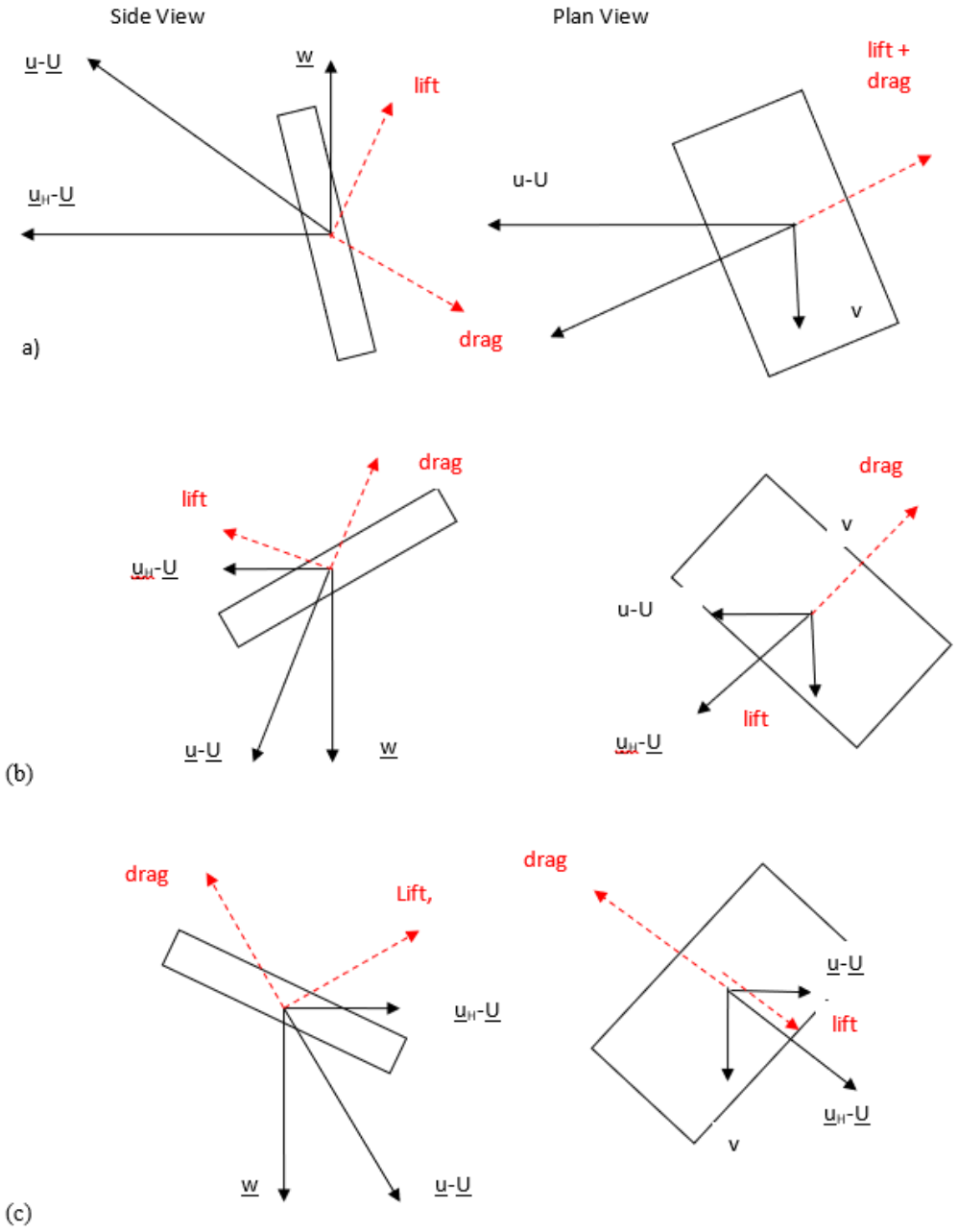

Figure 2.9: Three possible lift scenarios. All figures are in the plane defined by $\underline{U}$-$\underline{u}_H$ *and* $\underline{w}$*, and it is assumed that the plate-like ice fragment has its normal in that plane. The x axis is aligned with the wind,* $\underline{U}(z)$*, which is assumed to be horizontal and in the same direction for all heights, z.*

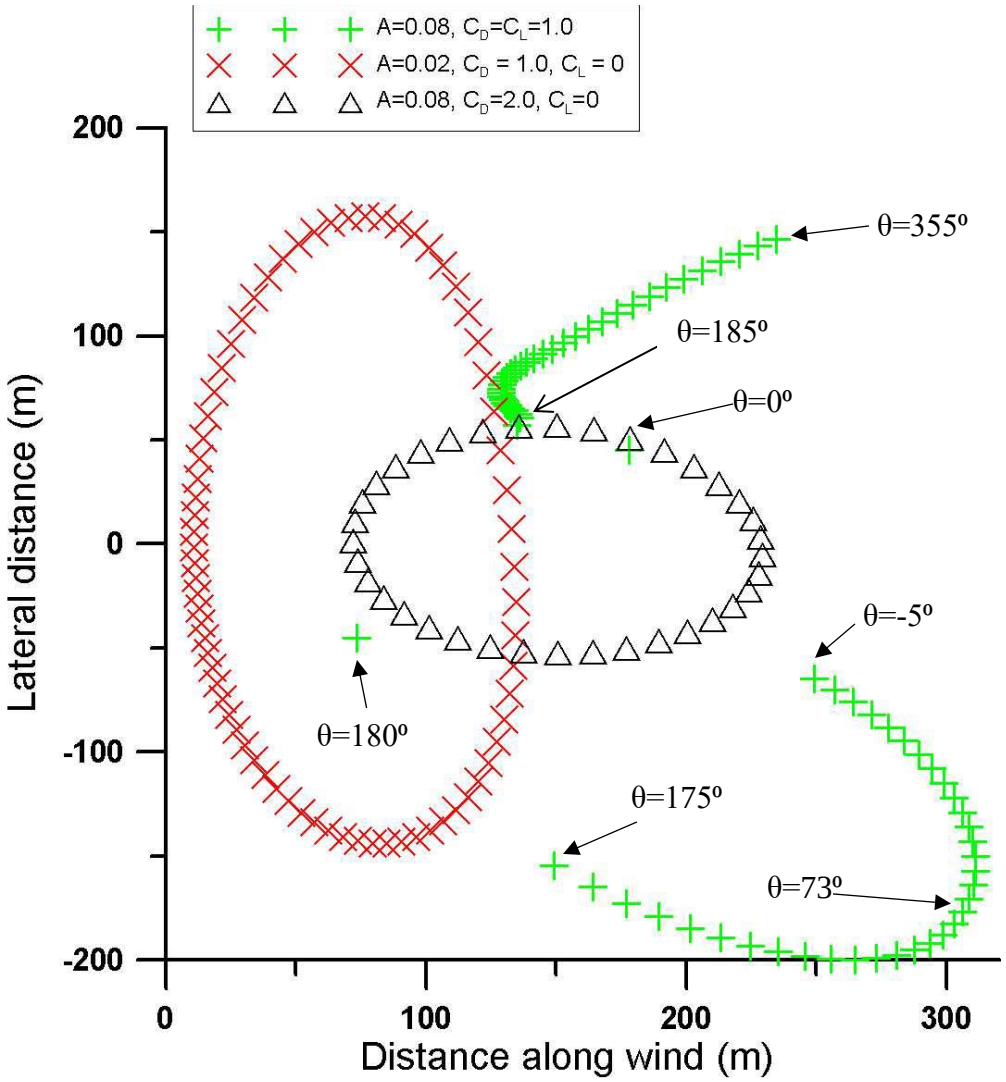

Figure 2.10. Landing positions for 1 kg ice fragments with and without lift. Fragments released from various angles, θ, at r = 45 m with U_H = 15 ms^{-1}. Basic compact fragment case has A= 0.02 m^2 and C_D = 1.0. Plate like fragments have A = 0.08 m^2. With no lift but oriented normal to the relative airflow C_D =2.0. With lift, and preferred orientations as discussed C_D = C_L = 1.0. Increments in θ are 10º except for the lift case with Δθ = 5º.

Sample landing position results are shown for 1 kg fragments in Figure 2.10. The lift case assumes A = 0.08 m^2 and C_D = C_L = 1.0. Also shown are compact fragment results with A = 0.02 m^2 and

results for a plate-like fragment with A = 0.08 m^2 and C_D = 2 - a typical value for a flat plate normal to the airflow. It is seen that the impact of lift can be to allow the wind to carry the fragments further, but not much further than about 350 m from the base of the turbine, even with the optimum lift scenario considered.

It is interesting to note the differences between the compact fragment and plate-like fragment case. The increase in C_DA/M limits the lateral distance travelled while allowing the wind to take the fragment further downwind, though not as far as when lift comes into play. Maximum downwind distance (based on calculations with 1º increments in θ) travelled with lift is 311 m when θ = 73º, while the lateral extreme of y = -200 m is for θ = 126º.

Looking at details of the trajectories with lift in Figure 2.11(a) and Figure 2.11(b) it is seen that θ = 0º and 180º are special cases with no lateral movement. This is an unstable situation and with small (1º) departures the trajectories eventually shift in the y direction as can be seen in Figure 2.10. This generally happens when the fragment has w < 0, since while the fragment has w > 0 and with $C_D = C_L$, a situation arises with both lift and drag forces opposing motion in the y direction as indicated in Figure 2.9a.

Any initial lateral velocity is quickly damped as shown in Figure 2.12. Once w < 0, the lift force can accelerate motion in the y direction until a balance exists between lift and drag forces.

Other effects such as rotation and possible Magnus effect forces are discussed by Baker (2007)

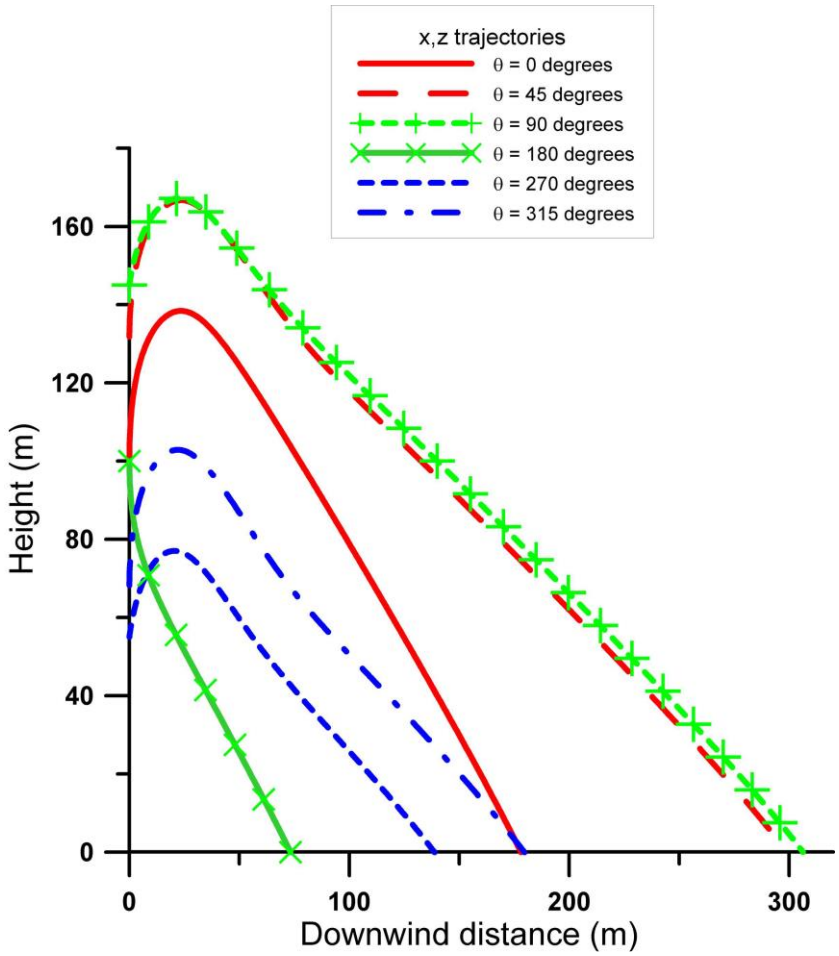

Figure 2.11(a): z-x traces for selected release angles (45º increments), at r=45 m with U_H=15 ms^{-1}. Plate like fragments optimally oriented; A=0.08 m^2, C_D=C_L=1.0.

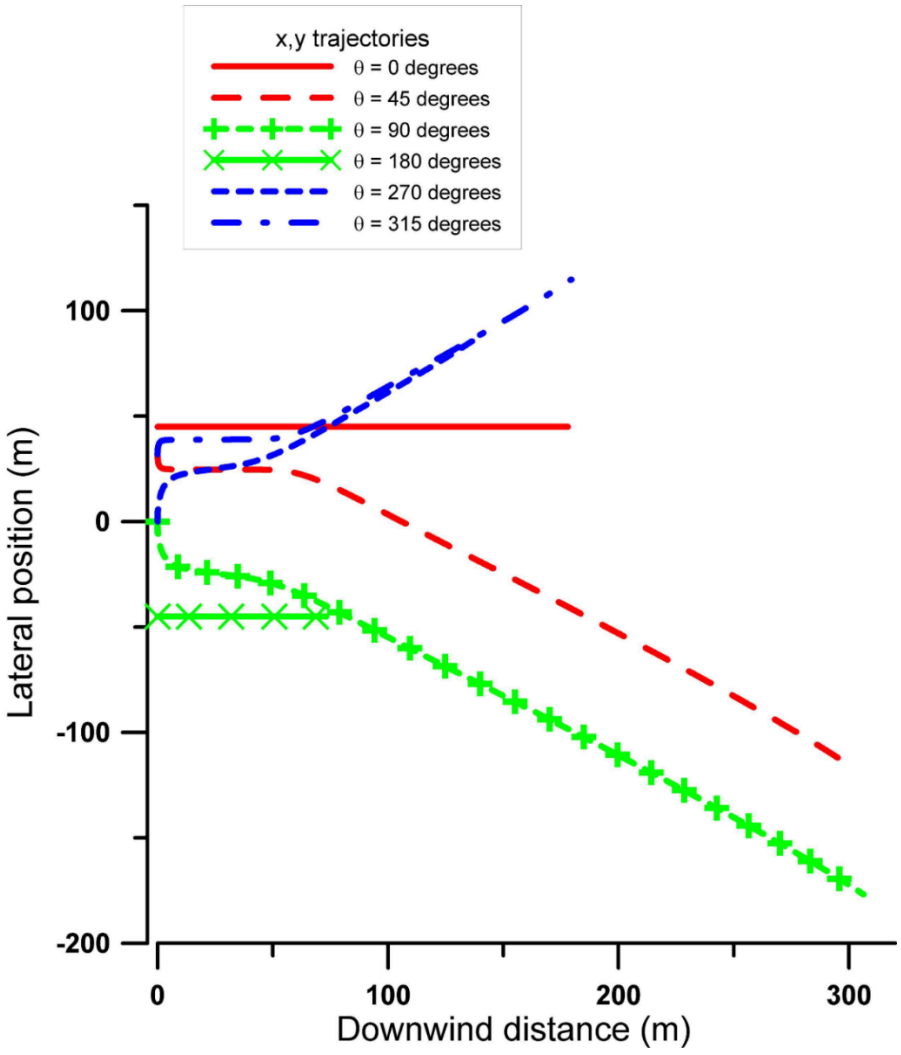

Figure 2.11(b): y-x traces for selected release angles (45º increments), at r=45 m with U_H=15 ms^{-1}. Plate like fragments optimally oriented; A=0.08 m^2, C_D=C_L=1.0.

and Richards *et al* (2008) in the general wind-borne debris context. Kordi (2009) indicates that the maximum lift coefficient associated with autorotation, C_{LA}, is 0.4 for a square flat plate. While this

may increase for a long rectangular plate it would appear that the Magnus or autorotation lift should be less than the value of $C_L = 1.0$.

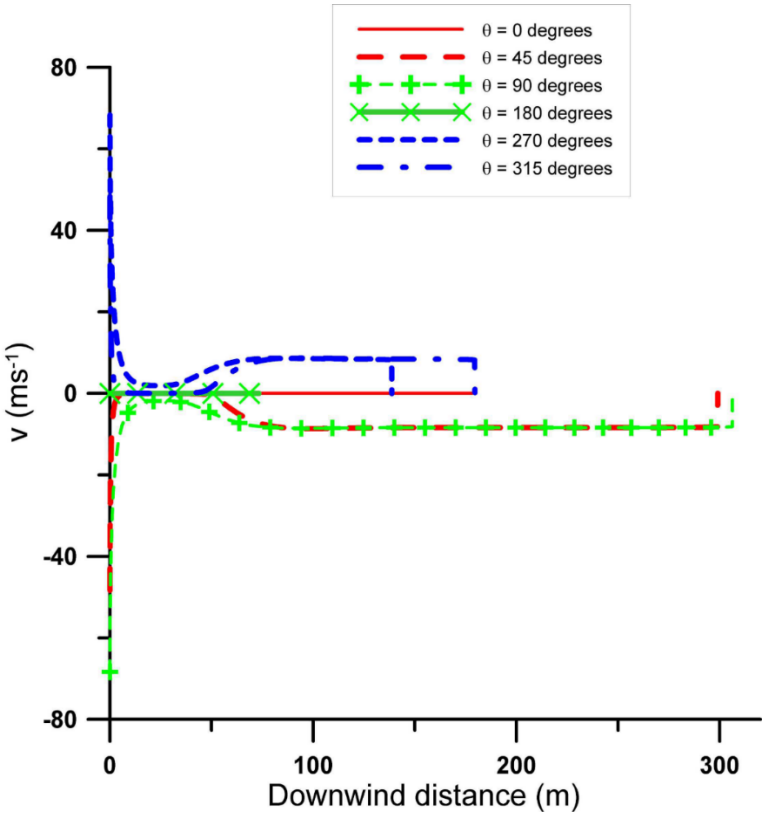

Figure 2.12: Lateral velocities for selected release angles (45 deg increments), at r = 45 m with UH =15 ms^{-1}. Plate like fragments optimally oriented; A = 0.08 m^2, $C_D = C_L = 1.0$. Velocities drop abruptly to zero when the fragment reaches the ground.

2.7 Ice throw summary

The author is not aware of any serious injury or damage caused by ice throw from large wind turbines, at least in part because they are not installed close to homes, schools, or businesses. The biggest risks may be associated with roads and the potential for vehicle impacts with large falling or fallen ice fragments. Compact debris calculations with no lift are relatively straightforward and the material in sections 2.4 and 2.5 provide a basic tool for risk assessments, as asserted by Krenn *et al* (2018). Better information on ice fragment mass, size and shape would be highly desirable but with limited occurrence and attempts to avoid ice throw situations this has been slow to appear. Section 3.2.2 of Krenn *et al* (2018), based on ice piece collection campaigns (Krenn, et al., 2018) does provide a histogram of A/M values. The average value is 0.09 m^2kg^{-1}. Lunden's study reports an average ice mass of 0.6 kg, and her photographs suggest somewhat flat ice fragments (Lundén, 2017).

Lunden *et al* (2017) conducted a field study in Sweden for three winter seasons. Three wind farms participated in this study where data were collected from nine wind turbines. The data collected during this study included mass, size, type (rime or glaze) of the ice fragments fallen on the ground, their impact locations, meteorological condition such as wind speed and direction, air temperature. All the information was recorded in a database. Analysis of the data shows that the weight of the ice lumps varies between 0.08 and 4.9 kg with an average mass of 0.6 kg. Most of the ice chunks (about 60%) weigh around 1 kg. Almost 75% of the total ice pieces were found between 20 m to 90 m from the base of the turbine. The least amount of ice lumps (around 1%) were found about 135 m from the turbine. There was no correlation between the mass of the ice and the distance it travelled before hitting the ground.

A model was also developed to calculate the level of risk while entering a wind farm using the information on ice fragments collected in the field study. The model uses the same equations as stated in this thesis to calculate the trajectory of the ice piece. The final output of the model is the energy of the ice lump when it lands on the ground. That impact energy was compared against a value of 40 Joules, which is lethal for human. The mass to reference area of an ice fragment was calculated to see its impact on the landing position. To do that, ice chunks were thrown from different blade positions. After they reached the ground, it was seen that if the impact points were connected, they formed the shape of an ellipse. The ice fragments which have the lowest mass to area value covered the smallest ellipse. The ice fragments with the highest ratio of mass to area value covered a larger area. The ice fragment that had the middle values covered the largest area on the ground. Therefore, it can be said that the ratio of mass to area is one of the governing factors that determines the trajectory of any ice fragment as well as the impact location on the ground. This result bears significance in the sense that if the mass to area ratio and other information are known for an ice chunk, it will be easier to predict its impact location on the ground.

Chapter 3
Wind turbine noise

This chapter gives an overview of the public concerns related to turbine noise. A summary of the research findings on the impact of noise on human health is provided. The current regulations and standards in effect to control noise are also discussed in detail.

3.1 Wind Turbine noise issues

The evidence based on the results of scientific research concerning the negative health effects of noise generated from wind turbines is inconclusive. The human perception of noise-related health effects is primarily based on opinion. There are specific sets of rules and standards to address the concerns of members of the public residing in residential dwellings in close proximity to wind turbines.

In Ontario, the provincial government has the most influence on the approval of wind energy projects. There is no national standard for wind turbine setback from dwellings or noise limits in Canada. Each province has established individual values of acceptable noise levels. The Ontario Ministry of the Environment Conservation and Parks (MOECP) has developed strict noise

guidelines for wind farms in order to protect public health and safety (Noise guidelines for Wind Farms, 2008). The current guideline states that there should be at least a 550 m setback of a wind turbine from a residence (Ontario Regulation, 2012). According to the MOECP guideline, the sound pressure level at the receptor cannot exceed 40 dBA. The decibel(dB) is the unit of sound pressure level. Due to large range of sound pressure human can perceive, it is expressed in a logarithmic scale. Human ear is more sensitive at certain frequency range (1kHz to 2kHz) (Kinsler, 1982). A-weighted decibel(dBA) is used to add weight to the sound levels at those frequencies. In this case, a receptor means 'any point on the premises of a person within 30 m of a dwelling'.

Health Canada is responsible for investigating public health related issues from radiating devices including noise radiation. A summary of their research and findings of effect of wind turbine noise on human health is discussed below.

3.2 Health issues and low frequency sound

The Government of Canada recently commissioned a study through the Ministry of Health to assess any causal relationship between exposure to wind turbine noise and adverse health effects. The Council of Canadian Academics assembled an expert panel of 10 medical practitioners and engineers to conduct this study. This section below provides a summary of the key findings and knowledge gaps highlighted by the panel in this report (The expert panel on Wind Turbine, 2015).

Insufficient Data

The Expert Panel on Wind Turbine Noise and Human Health (2015) has concluded that "there is not enough evidence to support a direct causal relationship between exposure to wind turbine noise

and reported adverse health effects". For example, health effects such as cardiovascular diseases can be linked to other secondary causes such as chronic issues with sleep deprivation or elevated level of stress. Therefore, further research is needed to understand how exposure to wind turbine noise affects sleep patterns or increases in stress levels in individuals. Available data on self-reported health problems was found to be insufficient. There have been no such studies conducted in Canada to be able to compare internationally the nature and extent of health problems in populations living in the near vicinity of a wind power generating facility. The report also concluded that exposure to wind turbine noise can cause annoyance which can lead to other health effects.

Characteristic of Wind Turbine Noise

One key characteristic of sound or noise generated from wind turbine is that the magnitude of the sound pressure level fluctuates as the wind speed varies at the height of the blade. Different sound pressure levels are established as guidelines in relation to the variation in wind speed. The variation causes periodic changes in noise pressure level from a swishing sound to thumping sound (Manwell, McGowan, & Rogers, 2010). The nature of the periodic fluctuation in amplitude of sound pressure levels is a phenomenon that warrants further study but will not be addressed in the present dissertation.

Technological developments

Technological advancements in relation to reduction or attenuation of noise generated from wind turbines mainly focus on three key areas. These three areas include methods to control different parts of the turbine during operation, geometry or shape of the blade and operating practices to curtail production in order to reduce excessive noise emissions under unfavorable conditions. One

such technique, known as the pitch control optimization (Manwell, McGowan, & Rogers, 2010), allows the operator to control the angle of the turbine blade along the long axis of the blade from the hub to the blade tip. Pitch control systems are used primarily to optimize power output by controlling mainly, the pitch angle of the blades. The same technology can be applied to reduce noise level over a range of wind speeds.

Modification of the shape of the turbine blade by installing serrations or brushes on the trailing edge helps to reduce aerodynamic noise (Oerlemans, 2011). This method is found to be quite effective during high wind speeds. The blade serrations can produce high frequency noise at low wind speed (Barone, 2011), but these frequencies are rapidly attenuated with distance from the turbine.

The third available option is to cut back production under meteorological conditions that are known to cause excessive noise based on previous knowledge of operation. Meteorological sensors such as LIDAR or SODAR can be used to monitor these conditions. Operating parameters can be adjusted accordingly for known conditions by reducing rotational speed or controlling blade pitch to reduce the noise level (Renewable UK, 2013).

Regulatory measures

Different levels of government including federal, provincial, and municipal regulate the wind energy sector in Canada. At the federal level, Health Canada has jurisdiction over measurement of noise and health effects established under the Radiation Emitting Devices Act (GoC, 2004). Sound waves emitted from wind turbines fall under this category. Provincial regulations govern the planning and approval of wind turbine projects. One such requirement is to conduct an environmental impact assessment for new wind energy projects under the provincial

environmental protection act. Local municipal regulations such as zoning bylaws and building permits set the requirements related to location of a turbine. Operating limits including noise limits and setbacks are established under the permit management process (Directive 038: Noise control, 2007). Noise limits guidelines are specified in provincial regulations (in Ontario, for example) in relation to background noise, wind speed, rural/urban areas, or time of the day. A setback is the minimum distance required between a turbine and the nearest residence.

Noise Monitoring

The expert panel (The expert panel on Wind Turbine, 2015) concluded that four key factors need to be considered in relation to measurement of noise. These four criteria include 1) background noise, 2) indoor noise measurement, 3) nighttime noise measurement and 4) measurement of periodic variation in amplitude of noise generated by wind turbines. It is important to measure background noise because sound perception is linked to the presence of background noise. Noise generated from a wind turbine located in a rural area will be more noticeable than it is in an urban setting where the background noise is high (Haugen, 2011) . Competing sound signals such as background noise conceal the hearing threshold. Variation in wind speed with height also creates similar effects. For example, a higher wind speed at the top of the swept area creates more significant noise than the lower wind speed closer to ground (Manwell, McGowan, & Rogers, 2010). As noted above, human perception of sound is dependent on the background noise in the surrounding area. Therefore, it is important to set noise limits based on background noise levels in urban and rural areas depending on the location of the wind turbine.

Indoor measurement of low frequency noise is relevant due to its association with the level of annoyance perceived by the receiver of sound. The loss of energy is less in the case of low frequency sound passing through walls, windows, and doors (Bullmore, 2011). The sound pressure

levels can vary in the same room depending on interference of high and low frequency noise levels (Findeis, 2004). Sometimes a computer-based simulation model can be used to measure indoor noise levels (Pedersen, 2007b). Existing methods to measure indoor noise levels are not adequate in terms of measuring the variation in sound pressure levels due to interference of sound pressure waves in low frequency.

Nighttime measurement of noise is also important for wind turbine noise. The wind turbines operate during nighttime and therefore generate noise perceived by the receiver. Other noise sources such as traffic noise subside during the nighttime. This condition makes the wind turbine noise more noticeable during the nighttime. Therefore, it is important to measure noise levels during the nighttime near the dwellings to be able to adequately assess human exposure to noise.

The sound generated from a wind turbine has some common characteristics. First, the wind turbine generates a range of noise ranging from high to low frequencies (Manwell, McGowan, & Rogers, 2010). The high frequency sound dissipates with distance and gets absorbed while passing through barriers such as walls, doors, and windows. It is the low frequency sound that is more prevalent in an indoor environment. Another key characteristic is that the sound pressure level varies depending on the wind speed. Current computer-based methods to predict noise pressure level at the receiver mostly rely on time dependent weighted average methods (Crocker, 2007). They do not adequately capture the periodic variation in amplitude of sound which changes from a swishing to thumping type of sound. Further refinement of the models is required to incorporate the common characteristic of sound generated from wind turbines in the form of mathematical equations.

3.3 Ontario Regulation

Wind farm planners in Ontario need to apply for a certificate of approval from the Ministry of Environment Parks and Conservation (MOEPC). They need to submit a list of documents to get approval. The list is available at "Interpretation for applying MOEPC technical publications to wind turbine generators." Recently there have been some amendments made to the Ontario Regulation 359/09. According to the new regulation effective May1, 2016 the proposed wind farms (excluding LRP I) need to add a turbine manufacturer specified positive uncertainty value to the sound power level of the wind turbine. Here LRP stands for "Large Renewable Procurement" which refers to projects that generate more than 500 kilowatts of electricity from wind turbines.

Another change in the noise guideline is reduction of ground factor value from 0.7 to 0.5. This parameterizes the level of sound that will be reflected/absorbed from the ground.

According to the World Health Organization (WHO) the noise level near to a dwelling should not exceed 50 dBA and inside a house the sound level should be below 35 dBA. During nighttime, the permitted sound level reduces to below 30 dBA (Ramani, 2007).

The Ontario regulations are as follows:

-In urban areas the sound pressure level should be below 45 dBA at wind speeds below 8 ms^{-1}.

Above 8 ms^{-1} sound pressure level can be above 45 dBA, but it should not exceed 51 dBA at

10 ms^{-1}.

-In rural areas at wind speed 6ms^{-1} the allowed sound pressure is 40 dBA. Above 6 ms^{-1} the maximum permitted sound pressure level increases and reaches up to 51 dBA at 10 ms^{-1} wind speed.

3.4 Alberta Regulation

In Alberta, every facility under the jurisdiction of the Alberta Utilities Commission needs to submit a noise impact assessment report according to AUC Rule 12 (AUC Rule 012 - Noise Control (draft Revised edition, March 2, 2011). According to the regulation, the facility should provide information comparing Cumulative Sound Level or CSL (*i.e.*, Sound Pressure Levels (SPL) that the facility generates combined with ambient sound level) to the Permissible Sound Level (PSL). The guidelines require that the CSL at 1.5 km from the facility fence line should not exceed the Nighttime Sound Pressure Level of 40 dBA L_{eq} when no dwellings are nearby.

One can determine the Permissible Sound Level from the Basic Sound Level (BSL). AUC Rule - 12 contains a table listing the Nighttime Basic Sound Levels based on the dwelling density and the proximity to the nearest highway. A value of 10 dBA is added to the Nighttime Sound Level to ascertain the applicable Daytime Sound Level. If the facility runs during wintertime, then a seasonal adjustment is required. An ambient monitoring adjustment is needed if the Basic Sound Level does not accurately represent the area's actual Ambient Sound Level. The facility owner may conduct a noise survey in pristine areas or where background noise is affected by non-energy related facilities. If the facility is active for less than sixty days, an additional adjustment is added. Usually, this adjustment is not required as most of the facilities operate throughout the year. The

Permissible Sound Level for any receptor is the summation of the Basic Sound Level, seasonal adjustment, ambient monitoring adjustment, and the adjustment based on activity duration, as summarized by the equation:

PSL = Nighttime Basic Sound Level + Daytime Adjustment + Class A Adjustment + Class B Adjustment

Once the Permissible Sound Level is established, the facility's sound level is computed at the most impacted dwelling or a surrogate receptor located at 1.5 km from the facility. The Cumulative Sound Level must include the Ambient Sound Level, sound from the existing/proposed facility, any current facility in the area and any approved, but not yet built facility. The Ambient Sound Level (ASL) can be estimated from the Basic Sound Level. This is usually 5 dBA less than the Basic Sound Level. It is then combined with the Predicted Sound Level from the facility to get the Cumulative Sound Level at the receptor. The Cumulative Sound Level is then compared with the Permissible Sound Level to ensure that the limit is not exceeded.

The SPL for day and night is described by a single value L_{eq} in dBA. Since the value can fluctuate when measured over a period of time, it is averaged over the interval of interest represented by L_{eq}, which stands for the average A-weighted equivalent SPL. While using L_{eq}, the duration should be mentioned in brackets. For example, if L_{eq} represents the A-weighted average SPL for 15 hours in the daytime, it should be written as $L_{eq}(15)$. The A-weighting is used to emphasize the frequencies around which the human ear is most sensitive, while C-weighting is used in combination with A-weighted values to determine the presence of low-frequency noise.

3.4 ISO-9613

The ISO 9613 Standard (ISO, 1996), Attenuation of sound during propagation outdoors – Part 2, presents an engineering method to calculate the attenuation of sound during outdoor propagation. This method can be applied to estimate sound pressure levels at receiver locations where the pressure levels are reduced due to various physical phenomena. During the propagation of sound, the sound pressure level can be reduced by physical factors such as a. geometrical divergence, b. atmospheric absorption, c. ground effect, d. reflection from surfaces, e. screening by obstacles. Algorithms have been developed to describe the method of sound attenuation for each of these physical phenomena. The method can predict both equivalent continuous sound pressure levels as well as long term averages based on a variety of meteorological conditions. It has been argued that the method can be applied to a variety of noise sources including stationary point sources. Environmental noise originating from ground-based sources such as road or railway traffic, construction activities or an industrial site requires modification of the source parameters. For example, industrial sites that can have multiple sources need to be divided into areas or sections. The sound pressure levels and direction of propagation at the center of each section are assumed to be representative of the entire section/cell.

The meteorological conditions to apply with this method also have been specified. It is assumed that sound propagation happens under moderate meteorological conditions, representative of a temperature inversion that is common during the nighttime. Temperature inversions over a water surface have been ignored. The method applies to wind directions within ± 45º from the centerline connecting the source and the receiver. The allowable wind speed limits are from 1 ms^{-1} to 5 ms^{-1} measured at a height of 3 m to 11 m above the ground surface.

In ISO-9613 a directivity correction factor can be added in the calculation of sound pressure levels at the receiver location. The correction factor addresses the deviation of sound pressure level along the direction of the receiver from the source in a situation where the sound from the source propagates in all directions.

The method for calculating ground attenuation during reflection by ground surfaces only applies to flat terrain that is either horizontal or with a constant slope. This method also includes attenuation of sound due to presence of barriers and obstacles.

Chapter 4
Atmospheric Sound Propagation

This chapter provides an overview of some basic properties of sound and a description of the process of sound propagation through the atmosphere as it applies to sound, or noise, associated with wind turbines.

4.1 Sound wave

A sound wave is the fluctuation of the pressure from its mean value in the medium in which it is traveling. A solid object, liquid or gas can act as a medium for the propagation of sound. The amplitude and frequency are two critical characteristics. The amplitude measures the increase and decrease in pressure from the average value of sound pressure. Similarly, the frequency measures the rate of pressure fluctuations in sound waves. One can use the amplitude and frequency of sound to express sound pressure as a function of time (Long, 2014).

The sound emitted by a source can generally radiate in all direction. The term "sound power" is used to quantify the amount of sound emitted from a source. The unit of sound power is the Watt (W).

4.2 Properties of Sound

The pressure variation of sound waves with a single wavelength or frequency has three main characteristics, i) intensity (amplitude), ii) wavelength (λ) and iii) frequency (f). The speed of propagation defines the relationship between the wavelength and frequency as per the equation, $c = \lambda f$. The distance between two identical points in adjacent cycles represents the wavelength of the sound wave. As shown in Figure 4.1, the wavelength is the distance between two successive crests or troughs in the pressure variations along the direction of sound propagation at a fixed point in time.

From a steady, continuous sound source the sound wave shape repeats itself. The number of cycles of the sound pressure wave propagating through a fixed point in the medium per second denotes the frequency of sound. A pure tone sound creates a single frequency wave. The amplitude or magnitude of the pressure wave represents the sound pressure or loudness of the sound. The intensity of sound, I_{av}, is defined as the square of the amplitude of the pressure wave divided by ρc, where ρ is the fluid density and c is the speed of propagation. It is measured in watts (Long, 2014).

The wave period is the time required by a sound wave to complete one cycle at a fixed point. Frequency, f, in cycles per second (Hertz, Hz), and period, T(sec) are related by the following equation.

$$f = \frac{1}{T} \qquad (4.1)$$

Frequency (*f*), wavelength (λ) and the speed of propagation (c) of a sound wave are related by the following expression.

$$c = f\lambda \qquad (4.2)$$

The amplitude and wavelength are shown in Figure 4.1. The amplitude of a wave is the distance to the highest point (crest) or the lowest point (trough) from the center line in a snapshot of p(x,t) for a plane harmonic wave.

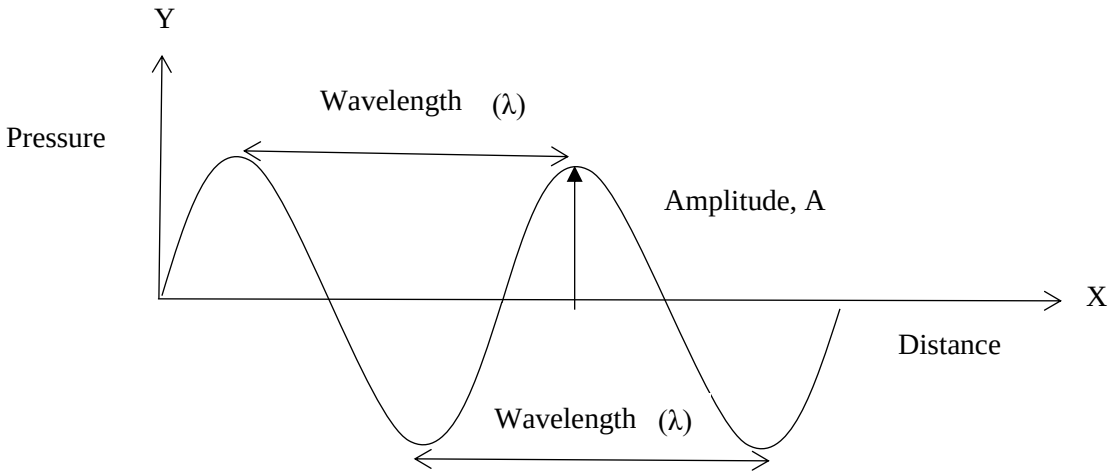

Figure 4.1: Wavelength, amplitude of a sound wave

4.3 Phase

The phase angle defines the position of a point on a waveform relative to an arbitrary starting point (time=0) and is measured in degrees or radians. In Figure 4.1 the waveform starts at the origin of the axis resulting in a zero-phase angle. If another wave begins before or after the origin, then a phase difference will exist between them.

The phase of a sound wave is a valuable property to determine pressure levels at a receiver location. The sound waves received at the receptor from a wind turbine, for example, may not be all in the same phase. A phase difference may exist between waves that reach the receiver directly and waves reflected from the ground surface. The frequency and time required to reach the receiver determine the phase of a waveform. Waveforms that are in phase with the fundamental wave amplify the intensity of the combined waveform. This property of sound can occur in computing sound pressure levels at receiver points where direct rays are combined with those reflected by the ground surface.

The equation of pressure(p) for a plane sound wave that starts at time, t=0 and travels in the x direction at position, r can be written as (Salomons, 2001),

$$p(r,t) = Asin(kx - \omega t) \qquad (4.3)$$

Here, k is the wave number, ω is the angular frequency and (kx-ωt) is the phase of the wave.

4.4 Sound wave spectrum

Most sounds are not monochromatic (pure tones) but contain multiple frequencies. A spectrum of sound can be expressed in the form of a relationship between the energy and frequency of the sound wave form. In the case of a single frequency signal, the spectrum shows energy for one frequency. On the other hand, in the case of a complex wave form, the power spectrum shows a dependency of the amplitude squared or energy (usually in dB) on the frequency or wavelength present in that wave form. Here, dB is the unit of sound pressure level and sound power level. Decibel (dB), to be defined in 4.7, is often used to express any quantity such as sound pressure relative to a reference value using a logarithmic scale. Noise generated by a wind turbine is characterized by a range of different frequency sound waves. A microphone can be used to measure sound pressure levels at the receiver location with respect to time. These sound pressure levels recorded at the receiver location can be analyzed to obtain spectra.

Machinery components such as gear box, cooling fans, *etc*., can generate sharp spikes in sound pressure level in the low frequency spectrum (Hubbard, 1990). The wind turbine noise spectrum also depends on several important factors including rotor diameter, blade tip speed and power output. Wind turbines with the same design parameters produce similar noise spectra.

4.5 Frequency bands

The measurement of sound pressure level generally utilizes two types of frequency bands (ISO 266: Acoustics Preferred frequencies for measurements, 1976). The Octave and one third octave

bands frequently appear in methods used to measure sound pressure levels. For Octave bands the 'preferred' center frequencies are at 16, 31.5, 63, 125, 250, 500, 1K, 2K, 4K, 8K, and 16k.

The calculation of the sound field is often carried out with these center frequencies. An octave band consists of three one third octave bands. Each one third band has a center frequency equal to $2^{-1/3}\, f_C$, f_C, $2^{1/3} f_C$ where f_C is the octave band center frequency (Salomons, 2001).

Sound pressure level is measured for a range of frequencies and weighting can be applied to assign more value to the desired frequency range. A, B, C, D and Z weightings (Long, 2014) are developed to act as a filter to add more weight to the desired frequency depending on the application. The A weighting is frequently used because it mimics the frequency response of the human ear. A-weightings for octave bands are shown in the Table 4.1.

Table 4.1: A-weighting (Long, 2014)

Octave band center frequencies (Hz)	16	31.5	63	125	250	500	1K	2K	4K	8K	16K
A-weighting (dB)	-56.7	-39.4	-26.2	-16.1	-8.6	-3.2	0	1.2	1	-1.1	-6.6

The calculation of sound pressure levels for noise generated from wind turbine uses the frequencies of the octave band as basis. The values presented in Table 4.1 are then added to the measured sound pressure level at the receptor to get the A-weighted value.

4.6 Loudness

The amplitude of a sound wave determines loudness of sound. Loudness is a subjective term as it depends on human perception of sound, which can vary from one person to another (The expert panel on Wind Turbine, 2015). The loudness of sound is also related to frequency and the sound pressure level. A sound with lower frequency and higher sound pressure level can produce the same level of loudness as a lower sound pressure level and higher frequency. The loudness of sound at the same pressure level increases with the f Similarly, the loudness of sound at the same frequency increases as the sound pressure level increases (Long, 2014).

4.7 Sound pressure level

The term "power" is used to express the rate at which energy is being transferred in unit time. The unit of power is a Watt or Joule per second (Js^{-1}). Sound power (in Watts) is the rate at which sound energy is emitted from a sound source per unit time. Sound pressure is the difference between the instantaneous pressure and the average pressure at some point in the atmosphere (Salomons, 2001). Sound pressure level is used to define the loudness of any source. As noted above, the relation between the amplitude of sound and human perception of sound is not linear and a logarithmic scale is used to represent both sound pressure level and sound power level.

Sound power level can be defined by

$$L_w = 10log\left(\frac{W_{av}}{W_0}\right) \qquad (4.4)$$

Here W_0 is a reference power. It is equal to 10^{-12} W. The unit of sound pressure level is the decibel (dB).

If P is the sound pressure at some point, the sound pressure level can be expressed as

$$L_p = 10log\left(\frac{P^2}{P_{ref}^2}\right) \qquad (4.5)$$

Here P_{ref} is the reference pressure and is equal to 2×10^{-5} Pa. This value corresponds to the lowest sound pressure that the human ear can typically perceive (Kinsler, 1982). The range of frequency of audible sound to humans is between 20Hz and 20 KHz. Similarly, the range of sound pressure level of audible sound starts at 0 decibel(dB) and can increase up to 110 decibels or higher. Sounds with pressure levels greater than 110 decibels can result in permanent hearing loss.

In a homogeneous, stationary-medium a sound wave emitted from a point source spreads spherically in the medium. The relation between the intensity, I and power of the source, W can be written as

$$I = \frac{p^2}{\rho c} = \frac{W}{4\pi r^2} \qquad (4.6)$$

$$\frac{p^2}{P_{ref}^2} = \frac{W}{W_{ref}} \times \frac{1}{r^2} \times \frac{\rho c W_{ref}}{4\pi P_{ref}^2} \qquad (4.7)$$

Taking logarithms of both sides of the above equation and multiplying by 10 yields

$$L_p = L_w - 20\log(r) + 10\log\left(\frac{\rho c W_{ref}}{4\pi P_{ref}^2}\right) \qquad (4.8)$$

In an inhomogeneous medium, atmospheric absorption, refraction due to wind gradient, ground absorption and irregular terrain effects are taken as possible sources of sound energy loss. These losses are called “excess attenuation”, over and above the spherical spreading. The loss due to spherical spreading is described in detail in Chapter 6. The loss due to spherical spreading occurs

due to distance travelled by the sound in the medium. If the medium is moving at speed U relative to the source there can be complications in the definition of r, but most discussions ignore this if U<<c (c=sound speed, ms^{-1}).

The equation for the sound pressure level at the receptor is then

$$L_p = L_w - 20\log(r) - A_{ground} - A_{refraction} - A_{absorption} + 10\log\left(\frac{\rho c W_{ref}}{4\pi P_{ref}^2}\right) \qquad (4.9)$$

Here

L_p = sound pressure level (dB)

r = distance from source to the receiver (m)

A_{ground} = attenuation due to ground absorption (dB)

$A_{refraction}$ = attenuation due to refraction(dB)

$A_{absorption}$ = attenuation due to atmosphere absorption(dB)

ρ = air density (kgm^{-3})

c = sound speed (ms^{-1})

W_{ref} = $1*10^{-12}$ W

P_{ref} = 20 μPa

Lw is the sound power level of the source. It is assumed that only spherical spreading occurs within 1 m from the source. The relationship between sound power level of the source and sound pressure level at 1m distance from the source can be expressed by,

$$L_p = L_w + 10log\left(\frac{\rho c W_{ref}}{4\pi P_{ref}^2}\right) \qquad (4.10)$$

4.8 Wind turbine sound characteristics

Noise generated by a wind turbine can be categorized in two types 1. Aerodynamic noise 2. Mechanical noise. The main sources of mechanical noise of the turbine are gear box, bearings, and accessories.

The aerodynamic noise can be narrow band or broad band. Narrow band noise is generated when the blade of the wind turbine crosses the support tower. The tower obstructs the flow of the wind hence there is a velocity deficit. It creates a fluctuation in the load on the turbine blade and generates acoustic pulses of short duration. This type of sound has a spectrum that contains pure tone of frequency equal to the rotation per minute multiplied by the number of blades and its integer harmonics. The directivity pattern is similar to an acoustic dipole (Hubbard, 1990) . Downwind rotor turbines which are not very common usually exhibit this kind of noise.

Broadband noises generally have a higher frequency range, greater than 100 Hz, and are mainly generated from the interaction between a moving blade and its boundary layer (Hubbard, 1990). This type of noise is subdivided into five groups as follows (Brooks, 1989).

1. Turbulent boundary layer trailing edge noise (TBL-TE)
2. Laminar boundary layer vortex shedding noise (LBL-VS) noise
3. Separation stall noise

4. Tip vortex formation noise

5. Trailing edge bluntness vortex shedding noise.

Turbulent boundary layer noise is generated at high Reynolds number from turbulent flow inside the boundary layer of the blade. At higher Reynolds number turbulent flow passes over the trailing edge forming wakes which contributes to noise generation (Brooks, 1989).

When flow of a fluid (air or water) is impeded by any bluff body an oscillating flow can be generated in the wake of the body. At low Reynold number, a laminar boundary layer exists over the airfoil. Interaction of the airfoil and the vortex shedding generated at the wake of the airfoil produces laminar boundary layer vortex shedding noise (LBL-VS) noise.

When air flows above the airfoil, a positive or negative pressure gradient can form above the turbine blade surface. A positive pressure gradient will oppose the wind flow and might separate the boundary layer from the blade. At higher angles of attack, a positive pressure gradient combined with surface friction may give rise to the boundary layer detaching from the surface of the airfoil. This condition is known as "stall". Separation stall noise is induced due to the separation of the flow and the turbine blade (Manwell, McGowan, & Rogers, 2010).

Tip vortex noise is produced due to interaction between the blade tip and the turbulence around it. Another kind of noise is created when blunt edge of the blade interacts with the vortex shedding in the wake of the previous turbine blade to pass through that patch of air. It is known as trailing edge bluntness vortex shedding noise (Brooks, 1989).

Apart from the regular noise from a wind turbine mentioned above, a stationary listener can hear a sound that fluctuates periodically. This type of variation is characterized as a 'swishing' or thumping sound. This noise is termed amplitude modulation of sound. Amplitude modulation can

be described by two parameters, modulation depth and frequency of modulation (The expert panel on Wind Turbine, 2015). Modulation depth is the distance between the highest (crest) and lowest point (trough) on the modulated sound. Frequency of modulation is the frequency at which this amplitude variation occurs. This is related to the rotational speed of the turbine blade. Amplitude modulation can be of two types, Normal amplitude modulation (NAM) can occur due to the interaction of the wind with the trailing edge of the blade which is also described as a “swishing” sound. The Enhanced or Other amplitude modulation (OAM) is referred as “thumping” sound. Ongoing research is being conducted to find out the reason and mitigation strategies for this latter kind of noise. Renewable UK led a study in two phases to investigate OAM (Renewable UK, 2013). The results of the second phase indicate that occurrence of OAM is related to the presence of turbulence or high wind speed. This type of noise can have modulation depth of 10dB at low frequencies (1 to 2 kHz) (van den Berg & Bowdler, 2011).

Chapter 5

Sound propagation model background

The propagation of sound in the atmosphere can be explained by different theories. In wave acoustics sound is considered to be a wave. When a sound wave propagates, it changes the properties of the medium. It displaces air particles in time and space. Air density and pressure also fluctuate. Sound propagation can be expressed by a wave equation relating the changes in all these parameters. In this chapter properties of a monopole source in one dimension (*i.e.*, a plane wave) will be explained followed by some discussion on ray theory in three dimensions. Previous studies on sound propagation modelling will also be presented at the end.

5.1 Simple sources, plane and spherical waves

When a sound wave is emitted from a source the path along which it will travel depends on the medium. Sound travels in every direction in the atmosphere. In some cases, sound only travels in one direction depending on the geometry of the source and the medium. For example, in a pipe or duct sound effectively propagates in one direction through the duct and a plane wave model is appropriate. A sound wave propagating through a medium generates fluctuation in physical

properties like pressure, density, and velocity. The one-dimensional wave equation that relates the variation of pressure (p) fluctuation in time and space can be written as (Kinsler, 1982),

$$\frac{\partial^2 p(x,t)}{\partial t^2} = c^2 \frac{\partial^2 p(x,t)}{\partial x^2} \qquad (5.1)$$

Here, the sound speed (c) is given by

$$c = \frac{\gamma p_0}{\rho_0} \qquad (5.2)$$

For typical atmospheric conditions where the specific heat ratio, $c_p/c_v = \gamma = 1.4$, the pressure, p_o=1.13*10^5 Nm^{-2} and air density, ρ_0 =1.18 kgm^{-3} then, the sound speed, c is 344.2 ms^{-1} in the air.

The ideal gas law states the relation between pressure (p) and temperature (T) of an ideal gas by the following equation

$$P = \rho R_{specific} T \qquad (5.3)$$

Here $R_{specific}$ is the specific gas constant ($Joulemole^{-1}$ $^oK^{-1}$) and ρ is the density of gas. From Equations 5.2 and 5.3 we get,

$$c = 20.05\sqrt{T_C + 273.2}\ ms^{-1} \qquad (5.4)$$

Where T_C is the air temperature in degree Celsius.

The speed of sound is different in different mediums. Sound travels faster in liquid than in gas and fastest in a solid. Sound speed in different mediums depends on their properties (Lighthill, 1978).

In the ray model developed here, sound is generated from a point source and radiates equally in every direction. This type of source is usually known as “a simple source” or “a monopole source”. In this section characteristics of a monopole source will be discussed.

An expression for a velocity potential, φ, which varies only radially in space and with time can be written as,

$$\varphi = \varphi(r, t) \qquad (5.5)$$

where, r is the distance from the source in all direction and t is the travel time. The radial velocity is $\partial\varphi/\partial r$ and taking the Laplacian of Equation 5.5 gives

$$\nabla^2\varphi = r^{-1}\frac{\partial^2(r\varphi)}{\partial r^2} \qquad (5.6)$$

The wave equation 5.1 can then be written for a monopole source as

$$\frac{\partial^2(r\varphi)}{\partial t^2} = c^2\frac{\partial^2(r\varphi)}{\partial r^2} \qquad (5.7)$$

A general solution of equation 5.7 can be (Lighthill, 1978)

$$\varphi = \frac{f\left(t-\frac{r}{c}\right)}{r} + \frac{g\left(t+\frac{r}{c}\right)}{r} \qquad (5.8)$$

Here, $f\left(t-\frac{r}{c}\right)$ is an outgoing wave and

$g\left(t+\frac{r}{c}\right)$ is an inwardly travelling wave,

The term, 1/r represents the spreading of the sound wave after emission from the source. If the shape of the sound source is a sphere with radius r, the "volume outflow from the center at time, t is."

$$m(t) = 4\pi r^2\frac{\partial\varphi}{\partial r} \qquad (5.9)$$

Now, the sound pressure is the measure of the deviation of pressure from its mean value at some point in the atmosphere. The measure of fluctuation from the mean atmospheric pressure is (Lighthill, 1978),

$$p - p_0 = -\rho_0 \frac{\partial \varphi}{\partial t} \qquad (5.10)$$

From equation 5.9 and 5.10 the sound pressure can be written as

$$p - p_0 = \frac{\dot{q}\left(t - \frac{r}{c}\right)}{4\pi r} \qquad (5.11)$$

Here, $q(t) = \rho_0 m(t)$ is the rate of mass outflow from a simple source. It is also known as the strength of a monopole source (Lighthill, 1978).

The results above are for ideal conditions of spherical symmetry and uniform, c, in an unbounded stationary medium and a stationary sound source. They do however provide the background to the ray theory that will be used in the model developed in this dissertation.

5.2 Ray theory

In ray theory our sound pressure calculation follows three steps. They are,

- Numerous rays are emitted from the source. The ray path for each of them is calculated between the source and a receiver plane or surface.
- Various losses are calculated along each ray and deducted from the source power level to get sound pressure level at the receptor.

- Sound pressures from each ray that reaches the receiver are combined to yield total sound pressure at locations on the receptor plane or surface.

Ray theory is used in this study to develop a mathematical model of sound wave propagation from a source, such as a wind turbine, in the atmosphere. A basic concept of the model is that the velocity of a ray in a moving medium is the vector sum of the medium velocity and the sound speed along the ray direction, normal to the wavefront. The model considers the source of the sound to be monopole and generating a spherical sound wave in all directions. The amplitude of the spherical wave decreases as the wave propagates away from the source and the reduction is inversely proportional to the square of the distance travelled. In a real atmosphere additional loss occurs due to atmospheric absorption. A layered atmosphere can be used where sound speed, temperature and wind speed change with height. Due to these factors and multiple reflections from the ground, multiple rays can arrive at the same receptor location and the phase difference needs to be considered during summation of the sound levels. Sound speed and wind variations in the air affect the ray trajectory and can cause diffraction variation along the ray. All of these variations during the propagation of sound are calculated and integrated in the model. The sound propagation model and results will be discussed in detail in the following chapters. A brief summary of the models that have been developed earlier based on ray theory are presented in the next section.

5.3 Previous studies

Prospathopoulos and Vobutsians (2007) developed a model based on Ray theory to calculate sound pressure level for both a single wind turbine and a wind park. The model included ground and

atmospheric absorption, wave refraction, diffraction, and atmospheric turbulence. The results from the model were compared with data from field measurement.

Chessell (1977) and Nicolas (1985) approximated formulas to compute ground impedance. That model calculates ground impedance in terms of specific flow resistivity but in some cases the ground surface was considered to be constituted of multiple layers of different materials. In that case impedance was calculated separately for each layer and an equivalent impedance was determined for ground impedance. The model was applied to five individual wind turbines and one Wind Park. Different values of flow resistivity were chosen depending on the nature of the terrain. Good agreement was found between the result predicted from the model and field data for flat terrain. However, for non-flat topography comparison was satisfactory for frequencies higher than 200Hz but for lower frequencies the model under predicted the sound pressure level.

Ray theory has been applied to calculate sound pressure level due to emission of low frequency noise from a wind turbine by Hawkins (1987). A model "MEDUSA" (Foreman, 1983) which was originally developed for ray tracing in an underwater environment was modified to fit the above ground sound propagation. The model uses a differential equation that gives position of a ray above the ground as a function of range. The model included loss due to ground impedance, reflection from the ground, and refraction of sound rays. As the model was used only to predict low frequency noise atmospheric absorption was ignored. The results of the model were used to explain field measurement data. The author concluded that the ray model could successfully predict sound pressure level in the downwind direction but was not suitable for the upwind field. The reason behind this was stated as due to formation of caustics. Caustics occur when separation between two adjacent rays is diminished and they intersect with each other. Therefore, a recommendation

was made to include caustic corrections in the model, but the model ‘Medusa” does not use any correction.

Evans and Cooper (2012) collected noise data from six measurement sites during a field study. Four noise prediction models for wind farms were selected and collected data were compared against the calculated results from the models. Comparisons were also made among those four models to see which model gave the most accurate result. The sites selected for noise measurement included varying terrain features such as flat, steady downward slope, and concave downward slope. The models selected for predicting noise level were ISO 9613-2 (ISO/DIS 9613-2: Attenuation of sound during propagation outdoors- Part 2: General method of calculation, 1996), CONCAWE (Manning , 1981), NZS 6808:1998, Nord 2000.

Nord 2000 is an outdoor sound prediction model which can be applied to various types of sources such as rail, road, industry, airports, wind turbines etc. The calculation is carried out based on geometrical ray theory. According to this model, a sound ray propagates in a straight line in the absence of refraction in the atmosphere. Strong refraction cases are included by using appropriate wind and sound speed profiles. Loss due to spherical spreading and air absorption are integrated in the model. Reduction of sound due to the presence of different types of acoustic screening is computed using a geometrical theory of diffraction. The model also considers propagation over irregular terrain and the terrain shape is approximated by an array of line segments (Nord2000:Comprehensive outdoor sound propagation model. Part 2: propagation in an atmosphere with refraction, Delta; Bateman, 1914-05).

CANCAWE stands for conservation of clean air and water in Europe. This model was originally developed for use in the petroleum and petrochemical industries but later modified to be used for all types of facilities (Marsh, 1982). The model predicts sound pressure levels at a receiver location

by computing various types of losses in the atmosphere and deducting them from the source power level. It includes loss due to geometric spreading, air absorption, ground effect, meteorological effects, source height effects, barriers and in plant screening effect (Bies, 2018).

NZS 6808:1998 is a standard for suitable methods to measure sound from wind turbines. It was originally composed in 1998 but has been modified after several revision. In its 1998 version, it computes sound pressure level by considering only spherical spreading and atmospheric absorption and only at 500 Hz (Bies, 2018).

It was found that none of the models accurately calculated sound pressure level for each measurement site (Evans & Cooper , 2012). One of the main reasons for this inaccurate prediction was taken to be the effect of topography on the sound pressure level. The authors also pointed out some other uncertainties that could be the potential sources of error. Those sources are the presence of background noise, wind shear and wind speed variation across the wind farm, or improper selection of sound power level. One suggestion for reducing background noise was to deduct the pre-construction noise level from the after-construction noise data. But studies show that this approach also incurs error as sound measurement sites for pre- and post-construction periods could be different and background noise is also not constant over the time. To eliminate this problem the measurement sites for their study were chosen where only noise level data strongly governed by wind speed were dominant. At the measurement sites where a downward slope exists between the base of the turbine and the receiver location the models under predict the sound pressure level. Several correction factors were developed and applied to the difference in the measured and predicted sound levels. One correction factor was calculated by dividing the cross-sectional area of the wind farm site by the area under the line connecting the turbine base and receiver location. But none of them were useful for all the models for every site. It was also recommended to collect

more noise data over varying terrain so that an accurate correction factor can be developed to include in the noise prediction models.

Prospathopoulos *et al* (2007) used the models: IEA (Expert Group study on recommended practices for W/Ts and evaluation. 4. Acoustic measurement of noise emission from W/Ts (3rd edn), 1994), NORD2000, ENM (Tonin, 1985) , CONCAWE in their project for different sites and measured noise data at those locations. The comparisons between the recorded data and model results showed that the all the models provide satisfactory results for regular flat terrain. The CONCAWE and ENM models provide the best data for irregular surfaces.

Modelling of both flow and noise issues in complex terrain wind farms developed at the Danish Technical University (DTU) for use with High Performance computers (HPC) have been discussed by Shen *et al* (2019) and Barlas *et al* (2017). The models calculate annual wind power output as well as sound pressure level at a receiver location in three different stages. In the first step, the power output of each turbine in the wind farm in calculated. To do this, the rotor is considered as a circular disk of zero thickness. This is known as the actuator disc method that virtually models the wind turbine. The flow field around the turbine blade is simulated by combining the Reynold's Averaged Navier Stokes Equations and the Actuator disc method. The output of this simulation is fed into the next stage that calculates noise source for each blade. The noise source model is based on the blade element (BE) method that was proposed in the work of Brooks *et al* (1989). According to the BE method, the wind turbine blade is divided into small segments. The noise from various mechanisms is computed for each blade section. The noise level is then integrated along the entire blade to give the total sound power level. The last step of the model is simulation of sound propagation over flat or irregular terrain from a wind farm to any receiver. The Generalized Terrain Parabolic equation (GTPE) method described by Sack and West (1995) is used to model sound

propagation between the wind farm and the receiver. This is based on a 2-D parabolic equation approach and has some limitations in a fully 3D situation, as discussed above in section 1.2.

DTU model flow simulation results are compared with measured data over a single hill for the widely used Askervein study described by Taylor and Teunissen (1987) and related papers. This field study was conducted in 1983 along a hill in Scotland where wind speed was recorded using 35 wind masts. The data of the field study are used to validate the result of the DTU CFD simulation, see also Cavar *et al* (2016). One comment would be that the DTU model does not appear to include Coriolis forces (Shen *et al* (2019) Eq 2, although they could potentially be included as a part of their f_{ext}) while Weng and Taylor (2011) found that their NLMSFD model performed better for Askervein with Coriolis terms included. Shen *et al* (2019) also report good agreement from another field study for a wind farm when comparing energy yield from the model. The wind farm was on an uneven terrain and had 25 wind turbines. In their field study wind speed was measured using cup anemometers at 30 m, 50 m, 70 m and wind vanes at 30 m, 60 m. Their Ellipsys 3D CFD (Computational Fluid Dynamics) model was run for twelve 30º sectors. In most of the cases the result from the model was in good agreement with the field measurement. Sheng et al note that computation times were 3-5 h with 300 processors for a single flow direction using 67.7×10^6 grid points. This seems high and the CFD model does not include the effects of thermal stratification. Multi-purpose CFD models are not always the best way to model the atmospheric boundary layer.

Turning to DTU sound level computations reviewed in Zhu *et al* (2019), these are coupled with a noise source model and the flow model to determine impacts of wind speed variations. Flat terrain results are discussed by Barlas *et al* (2017). In Shen *et al* (2019), the relative sound pressure level computed by the model over a 2D Gaussian hill is compared with the same case from a previous

result in Salomons (2001). The hill is 10m high and the surface flow resistivity is 200 kPa.s.m^{-2}. A downward refracting atmosphere is simulated with a logarithmic sound speed profile. The output from the model matches the result from Salomons (2001). In addition, the DTU approach is used to generate a noise map around a wind farm that has 25 wind turbines under four different circumstances. In the first two cases, a flat terrain is assumed. In the third case a noise map is generated over an uneven topography. In the last case the flow simulation by CFD is combined with varying topography. The noise level is higher in the downwind direction than the upwind. Downwind from the turbine, due to wake effects, wind speed decreases and this can affect the sound propagation path. The DTU PE sound propagation model is well tested and reported but a ray model is a good alternative and is investigated in this thesis.

A field study was conducted in Canada by Keith *et al* (2016) to validate sound power measurement data from a wind turbine manufacturer. For this study, two relatively flat regions were chosen in Southern Ontario and Prince Edward Island. There were 21 wind turbines from ten different models with hub heights between 78 and 80 meters. The microphones were placed on the ground on top of a plywood disk with a windscreen. The primary windscreen had a water-resistant spray put on it for weather proofing. A thin polyethylene cover was put on the microphone and pre-amplifier. Data collected during rainy days were excluded from further analysis. Background noise was recorded by turning off the nearest wind turbine over a short period of 15 min with the respective wind speed. Measurements above 3.15 kHz were not done as research shows higher frequencies contribute less than 0.5 dB to the cumulative sound power level (Keith & Feder Katya, Wind turbine sound power measurements, 2016b). The data were collected for low frequencies to get the C-weighted sound power level. A meteorological station was set up far from the microphone to record wind speed, wind direction, temperature and humidity, atmospheric

pressure, and wetness. Seven wind turbines had sensors at their nacelle to measure wind speed, direction, power output and rotor speed at a 10-minute interval. The wind speed of 8 ms^{-1} at 10m height was used to compare the sound power level supplied by the manufacturer and the SPL from measurement. From the comparison, a standard deviation of 2 dB is estimated.

In another field study by Keith *et al* (2016) sound pressure level was measured from 399 wind turbines at 1238 dwellings around them. The turbines are in Southern Ontario and Prince Edward Island in Canada. The sound pressure level is calculated with the software CadnaA (Computer aided noise abatement is a commercial software developed by DataKustik) which uses the ISO-9613 method. A Swedish software (SEPA) was used to compare the result. SEPA is written using Microsoft excel software to simulate sound propagation (Keith & Feder, 2016a). The sound power levels for the turbines were collected from the manufacturers. Most of the turbines had an 80m hub height and the rotor diameter was 80m. The terrain around the turbines was mostly flat with some trees with height ranging from 10 m to 30m. the wind speed was 8 ms^{-1} at 10m height. Results from both models showed similar output. The sound pressure level was calculated using A and C weighting. There was a strong co-relation between the SPL computed by these two-frequency weighting. The ambient noise level without the presence of wind turbines was also determined in this study. Ambient noise refers to the sound level from the nature and manmade sources excluding any energy industry. The result showed that sometimes the ambient sound level exceeded the wind turbine noise.

5.4 Numerical methods in sound propagation

Several methods have already been developed based on numerical solution techniques of the Helmholtz equation to predict sound pressure levels (Salomons, 2001). Three such methods are discussed in this section. Discussion topics include the mathematical equation used in the model, the computational technique, and how the medium and source are set up in the model. The purpose of this discussion is to find out the similarities and differences between the ray model discussed in this dissertation and the other numerical methods in relation to the discussion topics.

The alternative methods are as follows,

Fast Field Program Method (FFP)

Crank-Nicholson Parabolic equation method (CNPE)

Green's function parabolic method (GFPE)

In the FFP method the solution is derived in the frequency domain. In the frequency domain, the wave function is expressed with respect to frequency to represent variation over a range of frequencies. The atmosphere is divided in multiple layers extending vertically. The wave number can be viewed as changes in wave cycles per unit distance. The wave number is evaluated in the vicinity of each layer and the value remains constant throughout that step. The sound field is calculated in the frequency domain. The solution is again transformed back in the spatial domain by inverse Fourier transform. The original wave function is reconstructed by using known values of wave frequencies and phases. The limitation of this method is that any range dependent (function of distance) profile cannot be integrated into the model as calculation takes place in the wave number domain (Salomons, 2001).

The Parabolic equation (Salomons, 2001) method is developed based on the two-dimensional Helmholtz equation. The Helmholtz equation is,

$$\frac{\partial^2 q}{\partial x^2} + \frac{\partial^2 q}{\partial z^2} + k^2 q = 0 \qquad (5.12)$$

Here q is a function of position in the atmosphere and can be related to complex pressure amplitude, p(x,z) by

$$q = p(x,z)\exp(ik_0 x) \qquad (5.13)$$

The wavenumber k is equal to ω/c where ω is the angular frequency and c is the sound speed. The Helmholtz equation can be derived from the wave equation by using the separation of variable technique. The Helmholtz equation is independent of time and is widely used as a basis of sound propagation models.

Replacing q in equation 5.12 by 5.13 yields

$$\frac{\partial^2 p}{\partial x^2} + 2ik_0\frac{\partial p}{\partial x} + \frac{\partial^2 p}{\partial z^2} + (k^2 - k_0^2)p = 0 \qquad (5.14)$$

Neglecting the term $\frac{\partial^2 p}{\partial x^2}$ in equation 5.14 to make it parabolic we get

$$2ik_0\frac{\partial p}{\partial x} + \frac{\partial^2 p}{\partial z^2} + (k^2 - k_0^2)p = 0 \qquad (5.15)$$

This is the narrow angle parabolic equation.

In the PE method the atmosphere is structured as a grid. Here x and z define horizontal and vertical position on that grid. The position of the sound source can be defined by a suitable value of x and

z. The source wave is considered to be emitted from this point. The sound pressure can be evaluated at any point on the grid by solving equation 5.15.

Boundary conditions to satisfy the ground surface and the topmost layers are carefully chosen. A layer at the top of the grid is designated to prevent reflection of the sound wave to the ground. Sound waves that reach this layer are gradually absorbed and do not reflect towards the computation zone.

The GFPE method uses the same equation as the CNPE method but the computation is performed faster. In the CNPE method a limitation applies in selecting horizontal and vertical grid spacing. Ideally the spacing should not exceed this limit. The same restriction applies for vertical grid spacing in the GFPE method. But horizontal grids do not need to be coarser and a large gap between two adjacent grids can be chosen. So, the computation time is reduced in the GFPE method. In the three-dimensional GFPE method the sound field varies with azimuth angle as well. If φ is the azimuth angle, then sound pressure is calculated in a pie shaped area where φ ranges anywhere between 0^{o} to 360^{o}. The PE method is not suitable when the elevation angle of the sound wave exceeds 70^{o} (Salomons, 2001).

There is no sound wave equation used in the Ray theory method. Sound waves are presented as a combination of rays. The sound pressure level at the receiver location is estimated by tracking the rays emitted from the source. The wind speed and temperature vary with height. The medium can be inhomogeneous which allows calculation of various propagation losses due to reflection, refraction, and atmospheric absorption. It is relatively easy to integrate the propagation losses in calculating the sound pressure levels at the receiver. The method is also not dependent on frequency of sound sources which is the case for the FFP method. No initial function is required to represent the sound source in the model. The ray theory can be applied in the case of both flat

terrain as well as irregular terrain. One of the limitations of the ray model is that computation time is relatively higher as numerous sound ray can be emitted from the source. Another concern is if the receiver is a point not a single ray hits the receiver. In that case an interpolation technique can be used to predict sound pressure level at the desired receptor location.

Chapter 6

Ray Theory and applications

This section gives an overview of the ray theory and how the model in this dissertation is set up in relation to the source, medium and characteristics of the terrain. The determination of sound pressure levels estimated at the receiver location using the ray tracing equations are explained. The effects of terrain irregularities and propagation losses on sound pressure levels estimates are discussed.

6.1 Ray theory

In ray theory the sound source is considered as a combination of numerous rays emitted in all directions. Ray tracing equations are solved to connect the rays between the source and the receivers.

A model based on ray theory has been developed to calculate the trajectories of all sound rays emitted from a source such as a wind turbine. After sound is emitted from the source it travels in the medium as a wave. Wave front is a term that is used to describe the position of a sound wave at a given time. All the points on the wave front have same phase. In Figure 6.1 a wave front **$\tau(x)$**

at time t, $\boldsymbol{\tau}(\boldsymbol{x}) = t$ is shown at position A, as described by Pierce (1981). The wave front propagates in the same direction as the sound rays and after Δt of time the wave front moves to position B.

The direction of wave propagation is given by a vector **n** which is normal to the surface of the wave front. P is a point on the wave front which is also moving with the wave front (Pierce, 1989).

The speed of the wave front is c(x,t) and the medium the wave is moving through has a velocity of **v**(x,t). After Δt of time point P will still be on the wave front if it moves with the sum of the velocity of sound and the velocity of the medium (Pierce, 1989). If $\boldsymbol{x_p}$ is the position of the point P, then its velocity can be expressed by

$$\frac{d\boldsymbol{x_p}}{dt} = \boldsymbol{v}(\boldsymbol{x_p}, t) + \boldsymbol{n}(\boldsymbol{x_p}, t)c(\boldsymbol{x_p}, t) \qquad (6.1)$$

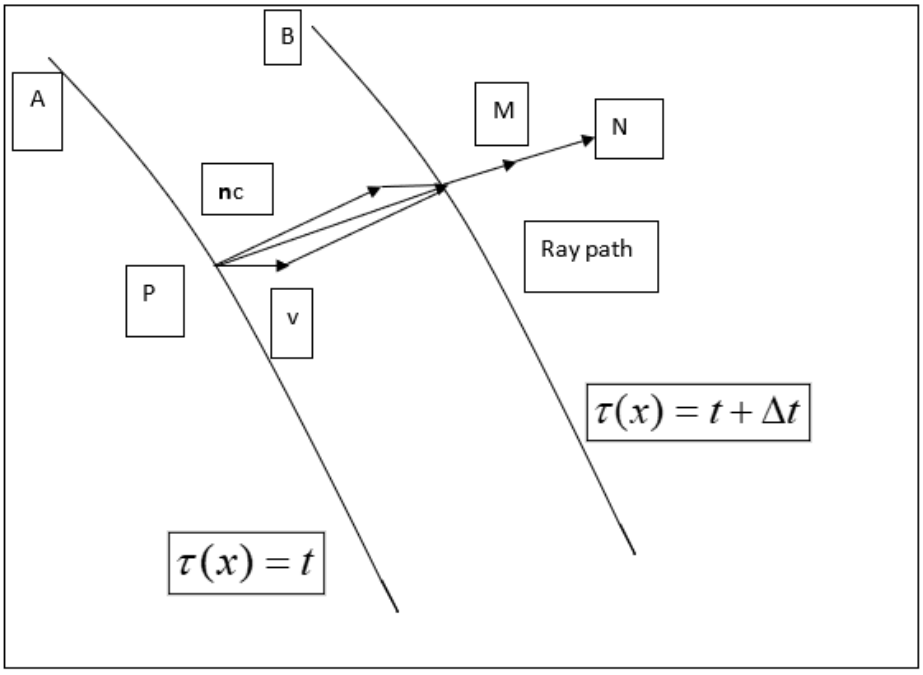

Figure 6.1: Wave front of a sound wave at two different times (Pierce, 1989).

Equation 6.1 represents a ray trajectory. In Figure 6.1 the point at P moves to position M and N after certain times. By calculating the locations of these points one can trace the ray.

In order to calculate the co-ordinates of the ray at a given time, the velocity of the wave front, **n**c and of the medium, **v** should be known. The vector **n** (normal to the wave front) can be calculated by constructing the wave front surface in the vicinity of the ray. Now, creating the wave front surface after each closely spaced time interval is potentially inefficient. To overcome this problem a new vector **s**(**x**) parallel to **n** is introduced. It is called the 'slowness vector', $\boldsymbol{s}(\boldsymbol{x}) = \boldsymbol{\nabla\tau}(\boldsymbol{x})$. The slowness vector is normal to the wave front and its magnitude is the reciprocal of the effective sound speed. The effective sound speed is the summation of sound speed and speed of the fluid.

Now **s** and **n** are parallel. So, as shown for example in Pierce (1981), and with the wave front at time t defined as $\boldsymbol{\tau(x)} = t$, we can define a scalar, Ω noting that,

$$\boldsymbol{s} = \frac{\boldsymbol{n}}{c + \boldsymbol{v}.\boldsymbol{n}} \qquad \boldsymbol{s}^2 = \frac{\boldsymbol{n}.\boldsymbol{n}}{(c + \boldsymbol{v}.\boldsymbol{n})^2} \qquad \boldsymbol{s}^2 = \frac{1}{\frac{c^{\,2}}{\Omega^2}}$$

$$\Rightarrow (\boldsymbol{\nabla\tau})^2 = \frac{\boldsymbol{\Omega^2}}{c^2}$$

So that,

$$\boldsymbol{s}^2 = (\boldsymbol{\nabla\tau})^2 = \frac{\boldsymbol{\Omega^2}}{c^2} \qquad (6.2)$$

This is an eikonal equation where $\boldsymbol{\tau}$ is the eikonal. Based on the eikonal equation, the slowness vector can be defined as the gradient of wave front $(\boldsymbol{\nabla\tau})$ at position **x** or as the gradient of travel time. The gradient of travel time also gives the direction of ray which changes with the change in c(**x**) (Pierce, 1989).

The trajectory of a ray with time t is $\boldsymbol{x_p(t)}$ and after a Δt interval of time the position can be written as $\boldsymbol{x}'_P(t)\Delta t + \boldsymbol{x}_p(t)$. So, the position at $t + \Delta t$ can be approximately equal to

$$t + \Delta t \approx \boldsymbol{\tau}\left(\boldsymbol{x_p} + \boldsymbol{\acute{x}_p}\Delta t\right) \approx \boldsymbol{\tau}\left(\boldsymbol{x_p}\right) + \left(\boldsymbol{\acute{x}_p} \cdot \nabla\boldsymbol{\tau}\right)\Delta t$$

Here $t = \boldsymbol{\tau}\left(\boldsymbol{x_p}\right)$ and $\boldsymbol{s} = \nabla\boldsymbol{\tau}$. Both sides of the above equation will be equal if

$$\boldsymbol{x_p^{'}} \cdot \nabla\boldsymbol{\tau} = 1 \qquad (6.3)$$

Inserting the value of $\boldsymbol{\acute{x}_p}$ from equation 6.1 into equation 6.3 yields

$$\boldsymbol{s}.(c\boldsymbol{n} + \boldsymbol{v}) = 1$$

$$c\boldsymbol{s}.\boldsymbol{n} + \boldsymbol{s} \cdot \boldsymbol{v} = 1 \qquad (6.4)$$

Since **s** is parallel to **n**, and **n** is a unit vector, the slowness vector can be also expressed by the following equation,

$$\boldsymbol{n} = \frac{\boldsymbol{s}}{\boldsymbol{s} \cdot \boldsymbol{n}}$$

Or $\boldsymbol{s} = \boldsymbol{n}(\boldsymbol{s} \cdot \boldsymbol{n})$

Therefore, substituting **s** = (**s.n**) **n** in 6.4 leads to

$$\boldsymbol{s} = \frac{\boldsymbol{n}}{c + \boldsymbol{v} \cdot \boldsymbol{n}} \qquad (6.5)$$

The expression for **n** can be written in terms of s by

$$c\boldsymbol{s} \cdot \boldsymbol{n} = 1 - \boldsymbol{v} \cdot \boldsymbol{s} \qquad \boldsymbol{n} = \frac{c\boldsymbol{s}}{1 - \boldsymbol{v} \cdot \boldsymbol{s}}$$

$$\boldsymbol{n} = \frac{c\boldsymbol{s}}{\Omega} \qquad (6.6)$$

Where

$$\Omega = 1 - \boldsymbol{v} \cdot \boldsymbol{s} \qquad \Omega = 1 - \boldsymbol{v}.\left(\frac{\boldsymbol{n}}{c + \boldsymbol{v} \cdot \boldsymbol{n}}\right) \qquad \Omega = \frac{c + \boldsymbol{v} \cdot \boldsymbol{n} - \boldsymbol{v} \cdot \boldsymbol{n}}{c + \boldsymbol{v} \cdot \boldsymbol{n}}$$

$$\Omega = \frac{c}{(c + \boldsymbol{v} \cdot \boldsymbol{n})} \qquad (6.7)$$

The solution of a ray trajectory involves determination of the slowness vector along the ray. The differential equation for rate of change of the slowness vector along a ray trajectory is

$$\frac{d\boldsymbol{s}(\boldsymbol{x_p})}{dt} = (\boldsymbol{x_p'} \cdot \nabla)\boldsymbol{s} \qquad (6.8)$$

From equation (6.4) and (6.6) we can write

$$\frac{d\boldsymbol{s}(\boldsymbol{x_p})}{dt} = c(\boldsymbol{n} \cdot \nabla)\boldsymbol{s} + (\boldsymbol{v} \cdot \nabla)\boldsymbol{s}$$

$$\frac{d\boldsymbol{s}(\boldsymbol{x_p})}{dt} = c\left(\frac{c\boldsymbol{s}}{\Omega} \cdot \nabla\right)\mathbf{s} + (\boldsymbol{v} \cdot \nabla)\boldsymbol{s}$$

$$\frac{d\boldsymbol{s}(\boldsymbol{x_p})}{dt} = \frac{c^2}{\Omega}(\boldsymbol{s} \cdot \nabla)\boldsymbol{s} + (\boldsymbol{v} \cdot \nabla)\boldsymbol{s} \qquad (6.9)$$

The first term on the right-hand side (R.H.S.) of equation 6.9 can be simplified in the following way,

$$(\boldsymbol{s} \cdot \nabla)\boldsymbol{s} = -\boldsymbol{s} \times (\nabla \times \boldsymbol{s}) + \frac{1}{2}\nabla \boldsymbol{s}^2$$

$$(\boldsymbol{s} \cdot \nabla)\boldsymbol{s} = 0 + \frac{1}{2}\nabla \frac{\Omega^2}{c^2}$$

The first term in the above equation is zero as **s** is a gradient.

$$(\boldsymbol{s} \cdot \nabla)\boldsymbol{s} = \frac{1}{2}\nabla \frac{(1 - \boldsymbol{v} \cdot \boldsymbol{s})^2}{c^2}$$

$$(\boldsymbol{s} \cdot \nabla)\boldsymbol{s} = \frac{-\Omega}{c}\nabla(\boldsymbol{v} \cdot \boldsymbol{s}) - \frac{\Omega^2}{c^3}\nabla c \qquad (6.10)$$

Inserting equation 6.10 into equation 6.9 results in

$$\frac{d\boldsymbol{s}(\boldsymbol{x_p})}{dt} = \frac{c^2}{\Omega}\left[-\frac{\Omega}{c^2}\nabla(\boldsymbol{v}.\boldsymbol{s}) - \frac{\Omega^2}{c^3}\nabla c\right] + (\boldsymbol{v} \cdot \nabla)\boldsymbol{s}$$

$$\frac{d\boldsymbol{s}(\boldsymbol{x_p})}{dt} = -\nabla(\boldsymbol{v}.\boldsymbol{s}) - \frac{\Omega}{c}\nabla c + (\boldsymbol{v} \cdot \nabla)\boldsymbol{s} \qquad (6.11)$$

Simplifying the first term in equation 6.11 gives

$$\nabla(\boldsymbol{v} \cdot \boldsymbol{s}) = -\boldsymbol{v} \times (\nabla \times \boldsymbol{s}) + \boldsymbol{s} \times (\nabla \times \boldsymbol{v}) + (\boldsymbol{v} \cdot \nabla)\boldsymbol{s} + (\boldsymbol{s} \cdot \nabla)\boldsymbol{v} \qquad (6.12)$$

The first term in the right-hand side (R.H.S.) of equation 6.12 is zero as the slowness vector, **s** is a gradient. Substituting equation 6.12 in equation 6.11 results in the following expression for slowness vector

$$\frac{d\boldsymbol{s}}{dt} = -\frac{\Omega}{c}\nabla c - \boldsymbol{s} \times (\nabla \times \boldsymbol{v}) - (\boldsymbol{s} \cdot \nabla)\boldsymbol{v} \qquad (6.13)$$

As shown by Pierce (1981) in Cartesian coordinate system the equation will be,

$$\frac{d\boldsymbol{s_i}}{dt} = -\frac{\Omega}{c}\frac{\partial c}{\partial x_i} - \sum_{j=1}^{3} \boldsymbol{s_j}\frac{\partial}{\partial x_i}\boldsymbol{v_j} \qquad (6.14)$$

Now the loci of ray can be computed by integrating the following equation,

$$\frac{d\boldsymbol{x}}{dt} = \frac{c^2\boldsymbol{s}}{\Omega} + \boldsymbol{v} \qquad (6.15)$$

Together with (6.14), there are six equations for the three position components plus the three slowness vector components. These are the basic equations for ray tracing. Note that **s** has dimensions of inverse velocity and Ω is dimensionless.

A ray model based on the equations derived above was developed by Lamancusa *et al* (1993). That model simulated sound propagation from a source in the atmosphere in two dimension and computed the sound pressure level at the receiver. In the model the calculation has been extended to compute sound propagation in three dimensions. In their model, a ray was emitted from a point source and traced until it reached a receiver location. They numerically solved equation 6.14-6.15 to compute the ray trajectory and the ray was traced until it reached the receiver range. Two different numerical techniques were used to solve the differential equations in the model by Lamancusa *et al* (1993). The medium was set such that temperature and wind speed varied in horizontal and vertical directions. Initially the program sent out a single ray and once the ray hit the receiver, losses were calculated along the ray. To calculate loss due to refraction additional

rays were emitted and traced for the same travel time. Then refraction loss was calculated from the area covered by those rays by applying the Blokhintzev invariant (Blokhintzev, 1946-10). If the ray hit the ground before reaching the receptor, a loss due to ground interaction was computed. Losses due to propagation and atmospheric absorption were also added.

In our model, a similar method has been used to calculate the loss. The model also included ray propagation over a hill with small curvature. We have also used uneven topography such as small hill, downward slope to show its effect on the ray trajectory. The sound pressure level was then calculated at the receiver.

The equation for the sound pressure level at the receptor is (Lamancusa & Daroux, 1993)

$$L_P = L_W - 20log_{10}d - A_{ground} - A_{refraction} - A_{absorption} + 10log_{10}\frac{W_{ref}\rho c}{P_{ref}^2 4\pi} \qquad (6.16)$$

Here, L_P = Sound pressure level in dB

L_W = Sound power level in dB

d = distance travelled in the fluid from source to the receiver along the ray in meter.

Lamancusa *et al* (1993) uses distance between the source and the receiver.

A_{ground} = attenuation due to ground absorption in dB

$A_{refraction}$ = attenuation due to refraction in dB

$A_{absorption}$ = attenuation due to atmospheric absorption in dB

W_{ref} =1*10^{-12} Watt

P_{ref} = 20 µPa

L_w is the sound power level of the source. It is assumed that only spherical spreading occurs within 1 m from the source. The last term in Equation 6.16 is introduced to express the relationship between sound power level of the source and sound pressure level at a 1m distance from the source.

All the losses mentioned above can be calculated using appropriate equations. The calculation method for individual loss will be discussed later in this chapter and in Chapter Seven.

The co-ordinates of a point on a single ray can be followed in time via the following nonlinear differential equations (Pierce, 1989). If r_x, r_y and r_z are the coordinates of a point along a ray referenced to the x, y and z axis then, expanding Eq. 6.15

$$\frac{d\boldsymbol{r_x}}{dt} = \frac{c^2 \boldsymbol{s_x}}{\Omega} + \boldsymbol{v_x} \qquad (6.17)$$

$$\frac{d\boldsymbol{r_y}}{dt} = \frac{c^2 \boldsymbol{s_y}}{\Omega} + \boldsymbol{v_y} \qquad (6.18)$$

$$\frac{d\boldsymbol{r_z}}{dt} = \frac{c^2 \boldsymbol{s_z}}{\Omega} + \boldsymbol{v_z} \qquad (6.19)$$

The slowness vector, **S(r)**, satisfies the equations, expanded from Eq. 6.14,

$$\frac{d\boldsymbol{s_x}}{dt} = \frac{\Omega}{c}\frac{dc}{dx} - s_x\frac{dv_x}{dx} - s_y\frac{dv_y}{dx} - s_z\frac{dv_z}{dx} \qquad (6.20)$$

$$\frac{d\boldsymbol{s_y}}{dt} = \frac{\Omega}{c}\frac{dc}{dy} - s_x\frac{dv_x}{dy} - s_y\frac{dv_y}{dy} - s_z\frac{dv_z}{dy} \qquad (6.21)$$

$$\frac{d\boldsymbol{s_z}}{dt} = \frac{\Omega}{c}\frac{dc}{dz} - s_x\frac{dv_x}{dz} - s_y\frac{dv_y}{dz} - s_z\frac{dv_z}{dz} \qquad (6.22)$$

Where

$$\Omega = \frac{c}{c + \boldsymbol{v}.\boldsymbol{n}} \qquad (6.23)$$

Solution of the trajectory equations starts with setting initial values for S_x, S_y, S_z, r_x, r_y, *and* r_z at t=0. The initial values for S_x, S_y, S_z are

$$S_x = \left(\frac{1}{c + \boldsymbol{v}.\boldsymbol{n}}\right) \sin\varphi \cos\theta \qquad (6.24)$$

$$S_y = \left(\frac{1}{c + \boldsymbol{v}.\boldsymbol{n}}\right) \sin\varphi \sin\theta \qquad (6.25)$$

$$S_z = \left(\frac{1}{c + \boldsymbol{v}.\boldsymbol{n}}\right) \cos\varphi \qquad (6.26)$$

Here φ and θ are used to define the initial direction of the ray. The rays considered are assumed to be emitted at turbine hub height. The zenith angle, φ, is taken relative to the z axis for each ray and the elevation angle is π/2-φ. The azimuth angle, θ is measured relative to the x axis. The initial positions of the ray were r_x=0, ry=0 and r_z= turbine hub height. The wind speed at each height is calculated from a logarithmic wind profile using the equation below.

$$U = \frac{u_*}{k} ln \frac{z}{z_0} \qquad (6.27)$$

Vertical variation of the wind speed is considered in the model and horizontal variation is set to zero in these initial computations. The sound speed is a function of temperature and calculated by $c = 20.05\sqrt{T + 273.15}$ (Lamancusa & Daroux, 1993) at each integration step. The unit of temperature is degree Celsius. Temperature can either increase or decrease with height. The standard value of atmospheric pressure, 101325 Pa is used in this model. In these initial calculations a flat ground surface is assumed without any obstacles such as high buildings or hills. The surface roughness length used is z_0=0.01 m.

The differential equations were solved by a simple forward Euler method. Euler method is a numerical procedure used to solve ordinary differential equations.

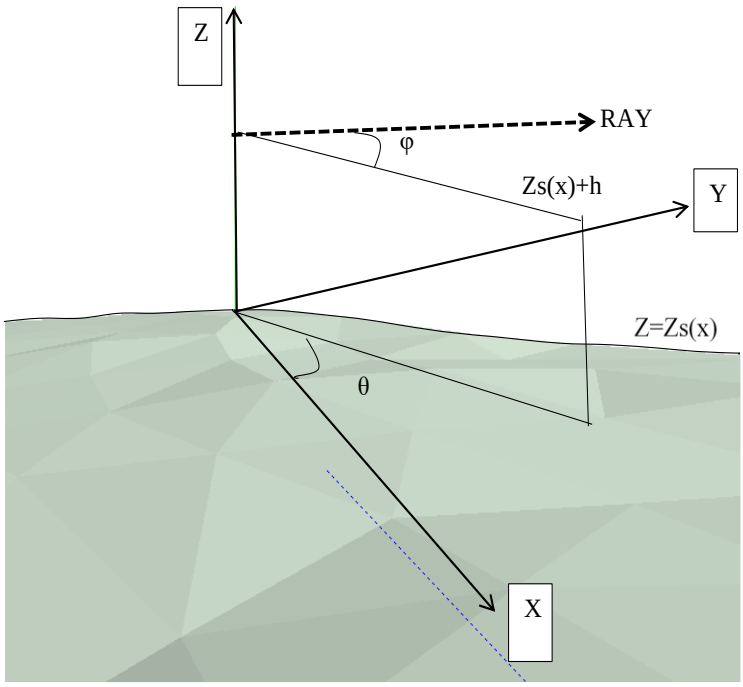

Figure 6.2: Initial position of the ray at a height of Zs(x)+h from the surface is shown in terms of angles. Terrain variation is also illustrated.

To calculate sound pressure level at the receiver it is important to know how sound propagates outdoors. Sound emitted from a point source or idealized wind turbine is attenuated in the atmosphere before it reaches the receiver. If only spherical spreading of sound is assumed, and it is assumed that the energy of the sound source at 1m is distributed over 1 m^2 area then the same amount of energy is distributed over 10,000 m^2 after travelling 100 m from the source (Salomons, 2001). Hence the intensity of the sound decreases with distance squared. In the case of spherical spreading the sound pressure level drops by approximately 6 dB ($-20log_{10}2$) per doubling of the distance from the source. A decibel (dB) is a logarithmic unit, and the definition has been provided in Chapter Four. Calculation of the sound pressure level at the receptor should consider all

additional sources of attenuation along the way. These include air absorption, effects due to spatial variations in the refraction of sound rays, ground absorption or reflection loss, and impacts of irregular terrain.

Reflection of the sound rays can occur when they touch the ground. The intensity of the sound rays decreases after ground interaction and this needs to be integrated into the model. During ray tracing the program checks for possible ground contact after each integration step. After a ground contact is detected, the intersection point of the ray and ground surface is carefully determined. In Figure 6.3 ground touch has been detected when the ray is predicted to travel from point B towards point A. The point O is the contact location on the ground and is computed from the information at point A and B. At point O the vertical distance, r_z=0. The coordinates of B and O are used to calculate the length, OD. The incident angle is computed from OB and OD.

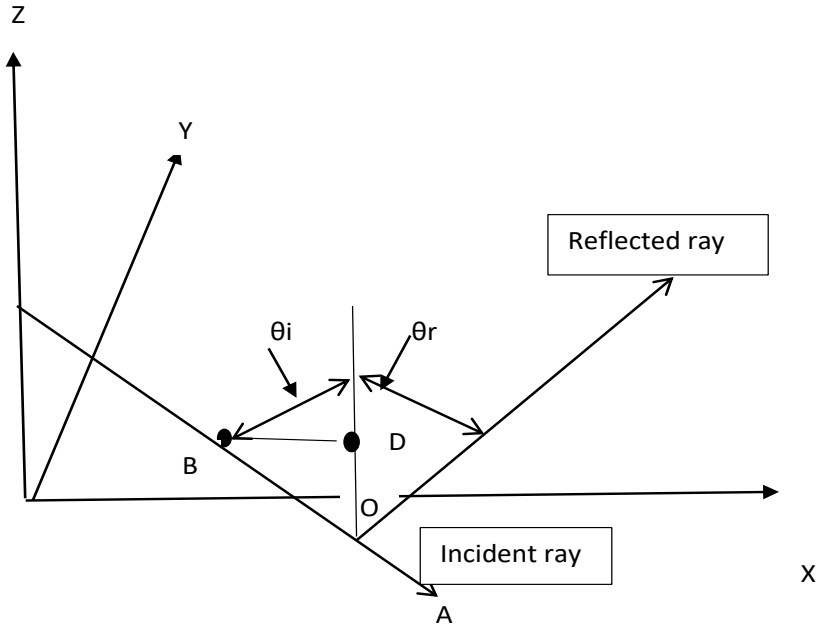

Figure 6.3: Reflection of a sound ray from the ground

According to the law of reflection the incident angle is equal to the angle of reflection. Using this theory, a new zenith angle is determined while the azimuth direction remains the same for the reflected ray over a flat surface. A new slowness vector is also calculated, and the entire calculation is repeated after every interaction with the ground. In the case of irregular terrain, the reflection calculation is more complex. If the surface is denoted by F(x,y,z) = constant then the direction cosine of the normal to the surface is grad(F)/|grad(F)|. For example, if $Z = Z_S(x,y)$ is the equation of a terrain then the direction cosine is

$$Direction\ cosine = \frac{\left(-\frac{\partial z_s}{\partial x}, -\frac{\partial z_s}{\partial y}, 1\right)}{\left|\frac{\partial z_s}{\partial x}, \frac{\partial z_s}{\partial y}, 1\right|} \tag{6.28}$$

If in a time step, the ray passes through the surface so that $z < z_s$ then an interpolation technique is used to determine the intersection point of the ray with the ground. If the direction cosine of the incident ray is l_i, i= (1, 2, 3) and the direction cosine of the normal to the surface is n_i, i= (1,2,3) then the direction cosine of the reflected ray is $m_j=l_i-2(l_jn_j)n_i$ or in vector notation **m**=**l**-2(**l**•**n**) **n.** The slowness vector is calculated based on the direction cosine of the reflected ray and the trajectory of the reflected ray is continued.

When a sound wave reaches a surface, it encounters an impedance mismatch due to a change in the medium. Whether the sound will be reflected, scattered, or diffracted depends on the nature and dimension of the surface. If the surface length scale is shorter than the wavelength of the sound than it will be scattered. Scattering of sound is dependent on the variability of the surface elevation and the frequency of the incident sound wave. If the dimension of a surface is A and wavenumber

is k then for kA>>1, sound wave specular reflection will occur. On the other hand, for kA<<1, the sound wave will be scattered.

Sound waves reflected from the ground can interfere with the direct rays. Reflected sound waves with the same phase as a direct ray will enhance the total sound pressure level at the receiver. This is known as constructive interference. Due to constructive interference of direct and reflected sound waves, the sound pressure level can increase by up to 3 dB at the receiver location (Salomons, 2001). If the direct and reflected waves are out of phase the total sound pressure level will decrease. The extreme case will arise when direct and reflected waves with the same amplitude and frequency intersect at 180^{o} out of phase. This is called destructive interference. So, it is important to measure the phase shift of the reflected wave after each ground touch. Whether the reflected wave will have a phase shift depends on the impedance of the two mediums. When sound wave travelling in the air strikes ground surface two different situations can arise: 1) A sound wave reflected from a hard, rigid surface 2) A sound wave reflected from a soft, yielding surface (Sen, 1990). If the ground is assumed to be hard, the impedance of the surface is higher than the air. In this case the incident wave will be reflected, and no phase change will occur. But if soft ground, say grass for example, is considered, part of the sound is absorbed by the ground and the rest is reflected and the reflected wave will have a change in phase (Sen, 1990). When a sound wave travels through two fluid mediums with different density, the phase change due to reflection depends on the characteristic impedance of the two mediums. For example, the impedance of water is greater than impedance of air. If sound travels from air to water the reflected sound wave will not experience any phase change. But a phase change will occur when sound travels from water to air. Lamancusa (1993) has addressed the issue of phase angle change and used the following formula to calculate it.

$$\Delta\beta = tan^{-1}\left\{\frac{Im(R_p)}{Re(R_p)}\right\} \quad (6.29)$$

Here *Rp* is the reflection coefficient can be written as

$$R_p = \frac{cos\theta_i - \left(\rho c / Z_{ground}\right)}{cos\theta_i + \left(\rho c / Z_{ground}\right)} \quad (6.30)$$

We denote θ_i as the angle of incidence, ρ is the air density (kgm^{-3}), c is the sound speed (ms^{-1}) and note that $Z_{ground} = R+jX$ is the ground impedance. Ground impedance is the measurement of resistance that a ground surface displays during interaction with a sound wave. The nature of the surface surrounding a wind turbine is assumed to be isotropic to compute the impedance of the ground. Delany and Bazley (Delany & Bazley, 1970) developed an empirical formula to evaluate characteristic impedance for fibrous absorbent material. If the medium is considered to be isotropic then the formula characteristic impedance becomes a function of frequency and specific flow resistance per unit thickness, σ of the material. The formula can be applied to calculate the impedance of the ground. The equations used to calculate ground impedance are,

$$R = \rho c\left[1 + 9.08\left(\frac{f}{\sigma}\right)^{-0.75}\right] \quad (6.31)$$

$$X = \rho c\left[11.9\left(\frac{f}{\sigma}\right)^{-0.75}\right] \quad (6.32)$$

The above equations are also used in loss calculation due to ground interaction of sound wave. Loss due to reflection is dependent on the frequency and increases at higher frequency.

6.2 Sound intensity and phase at the target site

A receptor location can be chosen at any horizontal distance x=D, in any direction from the base of the turbine. A set of equally spaced n×m rays are selected with small separation angles. These rays are emitted from the initial position on the rotor at (0, 0, h) with different azimuth and zenith angles. Each ray is followed with or without reflection from the ground until it intersects a receptor surface at x=D (or at r = R for example). When the x coordinate of the ray reaches the specified receiver distance (x=D) the program checks its position on the Y and Z axis and stores the co-ordinate. On the "receptor" surface the point of intersection of a single ray R_{ij} is defined as (y_{ij}, z_{ij}) where i and j are the azimuth and zenith angles. In Figure 6.4 two rays are emitted from the rotor center.

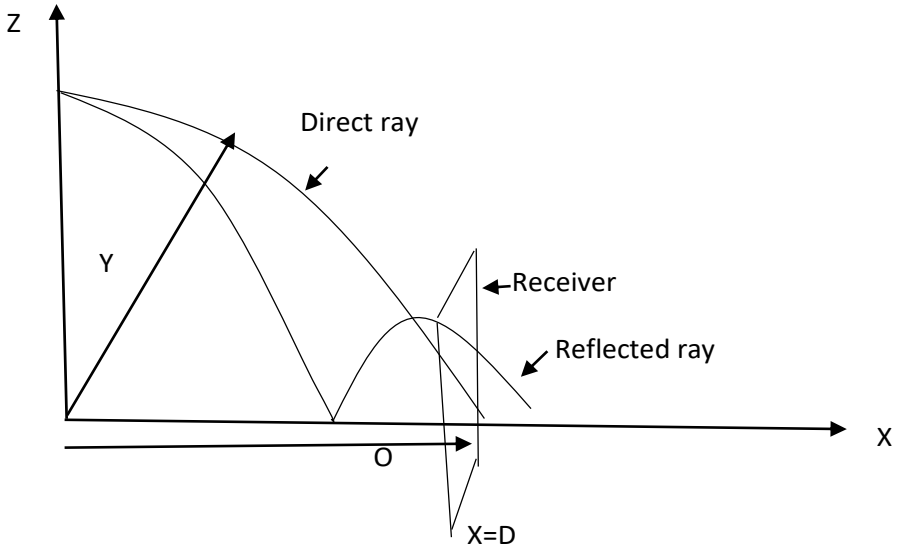

Figure 6.4: Receiver plane at x=D m from the base of the turbine.

One of them hit the receiver plane after reflecting once from the ground. The other ray reaches the receiver directly. Rays can reach the receptor surface with or without reflection, mostly once but potentially multiple times from the surface. The number of count of reflections, rc_{ij}, of each ray is recorded and rays can be grouped by counts of 0,1,2…. The time of arrival, tij values are also needed to compute the phase of the sound waves travelling along the rays.

The receptor point on the receptor surface if defined as (Y, Z) at x=D meter. The MATLAB interpolation scheme "grid data" can be used to find the values of desired properties at the selected location. The grid data takes a set of sample points, in this case intercept locations of the rays (y_{ij}, z_{ij}) and their corresponding values (e.g., angles, loss, sound pressure etc.). A grid surface can be defined by using a mesh grid command. Then the sound pressure, loss or other variables can be interpolated at the query point.

Before performing the interpolation, various losses need to be calculated to generate sound pressure level at the receptor location. When a ray reaches the receiver, losses due to spherical spreading, refraction and atmospheric absorption are calculated. These losses and their calculation methods are discussed in the following section.

6.3 Spherical spreading

A sound source that emits sound in all direction is called isotropic. A point source is shown in the center of a sphere in Figure 6.5. If the total power of the source is W and r is the radius of the sphere, then the intensity, I can be written as,

$$I = \frac{W}{4\pi r^2} \qquad (6.33)$$

If there were no total power loss then the intensity at different distances such as r_0, r_1, r_2 from the source can be related by the following equation,

$$W = I_0 4\pi r_0^2 = I_1 4\pi r_1^2 = I_2 4\pi r_2^2 \qquad (6.34)$$

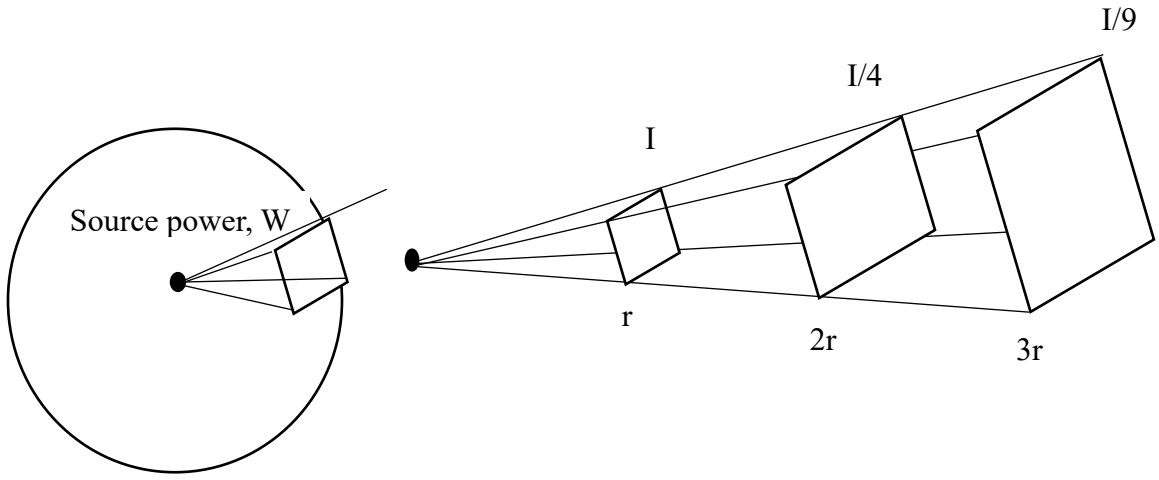

Intensity at the surface of sphere, I= $W/4\pi r^2$

Figure 6.5: Loss due to spherical spreading is shown. The sound source power is W, and the intensity is I. The intensity decreases with distance, r and is inversely proportional to the square of distance.

Propagation loss due spherical spreading after a certain distance is the ratio of sound intensity at 1m from the source and intensity at that particular distance. The equation is,

$$L_{propagation} = \frac{Sound\ intensity\ at\ 1m\ distance}{sound\ intensity\ at\ distance, r} = \frac{I_i}{I_0} \qquad (6.35)$$

By putting the value of I_i/I_0 from equation 6.34 into equation 6.35 yields in dB terms,

$$L_{propagation} = 10log\frac{r_1^2}{r_0^2} = 20log\frac{r_1}{r_0} \qquad (6.36)$$

Here r_0=1m and by replacing r_1 in equation 6.36 by r the equation to calculate transmission or propagation loss due to spherical spreading is simply,

$$L_{propagation} = 20\log(r) \qquad (6.37)$$

Where r is measured in meters.

Many ray model users, including Lamancusa and Daroux (1993), simply take r as the physical distance between the source and receptor, but it can be argued that, when wind is blowing past the source, it should be the distance travelled by the ray in the moving fluid, and r = ct_{ij}, is more appropriate. This change can account for different sound levels upwind (lower) and downwind (higher) of a source in a wind, although refraction effects and the source emission strength may vary with direction.

6.4 Refraction

Refraction of sound means the bending of sound rays. This bending can result from sound speed and wind speed variations in different layers of the atmosphere and depends on wind speed and temperature profiles.

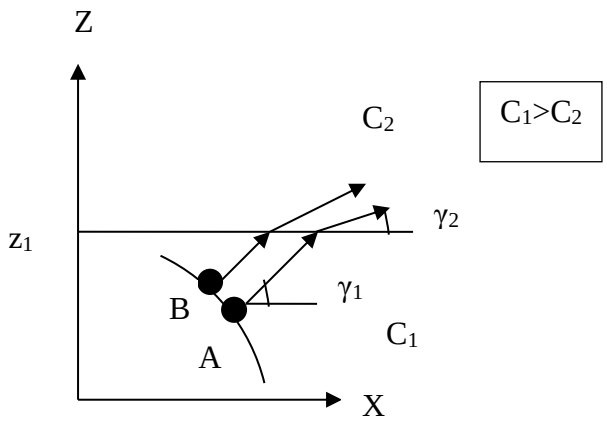

Figure 6.6: Refraction due to sound speed gradient (Salomons, 2001).

The travel time of a sound wave between the source and the receiver can also change due to refraction. In Figure 6.6 the sound speed, C_1 below z1 is higher than sound speed, (C_2), above point z_1. When a plane wave enters in the dense medium above z_1, the ray bends toward the ground. This is called downward refraction and, in this case, $\gamma_1 > \gamma_2$. The relationship between the angle of incidence with the interface and the sound speed can be expressed by Snell's Law. According to Snell's law of refraction the elevation angle, γ, varies with sound speed to preserve the ratio $\cos \gamma(z)/c(z)$ as a constant. As a result, when sound wave enters a medium sound travel at adiabatic sound speed in a non-moving atmosphere. But in a moving medium the sound speed can be calculated by the vector summation of the adiabatic sound speed and the wind speed. If sound travels in the same direction as wind, then the sound speed and wind speed are additive. When sound moves in the opposite direction then there can be increased attenuation due to a wind speed gradient. Due to this wind speed gradient the sound rays are often bent upward (Salomons, 2001).

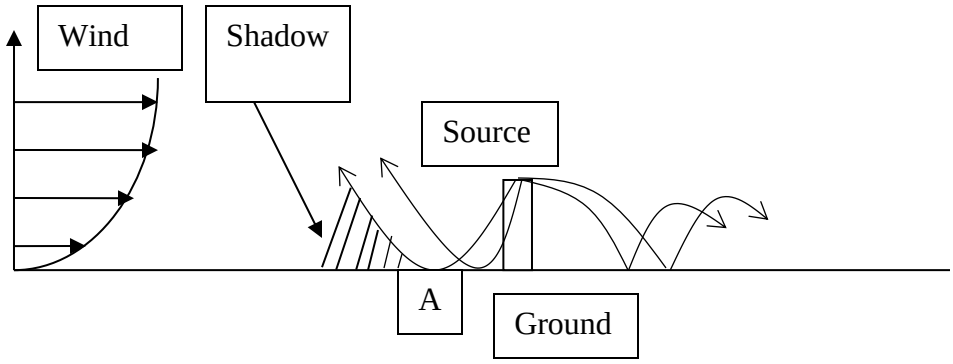

Figure 6.7: Bending of sound ray due to wind speed gradient (Hubbard, 1990).

In Figure 6.7 the sound emitted in the upwind direction from the source is bent upward. Due to this gradual bending of sound rays a 'shadow zone' can be created. In the shadow zone no ray can penetrate.

Refraction also results from a temperature gradient. If temperature decreases with height the speed of the sound will also decrease and bend upward due to upward refraction. If atmospheric temperature increases with altitude, then the sound rays will bend towards the ground.

If temperature decreases with increasing height, it means the upper air is cooler than the lower-level air. The sound travels slower in cooler air. The sound rays will bend upward. If temperature increases with height, as often occurs on the lowest 50-100m at night, then the sound rays will bend downward and enhance the sound field near the ground. The decrease of temperature with increasing height is called lapse rate. When sunlight heats the ground, air in contact with the surface warms, expands and moves upward. As the air parcel moves up it expands and loses

internal energy. This loss of internal energy results in a decrease in temperature of the air parcel with height. The rate of temperature decrease in this case is called the adiabatic lapse rate. If the air is dry the lapse rate is called dry adiabatic lapse rate. The value of dry adiabatic lapse rate is constant at 9.8°C/km. But if there is sufficient water vapour present in the air, and it condenses during ascent, the lapse rate is called the moist or saturated adiabatic lapse rate. The value of moist adiabatic lapse rate is dependent on the amount of water present in the air and is typically less than the dry adiabatic lapse rate. A typical value of moist adiabatic lapse rate is 5.8°C/km.

6.5 Terrain features

Sound is also attenuated by the presence of large obstructions such as trees, buildings, hills, and irregular terrain. Irregular terrain may develop a complex wind profile. There are several techniques that have been deployed to model terrain variation around a wind turbine. An advanced theoretical model for outdoor sound propagation method over complex terrain is described in the paper by Aballéa and Defrance (2004). Their model used a Green's function parabolic method as the basis for computation. A referential rotation technique is used to model the terrain here.

Two other approaches to define uneven terrain are discussed by Salomons (2001). One method is known as conformal mapping. In this method the terrain is imagined as a combination of convex and concave sections. Circles are drawn for each convex and concave part in such a way that those sections form a part of the circle. A coordinate transformation is then used to transform the atmosphere above the circle into a flat surface with a modified sound speed profile. If the surface is convex then an upward refracting sound speed profile is used and a downward refracting sound

speed profile is used if the curvature is concave. The crank-Nicholson parabolic equation method is used to compute the sound propagation.

In the ray model presented in the study we can include different types of terrain shape with appropriate equations. The computation method will be discussed in detail in the following chapter.

Chapter 7

Results

In this chapter results obtained from the ray model will be presented. The ray propagation will be shown above flat terrain and over topography. The effect of variation in the wind profile and sound speed profile on the sound ray will be discussed. Once the rays reach a user defined receiver location various types of losses will be computed. In this ray model loss due to spherical spreading, atmospheric absorption, refraction, and ground attenuation are calculated. Each type of loss will be described separately in detail. Calculations can be made for any initial zenith and azimuth angle but most of the figures we use limited ranges for illustration. From multiple ray calculations a contour plot of sound pressure level on a receptor surface can be generated.

7.1: Sound propagation over a flat terrain for a range of inclination and azimuth angles

The trajectories of rays emitted in a vertical plane parallel to the wind from the center of a wind turbine with 80 m hub height at different zenith angles are shown in Figures 7.2-7.4. Please note that the Figure 7.1 is mentioned afterwards as it is used to explain the atmospheric conditions

(lapse rate and wind profile) used during sound propagation of the rays. Hub height wind speed is 10 ms^{-1} and a logarithmic wind profile with z_0 = 0.01 m is assumed. The temperature gradient is -0.006 ºC/m, a typical lapse rate (6 ºC/km) in the near-neutral boundary-layer. In addition, a strongly stable temperature gradient of +0.05 ºC/m has been used in occasional cases (see section 7.3). This could exist in the lower atmosphere for up to 200 m but does not normally occur at higher altitudes apart from in capping inversions. The sound speed is a function of temperature as discussed in Chapter 5. Sound speed and wind speed are plotted with height in Figure 7.1. The temperature at the ground surface is 15 ºC in this case.

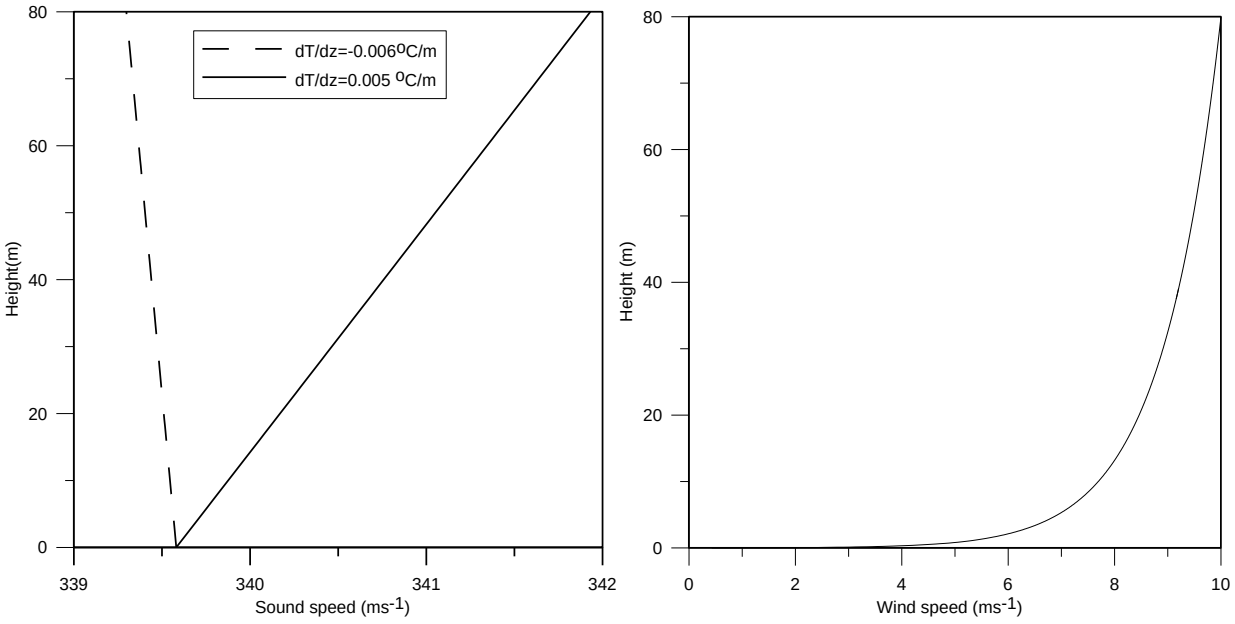

Figure 7.1: A) Sound speed plotted with height above the ground for two different sound speed gradients. The air temperature at ground surface is 15 ºC for this case. B) Wind speed variation is shown with height. The surface roughness length is 0.01 m.

The sound speed at the surface for both profiles are equal. In one case it gradually decreases with height as temperature decreases at a rate of -0.006 ºC/m while for a temperature gradient of +0.05 ºC/m it increases with height. In Figure 7.1, the sound speed line is very straight. The sound speed has been computed from, $c^2 = c_0^2 \left(\frac{T}{T_0}\right)$, where c_0 is the sound speed at temperature, T_0.

A group of twenty rays with zenith angles of between 85º-104º (separated by 1º) taken relative to the vertical axis and emitted in the downwind direction (zero azimuth angle) are shown in Figure 7.2.

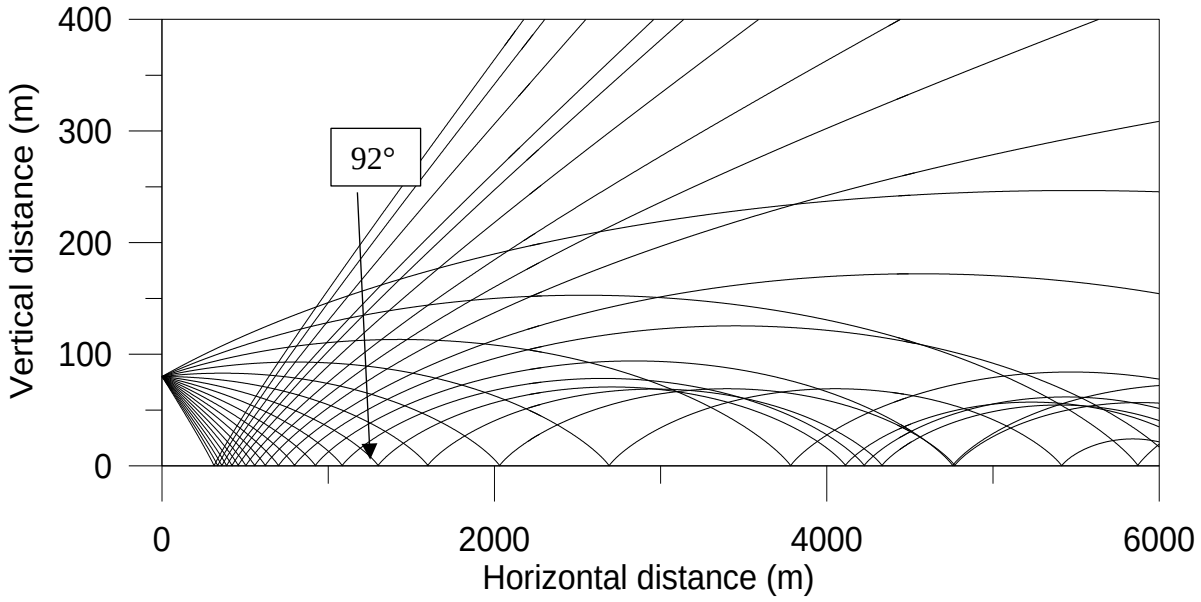

Figure 7.2: A group of 20 rays with zenith angle between 85º-104º (separation 1°) taken relative to the vertical axis are shown in the downwind direction for zero azimuth angle. Wind speed is 10 ms^{-1} at 80 m hub height, log profile with z_0 = 0.01 m. Lapse rate is 0.006 ºC/m.

The results indicate the horizontal distance that the rays travel before striking the ground increases with higher elevation (= 90° – zenith) angle. The wind speed is higher at higher levels which pushes those rays further downwind while temperature decreases at 6 °C/km. All the rays bend towards the ground due to presence of the vertical wind shear. In this case the temperature variation with height would have the opposite effect, but the wind shear dominates. The sound ray with zenith angle of 86° touches the ground at around 5,800 m from the base of the turbine and is reflected back into the atmosphere. The first ground touch point of rays decreases with higher zenith angle. The rays with higher zenith angle (above 92°) touch the ground within 1,000 m from the turbine and are reflected once. Those rays then continue to move in the upward direction after reflection. The rays with lower zenith angle (86°- 92°) are reflected multiple times from the ground as they propagate in the downwind direction. The amplitude of the sound pressure along the ray decreases after every reflection. These losses must be considered, as discussed later.

In Figure 7.3, rays are emitted at zenith angles between 95º to 125º and, again, the azimuth angle is 0°. These rays touch the ground once and then move away from the ground, although some could be bent back towards the ground by wind shear. In this case wind shear and the temperature gradient are working in opposite directions.

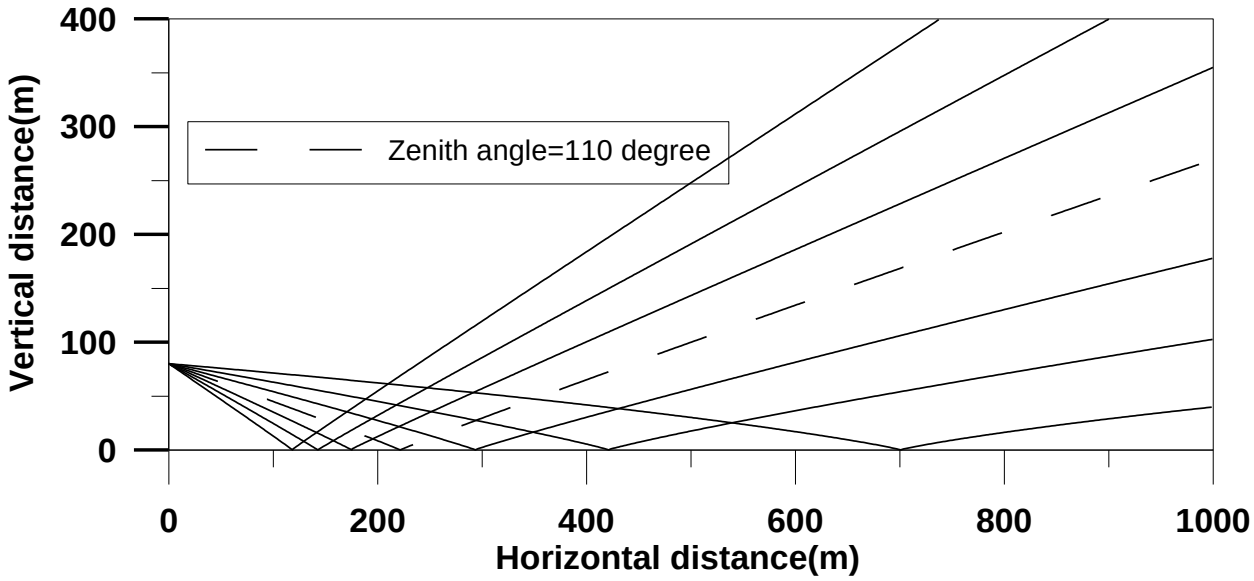

Figure 7.3: A group of seven rays with zenith angle of between 95º-125º (separation 5º) taken relative to the vertical axis are shown in the downwind direction for zero azimuth angle. Wind speed is 15 ms^{-1} at 80 m hub height, log profile with z_0 = 0. 01 m. Temperature at the ground surface is 10 ºC and a lapse rate of 0.006 ºC/m is used.

In the third scenario, as shown in Figure 7.4, a family of seven rays with zenith angles between 95º to 125º (separation 5°) are emitted where the azimuth angle is set to 180º. The results indicate that in the upwind direction, the impact distances on the ground are approximately the same as for rays with the same zenith angle in the downwind direction but there are slight differences associated with the wind shear. The point of ground touch in the upwind direction is 221.64 m from the source for the ray with zenith angle 110° while the distance for the same zenith angle ray in the downwind direction is 221.28 m. The rays reflected off the surface move in the upward direction and can leave a "shadow zone." In this example, the shadow zone starts to form before 600 m distance from the turbine base where a ray just "grazes" the surface. The shadow zone is created due to wind shear in the atmosphere. The wind moving in the same direction as the sound will push it further downwind. On the other hand, in the upwind direction, the rays emitted from

the source are moving opposite to the incoming wind flow. The effective sound speed in the atmosphere is the vector sum of sound speed and the wind speed. In this situation, wind speed is flowing in the opposite direction that reduces the overall speed of the sound. The wind speed is higher at a higher height so, the reduction in the effective sound speed is higher in the upper atmosphere. The sound waves close to the ground then move faster than those above. As a result of this difference in speed, the rays eventually bend in the upward direction creating a shadow zone. In this example, the shadow zone starts to form shortly before 600 m distance from the turbine base.

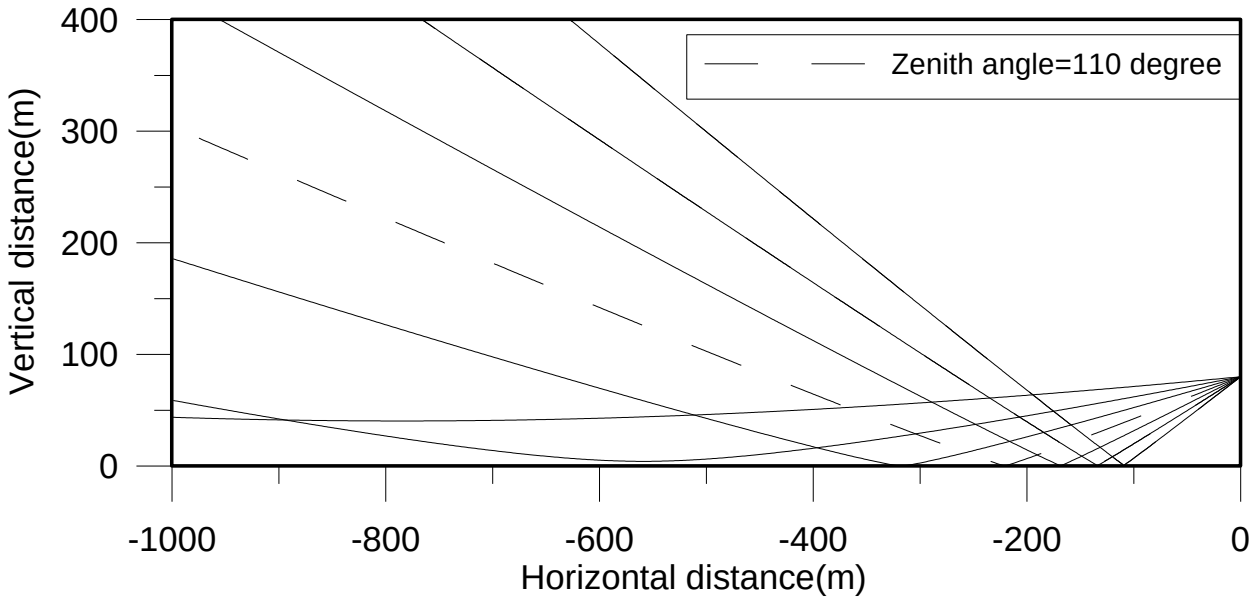

Figure 7.4: A group of seven rays emitted at different zenith angles between 95º-125º and an azimuth angle 180º. Wind speed is 15 ms^{-1} at 80 m hub height, log profile with z_0 = 0.01 m. Lapse rate is 0.006 ºC/m.

To show the variation in trajectory of the rays with azimuth angle, rays are emitted at various azimuth angles between 0º to 50° with 10° increments and a fixed, 95º zenith angle in Figure 7.5. The trajectories of the rays are shown in 3 dimensions. The first impact location for the ray emitted at 0º azimuth angle is, x=589.57 m. The ray emitted at 40º azimuth angle touches the ground at, x=471.578 m which is roughly cos (40º) times the impact location of the ray ejected at 0º azimuth angle. The rays continue to propagate in the same direction after reflection and strike the ground two times more within 6 km in the horizontal direction.

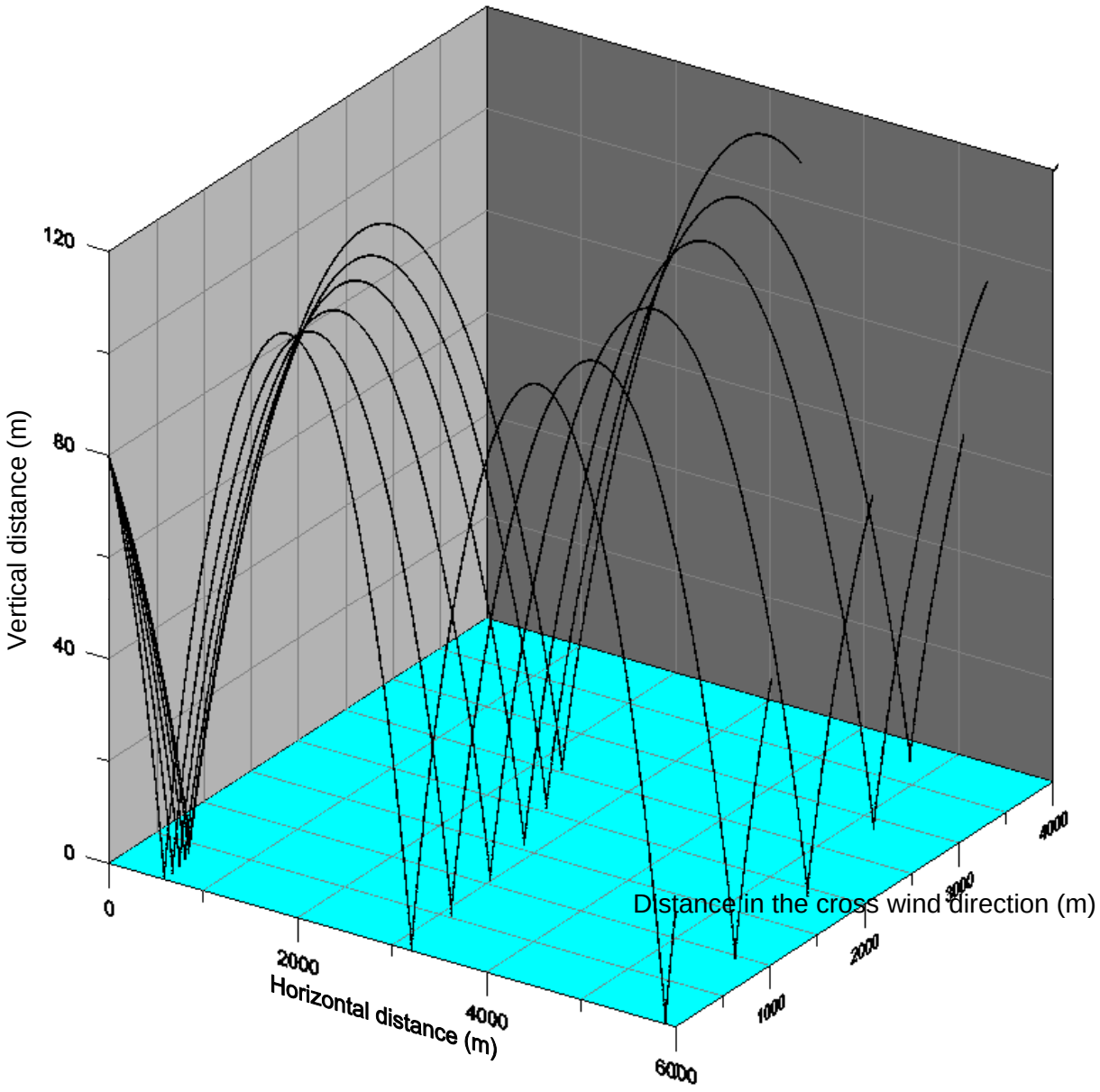

Figure 7.5: A group of rays emitted at different azimuth angles between 0º-50º with an increment of 10ºand zenith angle 95º. Wind speed is 15 ms^{-1} at 80 m hub height, log profile with z_0 = 0.01 m. A positive temperature gradient of 0.05 ºC/m is chosen for this case.

7.2: Sound propagation over uneven landforms

In principle, effects of the terrain on the flow and the sound speed could be computed with models of flow in complex terrain but here we will simply assume that U and T fields are displaced vertically, and z is replaced by $Z = z\text{-}z_s$ where z_s is the surface elevation relative to surrounding terrain. The main impact will be reflection from the surface, occurring in the plane containing the incident ray and the normal to the surface.

Case A – a single 2D ridge

The terrain in Case A is a 2-D ridge of height 50 m. The wind is assumed to be normal to the ridge. In Figure 7.6 the turbine is located on the top of the 50 m hill. The elevation of the surface decreases with distance from the base of the turbine. The height of the turbine hub is 80 m. Due to the uneven nature of the topography; the elevation of the source becomes 130 m above the surrounding terrain. A logarithmic wind profile with $U = (u^*/k) \log ((Z+z_0)/z_0)$, with Z the height above terrain is used to describe wind flow over the ridge. The lapse rate is 0.006 ºC/m in all the cases presented over irregular terrain.

In order to illustrate potential convergence a group of twenty-one rays shown in Figure 7.6 are emitted at zenith angles between 125º-145º, with a separation of 1º, in the downward direction. The rays that reach the ground within the range of the hill are reflected back into the atmosphere. Due to this reflection, a convergence of rays occurs at about 230 m along the x axis. Rays that reach the surface of the hill are reflected and, in this case, all move in the upward direction after reflection. However, curvature of the surface leads to a situation where the rays that are reflected from the steeper slope section do not reach as high as the rays reflected from the downhill, more level section. This leads to a convergence of rays which in this case focusses them at about 250 m

downwind of the turbine. Simple ray theory breaks down near these regions where reflection or refraction leads to the creation of a caustic surface to which rays are tangential. Lighthill (1978) shows that these local difficulties can be overcome in a "healed" version of ray theory.

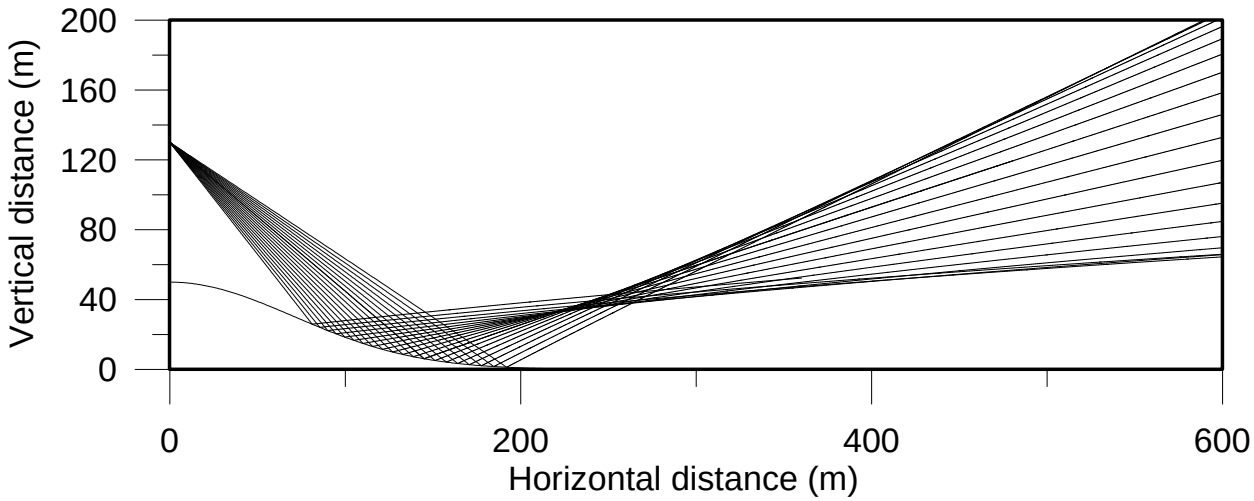

*Figure 7.6: (Case A) Sound propagation over downward slope. The ridge is 50 m high, and the topography can be represented by the equation z_s=50*exp [-(x/R)^2] m where the value of R is 200. A group of twenty-one rays with 1° separation were emitted with zenith angles between 125^o-145^o and zero azimuth angle. The coordinate of the rotor center is (0, 0,130). Lapse rate is 0.006 ^{o}C/m.*

Case B: Sound propagation over an undulating idealized surface due to variation in horizontal and vertical angles

The terrain in Case B is arranged with varying landforms surrounding the base of the wind turbine. The terrain is represented by z=amp*sin (2πx/100) *cos (2πy/200). The height of the terrain can be varied by using different values for 'amp' in the equation. Fifteen rays are emitted at different

zenith angles between 107º and 121º (1° separation) in the downward direction in Figure 7.7. Due to the presence of uneven topography, interference among the rays can occur after reflection from the surface. There is a possibility of an increase or decrease in the sound pressure level at 210 m downwind and at 10 m above the ground. Several rays can interfere at this location and may intensify or weaken the sound pressure depending on the phase of the rays. With variation in the azimuth angles things would be more complex.

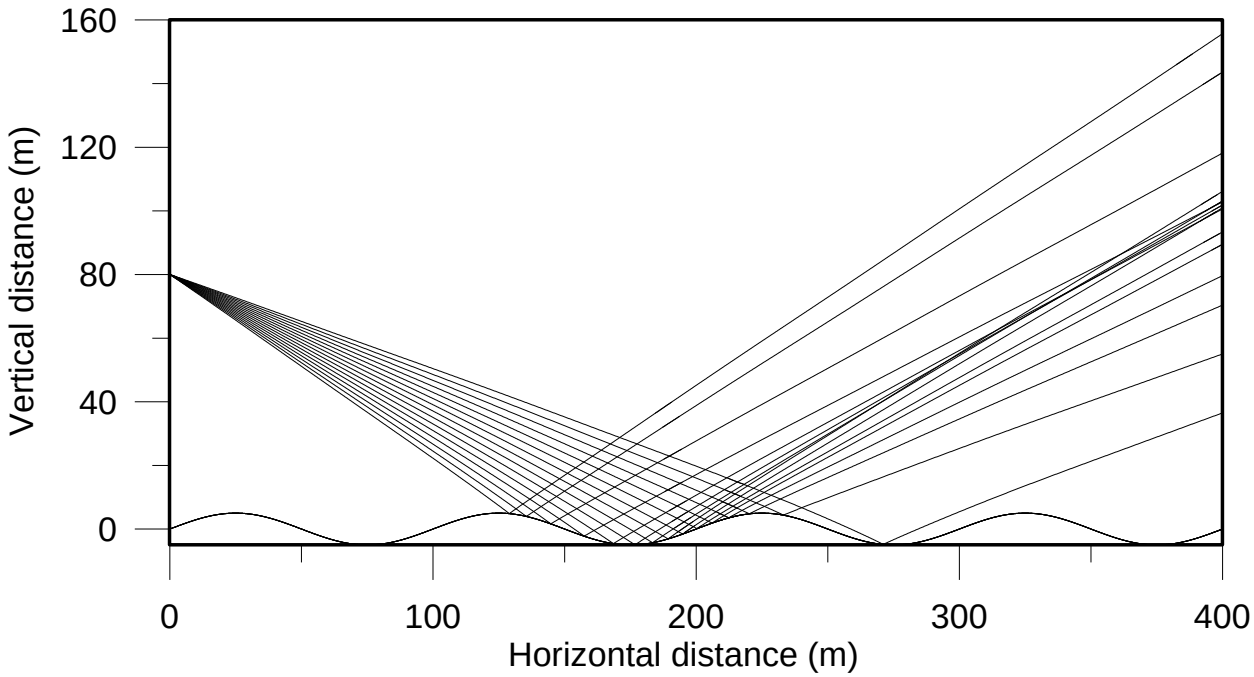

Figure 7.7:(Case B) Rays (a family of fifteen) are emitted at 0º azimuth angle and at various zenith angles between 107º and 121º (1º separation). Wind speed is 15 ms^{-1} at 80 m hub height and the surface roughness length, z_0 = 0.01 m. The equation of the terrain is $z=amp*sin(2\pi x/\lambda_x)$. Downwind horizontal direction is x and λ_x is 100. The elevation of the uneven terrain is amp and set to 5 m. Lapse rate is 0.006 ºC/m.

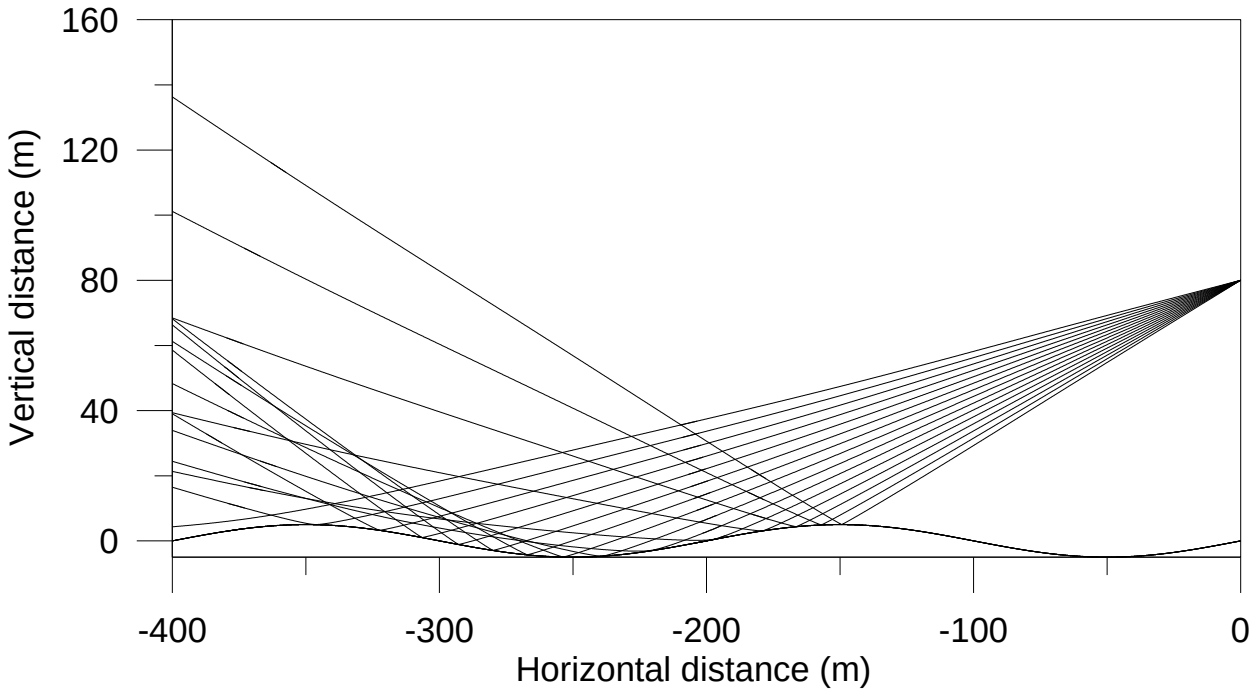

*Figure 7.8: (Case B) Rays (15) are emitted at 180° azimuth angle and at various zenith angles between 102° and 116° (1° separation). Wind speed is 15 ms^{-1} at 80 m hub height and the surface roughness length, z_0 = 0.01 m. The equation of the terrain is z_s=amp*sin (2πx/λ). Here, amp=5m is the amplitude of the uneven terrain, λ is 200. Lapse rate is 0.006 °C/m.*

Figure 7.8 illustrates possible effects of topography on sound wave propagation in the upwind direction over the same terrain. Multiple (15) rays are emitted at different zenith angles between 102º to 116º with 1º separation. Some of the rays with higher zenith angle reach the downward slope of the ridge surface. Those rays get reflected from the ground and propagate through the air. here is significant increase in the occurrence of interference of these rays on the hilltop at -330 m.

Case C: Sound propagation over a complex terrain (flat combined with small hills)

In case C, the terrain features are defined to include flat terrain up to 200 m from the base of the wind turbine followed by a 2-dimensional ridge. Both the wind turbine base and the base of the ridge are assumed to be at the same elevation. Two downwind ridges of different heights and widths are considered. In the first example, the height and width of the first ridge have been set to be 10 m and 100 m, respectively. In the second example, the height of the ridge is increased to 30 m with the same width. The rays were emitted with zenith angles between 100º-120º, and the azimuth angle is set to zero. The azimuth angle can be varied in case of a three-dimensional terrain feature. The following equation has been used to characterize the terrain:

$z_s = A \sin [2\pi(x-200)/200]$ for $200<x<300$, where A = elevation of the ridge

The hub height of the turbine is set at 80 m, as indicated in Fig 7.9.

In this example, some rays strike the ridge and get reflected in the air. The direction of rays reflected from the ridge are different from rays reflected from the flat surface. The reflected rays from the ridge do not interfere with each other. Some of the rays that are reflected from the flat surface can interfere with the reflected rays from the hill surface. The rays that reach the downwind slope of the hill on the other hand move forward and may converge. In case of the smaller hill, more rays will reach the downward slope. Fewer rays reach the downward slope when the height of the hill is increased to 30 m (Fig 7.10). Rays reaching the flat terrain upwind of the ridge can be reflected twice. The first reflection occurs in the flat surface. Then they reach the uneven surface and get reflected again. The rays that are reflected from the bottom of the hill, move in the upwind direction after reflection.

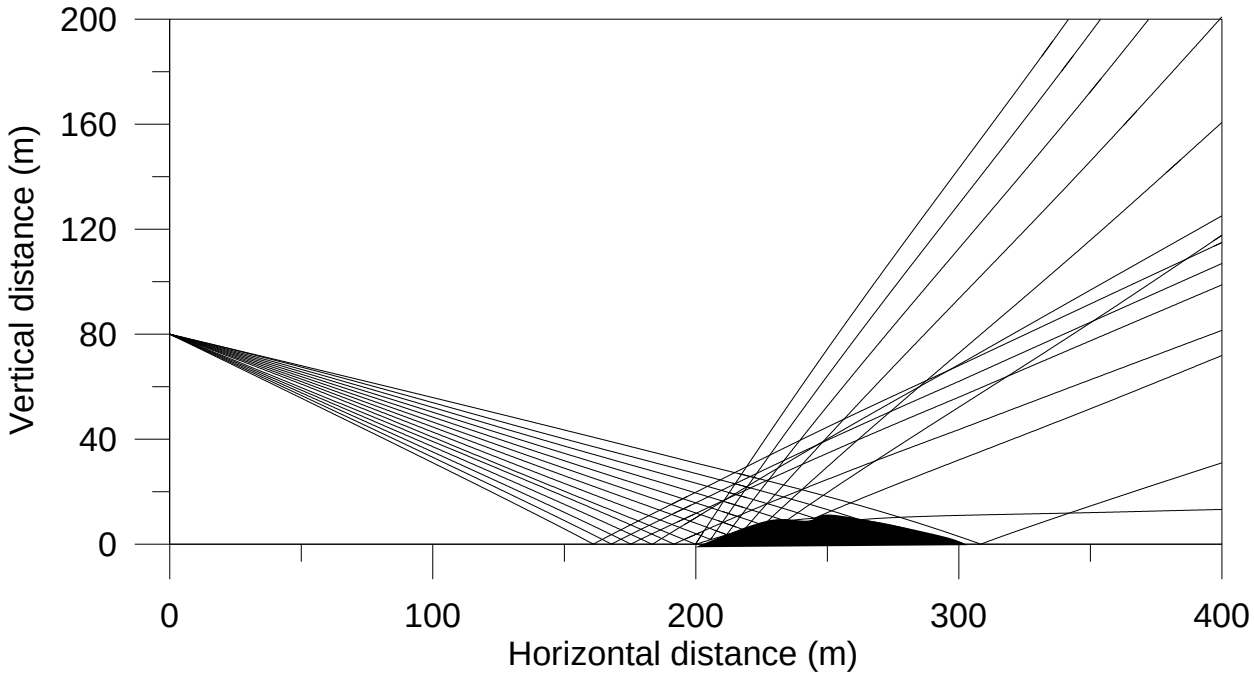

Figure 7.9: (Case C) Sound propagation over a hill. The hill is 10 m high and 100m wide. The rays were emitted between 95^o-120^o and the azimuth angle was zero. The equation of the uneven terrain is z=10 sin [2π(x-200)/200]. The wind speed at the hub height of the turbine is 15ms^{-1}. Lapse rate is 0.006 ^{o}C/m.

The effect of variations in the topography has been shown with different examples of terrain type. Variation in topography can attenuate ray sound pressure levels or can create shadow zones. For example, in Figure 7.10 there is a region behind the hill between 300 m to 340 m where no direct ray has penetrated. Also, after reflection from the hill the rays bounce back in the air and do not reach the ground again. So, this also reduces the number of rays that can reach a certain receiver distance. Another effect of uneven terrain is interference among the direct and reflected rays. This phenomenon can contribute to the increase or decrease in the sound pressure level at a specific location. In the following section the dependency of ray trajectories on the wind speed and temperature profiles will be explored.

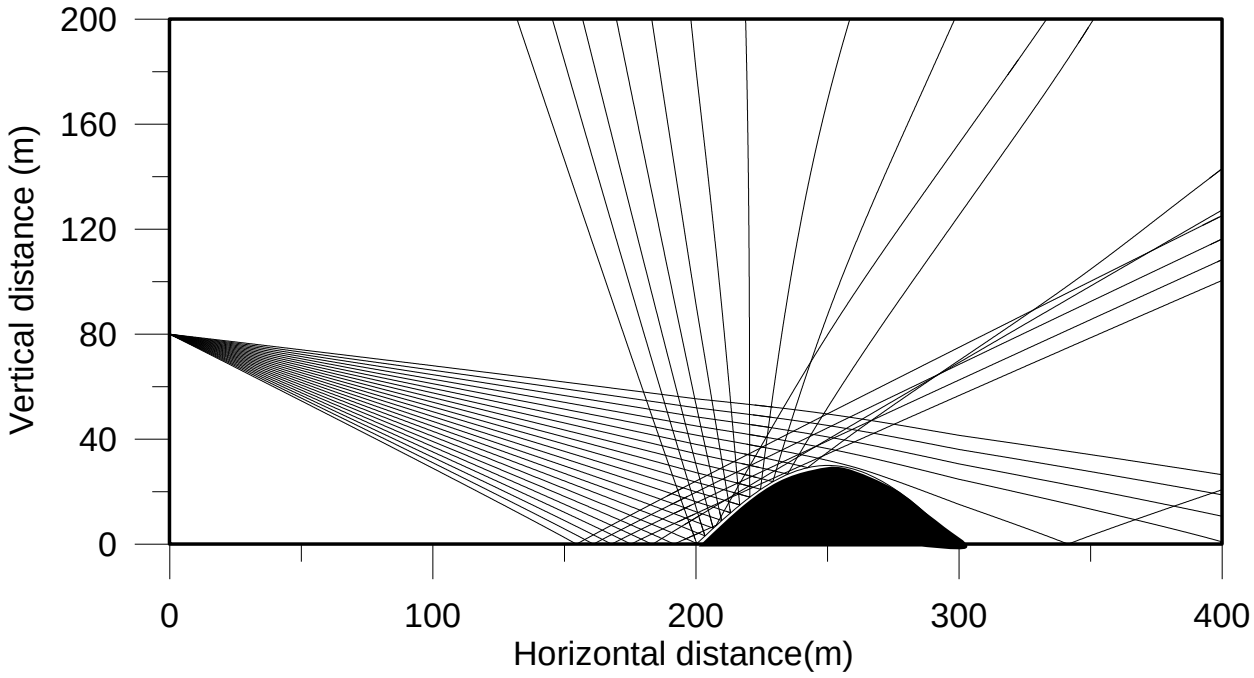

Figure 7.10: (Case C) Sound propagation over a hill. The hill is 30 m high and 100 m wide. A group of twenty-two rays were emitted between 100º-121º and the azimuth angle was zero. The equation of the uneven terrain is z=30 sin [2π(x-200)/200]. The wind speed at the hub height of the turbine is 15 ms^{-1}. Lapse rate is 0.006 ºC/m.

7.3 Refraction effects

Refraction of sound means the gradual bending of sound rays. This bending can result from variation of sound speed with height in the atmosphere, and/or wind speed gradient. Sound speed is dependent on air temperature and temperature generally varies with height. The equation showing the relation between sound speed and temperature is given in chapter 5 (equation 5.4).

Wind speed and sound speed profiles have a significant effect on the propagation direction of rays. In most of the cases presented earlier the wind speed was 15 ms^{-1} at 80 m hub height. The temperature was 10 ℃ at the ground and decreased at a rate of 0.006 ℃ per one-meter increase in height. The sound speed is a function of temperature. In this section various test cases have been run with variation in the temperature and wind speed profile. Results from those cases will be presented in the following sections.

Case 1: Constant temperature, various wind profiles

This test case has been set up by using constant temperature and different wind profiles. A group of five rays are emitted with a zenith angle between 85º-105º (increment of 5º) and zero azimuth angle. Temperature at the ground surface is 10 ºC. As sound speed is a function of temperature, it is also invariant in this particular case. The wind speed starts with a value of 15 ms^{-1} at 80 m hub height and decreases logarithmically with decrease in height. The variation in wind speed profile is achieved by taking three different values of surface roughness length. Surface roughness length (z_0), with a value of 0.0001 m represents a smooth surface without any obstacle and is similar to a sea. A surface with short grass can have a roughness length of 0.01 m. A ground with long dense trees like a forest has a higher roughness length, close to 1 m. As temperature is constant, refraction can occur due to wind shear. It is seen that sound rays bend the most for the wind profile with a roughness length of 1m. The degree of refraction diminishes at lower values of roughness length and rays bend less toward the ground. The rays follow a trajectory of a straight line in the absence of any refraction. The rays would travel a longer distance before reaching the ground compared to the distance they travel in a refracting atmosphere.

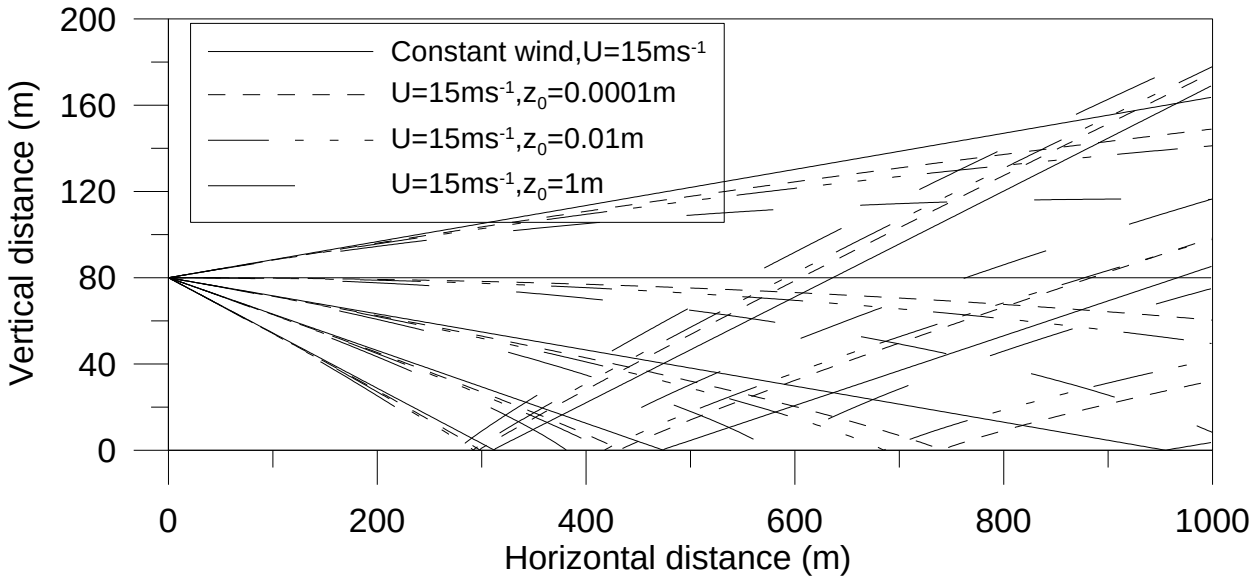

Figure 7.11: Sound rays are traced for constant sound speed and varying wind speed profiles. The hub height is 80 m, and the zenith angles are between 85^o-105^o.

Case 2 Variation in temperature and wind speed

To illustrate potential effects, three scenarios have been created using three separate temperature profiles. In the first scenario temperature is constant and the wind speed varies logarithmically. In the second scenario temperature decreases with height at a rate of 0.006 ºC/m. A third scenario includes a temperature inversion. For this scenario, the wind profile remains the same and the temperature gradient is positive at 0.05 ºC/m. It is a situation of strong refraction and as a result most rays travel towards the ground. This type of atmospheric condition is mostly common at nighttime. At night, the air near the ground is cooler than the air at higher elevation. In this case there will be more rays near the ground and sound level will be higher at lower altitude.

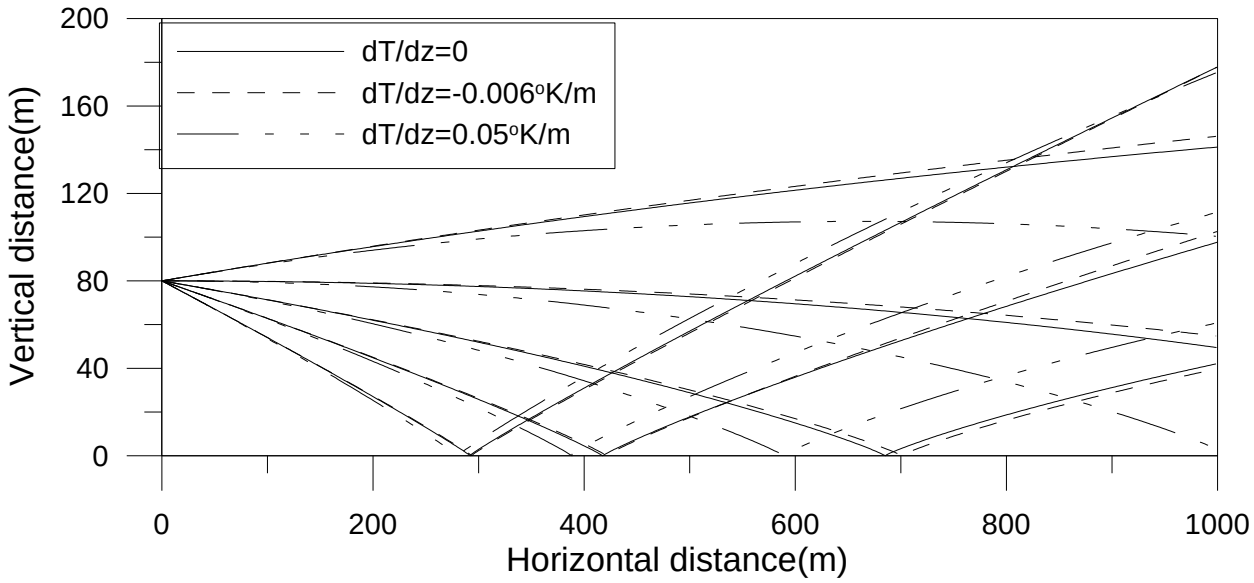

Figure 7.12: Ray trajectories are shown for three different temperature gradients. The ambient temperature at the ground surface is 10 ^{o}C, sound speed, c=336 ms^{-1}. The temperature variation with height is zero for the first case. So, there is no stratification in the atmosphere. The wind speed is 15 ms^{-1} at a hub height of 80m and varies logarithmically with height (z_0 =0.01 m) in all cases. The second scenario has the same temperature at the ground and the lapse rate is 0.006ºC/m. In the third scenario the temperature gradient is 0.05 ºC/m. Rays are emitted at zenith angles between 85º to 105º (increment 5º) in all cases.

Case 3: A compound profile of temperature and logarithmic wind speed

In this case two different scenarios will be presented. A composite temperature profile is used where the temperature decreases with height at a rate of 0.006 ºC/m for the first 100 m elevation from the ground and then increases with height after that at 0.05 ºC/m. The other scenario has a lapse rate of 0.006 ºC/m. The same wind profile is used in both scenarios. Rays are emitted at zenith angles between 85º-105º (separation 5º), and results are shown in Figure 7.13. The rays in the compound temperature profile bend towards the ground after 100 m height because of the

positive gradient. The inversion condition in the upper layer bends some of the sound rays back into the lower region of the atmosphere.

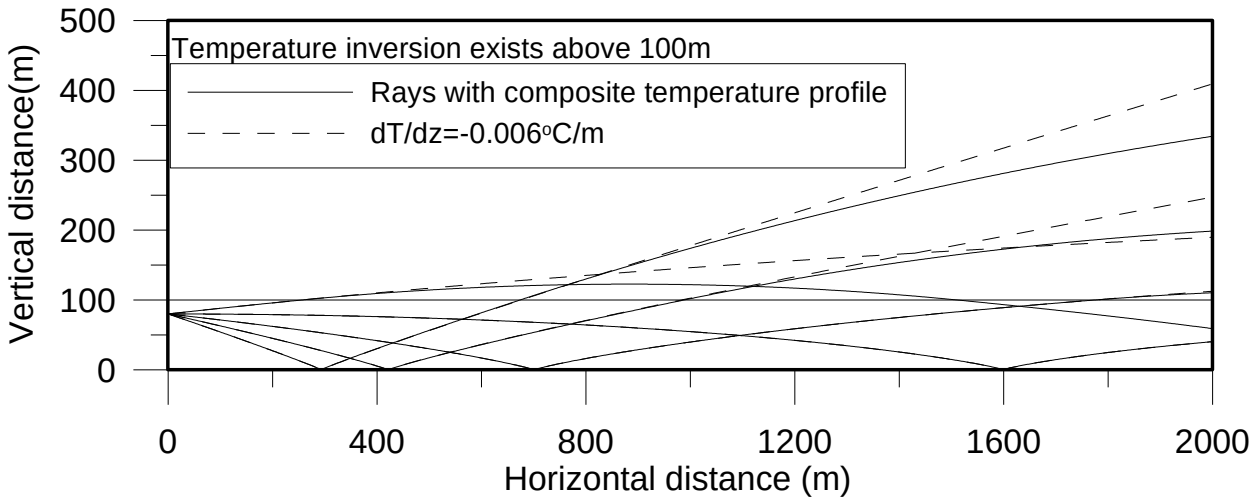

Figure 7.13: A group of rays are emitted with zenith angle between 85º-105º with 5º increment. Results are for a logarithmic wind profile and temperature gradients dT/dz= -0.006 ºC/m from 0 to 100 m and dT/dz= 0.05 ºC/m above 100 m.

7.4 Loss calculations

When ray trajectories are successfully traced the next step is to calculate the different types of losses at a specific location. In this model the receiver can be specified in any direction surrounding the turbine. In the next couple of sections, the calculation method of losses and gains from various

effects will be explained with corresponding results. Losses due to spherical spreading were discussed in Section 6.3.

7.4.1 Refraction effects

When a group of rays propagate in the atmosphere the cross-sectional area(A) and volume covered by them can be considered as a ray tube. The energy contained in it remains constant along the ray tube. This theory can be used to determine the loss or gain due to refraction. This is often termed as refraction loss, but it can be positive or negative. The relation among pressure variation along a ray *(P*), ray velocity (V_{ray}), and cross-sectional area of the ray tube (A_{ray}) can be expressed by equation 7.1 which is also known as Blokhintzev invariant (Blokhintzev, 1946-10). It is constant along any ray tube of varying cross-sectional area (Pierce, 1989).

$$\frac{P^2 V_{ray} A_{ray}}{\rho c^2 \Omega} = constant \qquad (7.1)$$

Here

$$\Omega = \frac{c}{c + \boldsymbol{v}.\boldsymbol{n}}$$

$\boldsymbol{v}$ is the medium velocity, $\boldsymbol{n}$ is a unit vector, ρ is the medium density and c is the sound speed. The refraction loss can be calculated from the ratio of the cross-section of a set of closely spaced rays travelling in a homogeneous medium and the area of the same group of rays moving in non-homogeneous medium (Lamancusa & Daroux, 1993). In order to determine refraction loss when a ray reaches a receiver location four more adjacent rays with small separation angles are emitted from the source. Those four rays are then traced for the same amount of time as the central ray. In Figure 7.14 one central ray and four adjacent rays are shown in a refracting medium and in a non-refracting medium. The area surrounded by the points ABCD under those rays is calculated.

The area in the refracting medium is, S_{refrac} =ΔABC+ΔACD

The area in the non-refracting medium is $S_{non\text{-}refrac}$=ΔPSR+ΔPQR

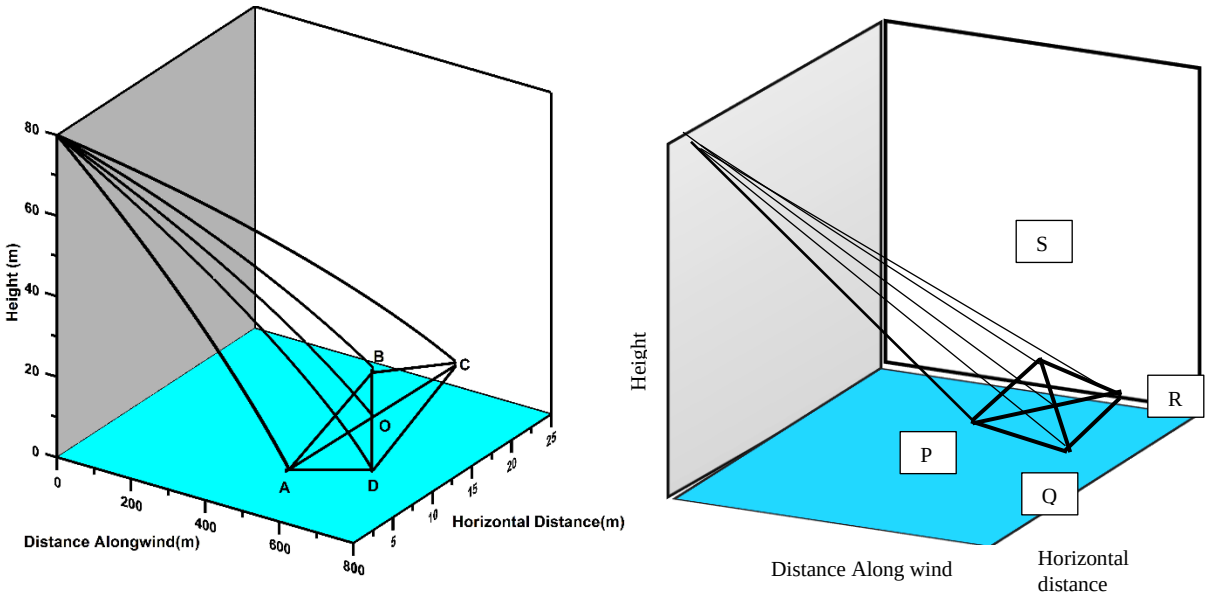

(a) (b)

Figure 7.14: (a) Area enclosed by rays in a refracting medium. (b) Area enclosed by the same rays in a non-refracting medium.

Now in a non-refracting medium, rays do not deviate from their initial paths and advance in the same direction. The calculation procedure of the area covered by the rays in a non-refracting medium is similar to the calculation in a refracting medium. If ρ′ and c′ are medium density and sound speed in the non-homogeneous medium then refraction co-efficient, α is defined by using equation 7.1 as,

$$\alpha = \frac{P_{refrac}^2}{P_{non-refrac}^2} = \frac{S_{refrac}|V_{ray}|\rho c}{S_{non-refrac}\Omega\rho' c'^2} \qquad (7.2)$$

The refraction loss (attenuation) in dB is, $A_{refraction} = 20log_{10}\alpha \;\; dB$ (7.3)

To illustrate the calculation of refraction loss at different distances from a point source of sound a group of rays with various azimuth angles are chosen. For this case rays were emitted at three different azimuth angles and the zenith angle 85º. Refraction was then calculated at multiple receiver locations in the downwind direction. The first receiver was set at 200 m from the turbine base. Additional receivers were set at each 50 m increment after that (*e.g.,* 550 m, 600 m…) that until 700 m distance is reached. The result is presented in Figure 7.15. The wind speed is 15ms^{-1} at the hub height of 80 m. The temperature gradient is 0.05 ºC/m. Due to this increase in temperature with height, rays bend more towards the ground. The emitted ray may hit the receiver directly or after reflection from the ground. When the ray is reflected from the ground additional calculation is necessary to determine refraction loss. In that situation the four adjacent rays that are used initially in the loss calculation also get reflected from the ground. The four adjacent rays used in the refraction loss calculation are 0.1º apart from each other at the time of emission. Refraction loss can be positive or negative (gain) depending on the temperature gradient. From figure 7.15, it is seen that the refraction gain is increasing with increase in distance for all azimuth angles. The ray bends more as it travels further in the air, which causes the change in refraction gain. The gain is small (0.02-0.03 dB) at 200 m from the turbine but can go up to 0.2 dB at 700 m. This value will enhance the total sound pressure level at the receiver. It is also seen that the gain is lower when the ray travels precisely downwind (azimuth angle = 0º) from the source.

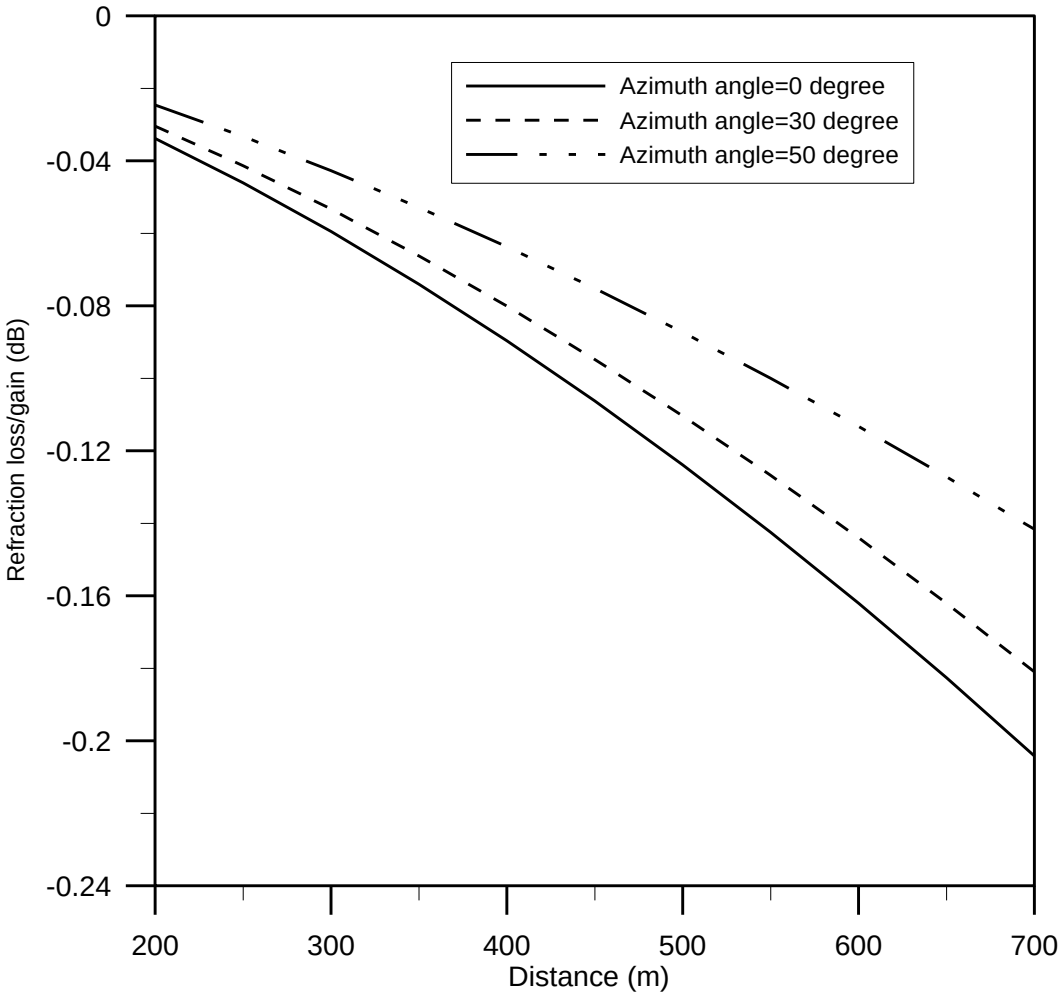

Figure 7.15: Loss due to refraction is plotted with horizontal distance from the turbine in the downwind direction for various azimuth angle. Wind speed is 15 ms^{-1} at the hub height of 80 m. The surface roughness length is z_0=0.01 m. The temperature gradient is 0.05 ºC/m.

7.5 Summation of rays/calculation at the receiver

The computation of ray position after travelling a specific horizontal distance (receiver at 200 m) from the turbine is shown in Figure 7.16. The advantage of this ray model is that the receptor location is not restricted to the downwind direction from the source. It facilitates generation of a contour plot of sound pressure level surrounding the turbine. The rays shown are emitted at zenith angles between 85º-130º, and azimuth angle is varied between 0º-40º. The wind speed is 15 ms^{-1} at the hub height of 80 m and the surface roughness length is 0.01 m. In Figure 7.16 it is seen that the direct rays and reflected rays are distributed over the receiver surface. Receptor plane sound pressure are only considered for z <100 m. The impact points of direct rays and reflected rays on the receiver can be close. The distance in the crosswind direction increases with the increase in the azimuth angle. Care has been taken in differentiating among the direct rays and reflected rays at the receiver. They are presented with different symbols in Figure 7.16.

In Figure 7.17 the positions of the rays on the YZ plane are shown. The rays are mostly evenly distributed, and from the ray positions in this figure, the zenith and azimuth angle for each data point can be worked out. For example, the data points at y=0 are for the rays emitted at azimuth angle zero and zenith angle between 85º-130º. The data point that is at the top on the z axis (and y=0) is emitted at the zenith angle 85º. Then the data points below it corresponds to the rays that emitted at higher zenith angle (> 85º).

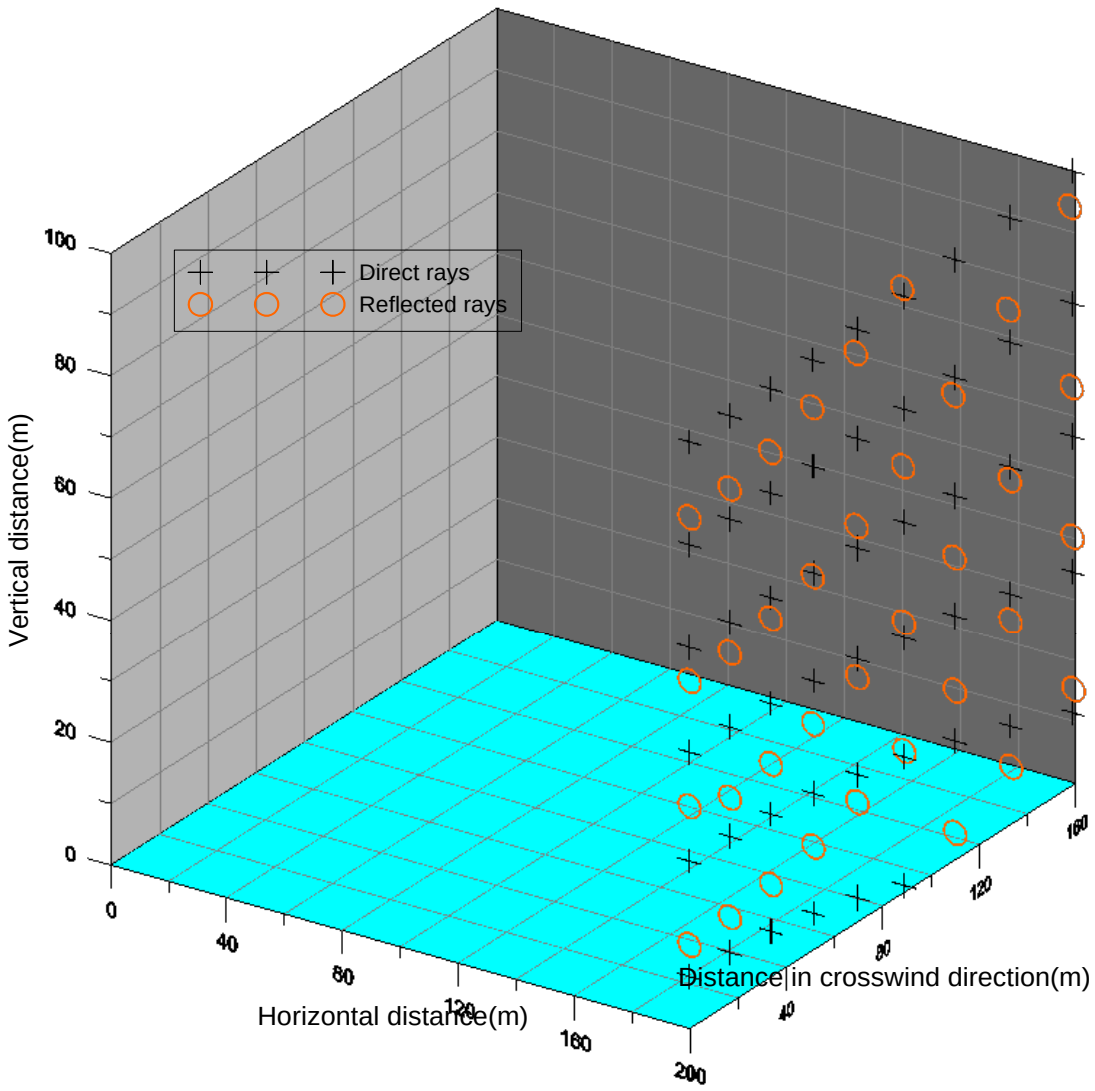

Figure 7.16: Position of rays at 200 m downwind from the turbine. Rays are emitted at 5º separation in the zenith angle between 85º-130º. The azimuth angle was also varied from 0º to 40º with a 5º increase. The wind speed is 15 ms^{-1} at the hub height of 80 m and the surface roughness length is 0.01 m. The lapse rate is 0.006 ºC/m.

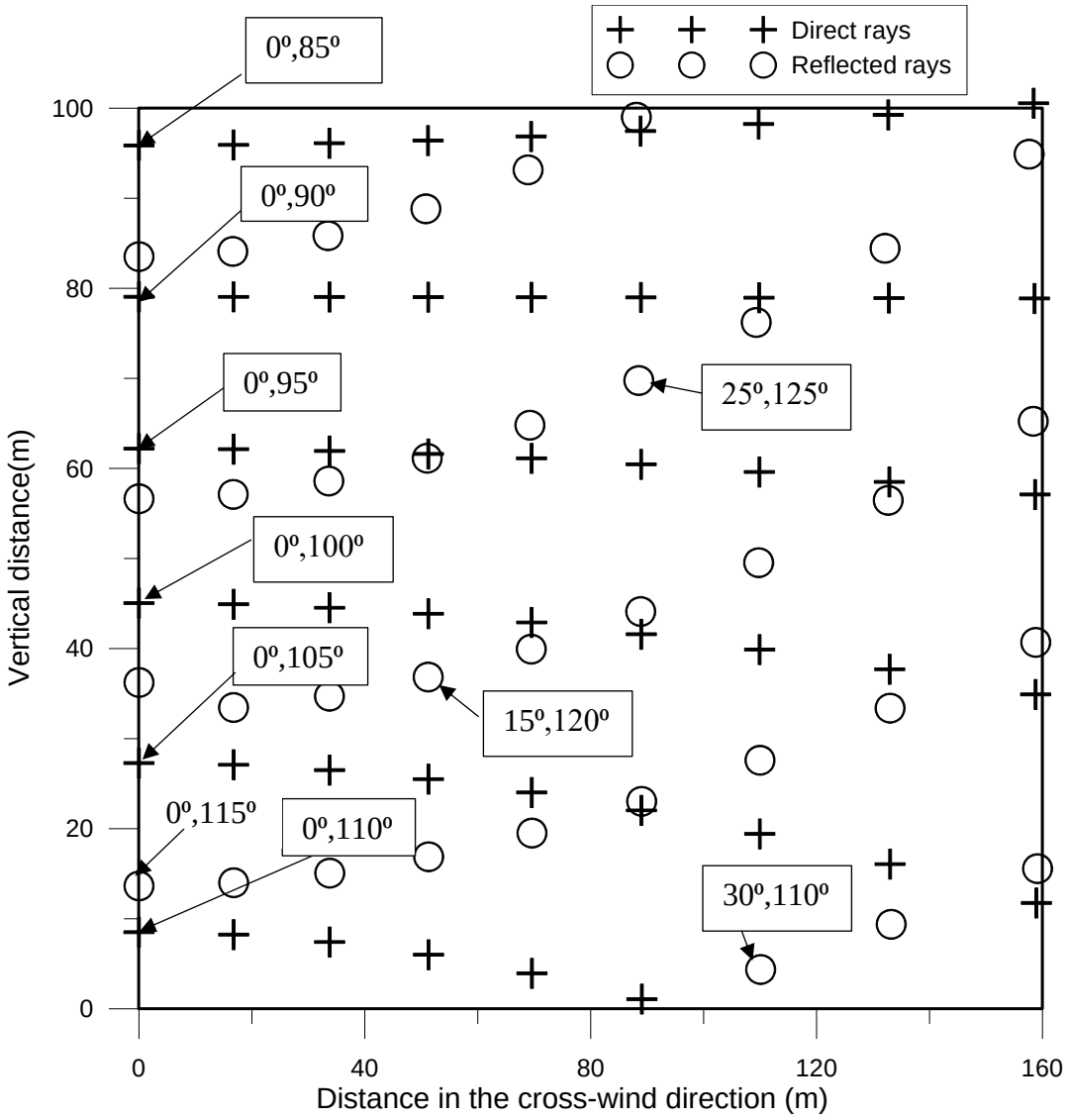

Figure 7.17: Position of the rays from Figure 7.16 are plotted for positions in the vertical and crosswind direction. Rays are emitted at 5º separation in elevation angle between 85º to 130º. The azimuth angle was also varied from 0º to 40º in 5º increments (left to right in the figure).

Once the rays reach receiver, losses are calculated for those rays. Different types of losses are calculated and are discussed below. To establish sound pressure levels for a receptor at a specified y,z position one can interpolate between surrounding 4 direct and 4 reflected rays.

7.6 Relative sound pressure level and excess attenuation

When a sound wave travels in the air it is mostly attenuated in the environment due to spherical spreading and atmospheric absorption which are explained in detail in the previous Chapter 6. Any other attenuation in addition to these two factors is known as excess attenuation. Excess attenuation can be caused by reflection from the ground, barriers such as screens, walls or buildings, refraction, turbulence etc. In the ray model attenuation due to interaction of rays with the ground and refraction are sources of excess attenuation. A term that describes the excess attenuation is relative sound pressure. In Figure 7.18 relative sound pressure associated with interference of direct and reflected rays is calculated for the center frequencies in the one third octave bands. The excess attenuation is calculated here only for two receiver heights, z = 1 m and z = 3 m. The wind speed is 21 ms^{-1} at the hub height of 100 m and varies logarithmically. The sound speed is 340 ms^{-1} at ground level and varies with temperature. The lapse rate is 0.006 °C/m. The receivers are set at 100 m horizontal distance from the turbine base. To compute the relative sound pressure level knowledge about the phase difference between the direct and reflected ray is required. The phase of a ray is determined from the time to reach the receptor and frequency. For each receiver height (*e.g.*, 1 m), two direct rays that reach just above and below that receptor point are traced, and their travel times are recorded. Then the time required by a ray to reach the desired height (1 m) is computed by interpolating between those travel times. The same calculation procedure is repeated for reflected rays. The relative sound pressure level also varies with frequency due to constructive and destructive interference from direct and reflected sound ray. A rigid ground is considered for this case which means 100% of the ray's energy that hits the ground will be reflected. From Figure 7.18, it is seen that the first minimum value of relative SPL occurs at lower frequency for higher receiver height than the lower receiver height. This arises because the frequency at which the

minima occur is inversely related to the receiver height. This relationship will be discussed in detail using equation 7.32 in section 7.11 later in this chapter.

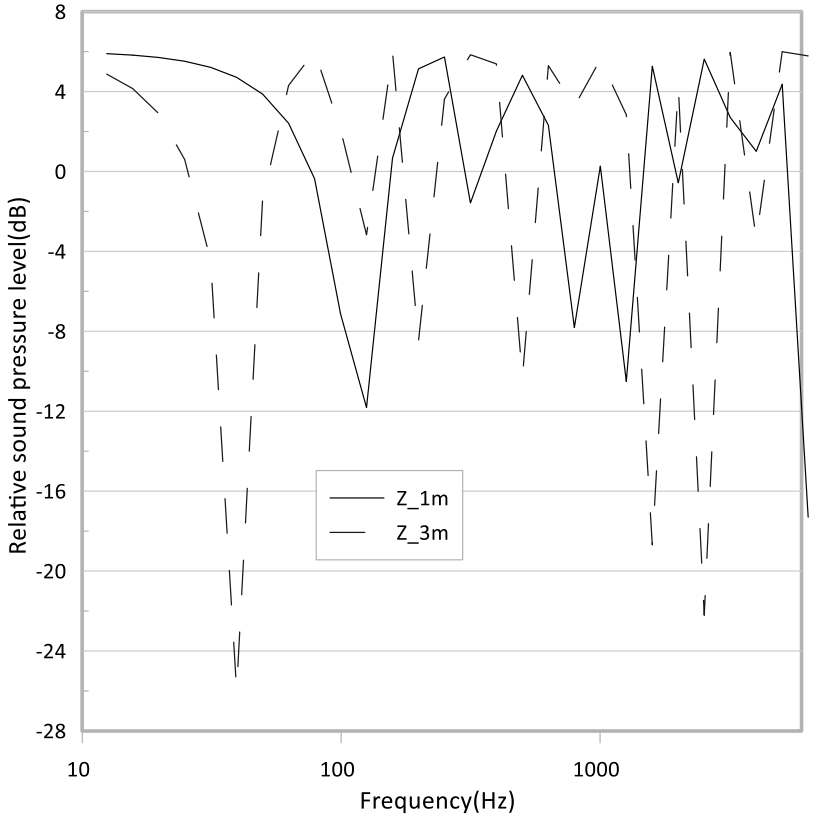

Figure 7.18: Excess attenuation is computed for a single ray for different frequencies at two receiver heights, z= 1 m and 3 m. The parameters chosen for this plot are as follows, rigid ground and lapse rate 0.006 ℃/m. Temperature and relative humidity of the air are 10 ^{o}C and 80%. Wind speed is 21 ms^{-1} at hub height of 100 m, the surface roughness length is, z_0=0.01 m. The receiver is set at a horizontal distance of 100 m. The azimuth angle is 0^{o}.

The total loss including the spherical spreading, atmospheric absorption, reflection and refraction effects is shown in Figure 7.19 with respect to frequency. The receiver is set at three different distance, x=100 m, 300 m and 500 m in the downwind direction from the turbine. The ray is emitted at 100º zenith angle and zero azimuth angle. The ray reaches the receiver at 100 m and 300 m directly. It reflects from the ground once before it reaches the receiver at 500 m. The losses at 500 m for octave band center frequencies are shown in table 7.1.

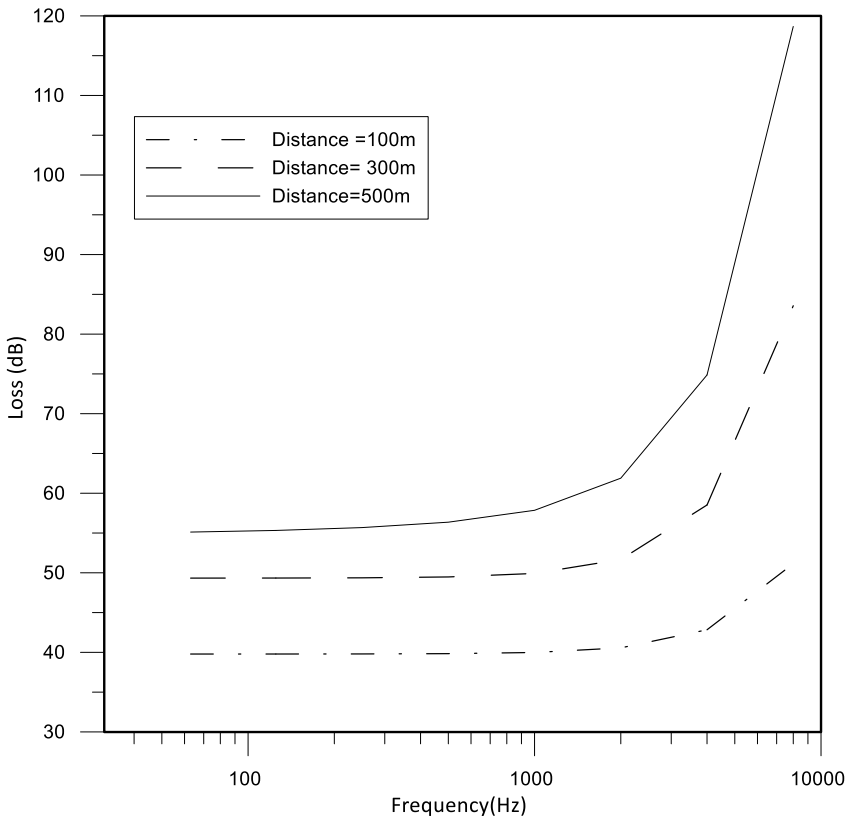

Figure 7.19: The total loss (loss due to spherical spreading, refraction, ground interaction, and atmospheric absorption) is presented along a single ray at 500 m horizontal distance from the turbine. The ray was emitted at 100º zenith angle and zero azimuth angle. The center frequencies (63 Hz-8 kHz) of the octave band are used to produce the results.

Table 7.1: Total loss at 500 m

Frequency (Hz)	63	125	250	500	1000	2000	4000	8000
Aprop* (dB)	53.85	53.85	53.85	53.85	53.85	53.85	53.85	53.85
Aground* (dB)	0.304	0.496	0.807	1.30	2.05	3.14	4.61	6.37
Aatm*(dB)	0.037	0.049	0.095	0.281	1.02	3.97	15.47	57.52
Arefraction* (dB)	0.92	0.92	0.92	0.92	0.92	0.92	0.92	0.92

*Aprop-spherical spreading, Aground-reflection loss, Aatm-atmospheric absorption loss, Arefraction-refraction loss

It is seen that in these three cases, the attenuation does not change significantly for frequencies< 1kHz but increases after 2 kHz. The loss due to spherical spreading usually comprises the highest portion in the total loss. The losses due to atmospheric absorption and ground interaction vary with frequency. Loss due to atmospheric absorption is very low relative to the propagation loss at low frequency and does not have significant impact on the combined loss. But it can be significant at higher frequency and the impact is more evident after 2 kHz. In Figure 7.19, at 500 m distance the total loss is 61.89 dB at 2 kHz. This loss encompasses spherical spreading (53.85 dB), ground interaction (3.14 dB), refraction loss (0.92 dB) and atmospheric absorption loss (3.97 dB). When the frequency approaches 8 kHz then the losses due to reflection and atmospheric absorption increase which changes the total loss. This explains the hike in the loss at 8 kHz in Figure 7.19. The contribution from each frequency band can be added logarithmically to evaluate the overall sound pressure level at a certain distance (not shown in this example). Also note that summation of two decibel values requires converting the dB level to linear scale (dB to Pascal for sound). Then after addition of the losses in the linear scale the resultant is again converted back to logarithmic scale to get the value in decibels.

7.7 Atmospheric absorption of sound

Loss due to atmospheric absorption is also included in the model. The energy from the sound gets absorbed in the surrounding medium during propagation of sound through the medium. Key factors contributing to atmospheric absorption include thermal conductivity, molecular relaxation and shear viscosity (Evans & Bass, 1971-09). The sound wave energizes the air molecules and energy is transmitted into the medium.

Loss due to viscosity and thermal conductivity is termed “classical absorption” (Salomons, 2001). Another type of absorption occurs when the sound moves through the air and excites the diatomic nitrogen and oxygen molecules. The water, nitrogen and oxygen molecules collide among each other and the excited electrons within each atom jump to a higher energy state. The vibrating electrons in the higher energy shell move back again to their normal state and dissipate the excess energy as heat. The time required by the electrons to go back to their relaxed states is known as relaxation time. It takes several collisions to come back to the translational or relaxed state. The relaxation time is different for different mechanism of energy transfer and results in three different scenarios. First scenario occurs when the relaxation time is longer than the time required to complete one cycle of the sound wave. In this case the time taken by the electrons to jump to the excitation level and come back again to the initial relaxed mode is so long that it does not affect the compression and expansion of the sound wave. In scenario number two, the relaxation frequency is very short and does not affect the sound wave. In the third case, the relaxation time matches the frequency of the sound and hence poses added attenuation. The relaxation period is dependent on the presence of water particles in the air. Vibrational relaxation time is greatly

reduced by the presence of water molecules. So, absorption is considerably higher in dry air (Sen, 1990).

The loss due to atmospheric absorption can be measured by computing the absorption coefficient. It is calculated from the absolute temperature, the relative humidity and the atmospheric pressure (Salomons, 2001). The absorption coefficient(dB/km) is multiplied by the distance travelled by the ray to compute the loss. The equations for the absorption coefficient are as follows,

$$\alpha = 8.686 f^2 \tau_r^{0.5} [1.84 \times 10^{-11} \rho_r^{-1} + \tau_r^{-3} (b_1 + b_2)] \qquad (7.20)$$

Here,

$$\tau_r = \frac{T}{T_{20}}$$

and

$$\rho_r = \frac{P_a}{P_r}$$

T= temperature in Kelvin, T_{20}= 293.15 K, P_r= 1 atm or 101325 Pascal, P_a=atmospheric pressure

$$b_1 = 0.1068 exp \frac{\left(\frac{-3352}{T}\right)}{\left(f_{r,N} + \frac{f^2}{f_{r,N}}\right)} \qquad (7.21)$$

$$b_2 = 0.01275 exp \frac{\left(\frac{-2239.1}{T}\right)}{\left(f_{r,O} + \frac{f^2}{f_{r,O}}\right)} \qquad (7.22)$$

Where $f_{r,N}$ and $f_{r,O}$ are relaxation frequencies of oxygen and nitrogen. The relaxation frequency is the frequency where the maximum loss occurs. These can be computed by the following equations.

$$f_{r,N} = \rho_r \tau_r^{-0.5} \left(9 + 280h \, exp\left(-4.17\left[\tau_r^{-\frac{1}{3}} - 1\right]\right)\right) \qquad (7.23)$$

$$f_{r,O} = \rho_r \left(24 + 40400h \, \frac{(0.02 + h)}{(0.391 + h)} \right) \qquad (7.24)$$

Here *h* is the molar concentration of water vapour in the air calculated from the relative humidity, water vapour pressure and saturation vapour pressure. Loss due to atmospheric absorption is frequency dependent and increases with increase in frequency.

The absorption coefficient calculated using the equations (7.20-7.24) is shown in Figure 7.20 as a function of frequency. It is seen that there are three distinct regions where the total absorption coefficient is dominated by three mechanisms of absorption. The frequency region below the relaxation frequency of nitrogen ($f_{r,N}$ = 272.3 Hz*)*) is dominated by nitrogen relaxation. The region between $f_{r,N} < f < f_{r,O}$ is governed by oxygen relaxation. Above the relaxation frequency of oxygen ($f_{r,O}$ = 28510.41 Hz) the total loss coefficient approaches the classical attenuation (Salomons, 2001).

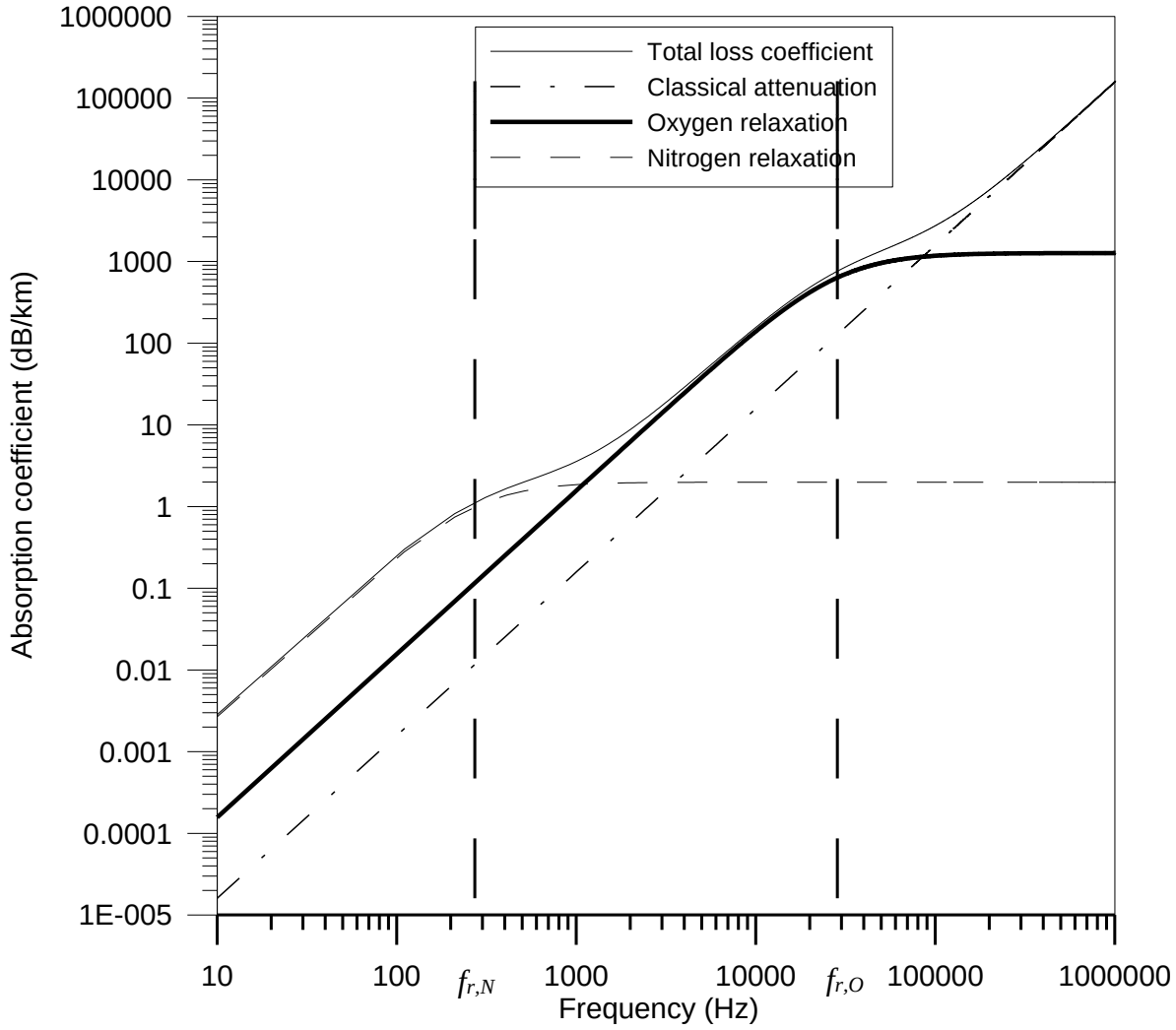

Figure 7.20: Absorption coefficient is presented as a function of frequency. The temperature is 10°C, the relative humidity is 80% and the atmospheric pressure is 1atm.

A theoretical method is described by Evans and Bass (1971) to predict atmospheric absorption. The results from the model are compared with their experimental data. The atmospheric absorption can be divided into two categories based on the mechanism. One is classical absorption where

during sound wave propagation through the air the kinetic energy of the air molecules converts into heat. Classical absorption can be subdivided into four groups. They are viscous loss, heat conduction loss, diffusion loss, and loss due to radiation. The viscous loss and heat conduction loss are known as Stokes-Kirchhoff loss and constitute the major contribution in the classical absorption loss calculation.

Sound absorption due to vibrational relaxation can be calculated from the concentration of each gas present in the air and the energy transfer rates (Evans & Bass, 1971-09). Evans and Bass (1971) predicted the energy transfer rate for 24 energy transfer mechanisms. If the constituent gases in the air are known, sound absorption can be computed using the energy transfer rates. The reason behind using 24 mechanisms is that different mechanisms are dominant in different atmospheric situations. It was concluded that if the constituent gases are known in an unknown atmosphere and the energy transfer rates among those gases are determined, then atmospheric absorption can be calculated from that information. Their final result was a graphical presentation of absorption coefficient as a function of frequency for a range of relative humidity values. This is shown is Figure 7.21. Data from the graph can be used to calculate air absorption. From the graph it is very clear that absorption is dependent on the presence of water vapour in the air. For instance, at 4 kHz, the value of absorption coefficient is 109 dB/km at 10% RH, but this value goes down to 10 dB/km at 100% RH. To further simplify the computation of this type of loss, equations (7.20) - (7.24) were developed later.

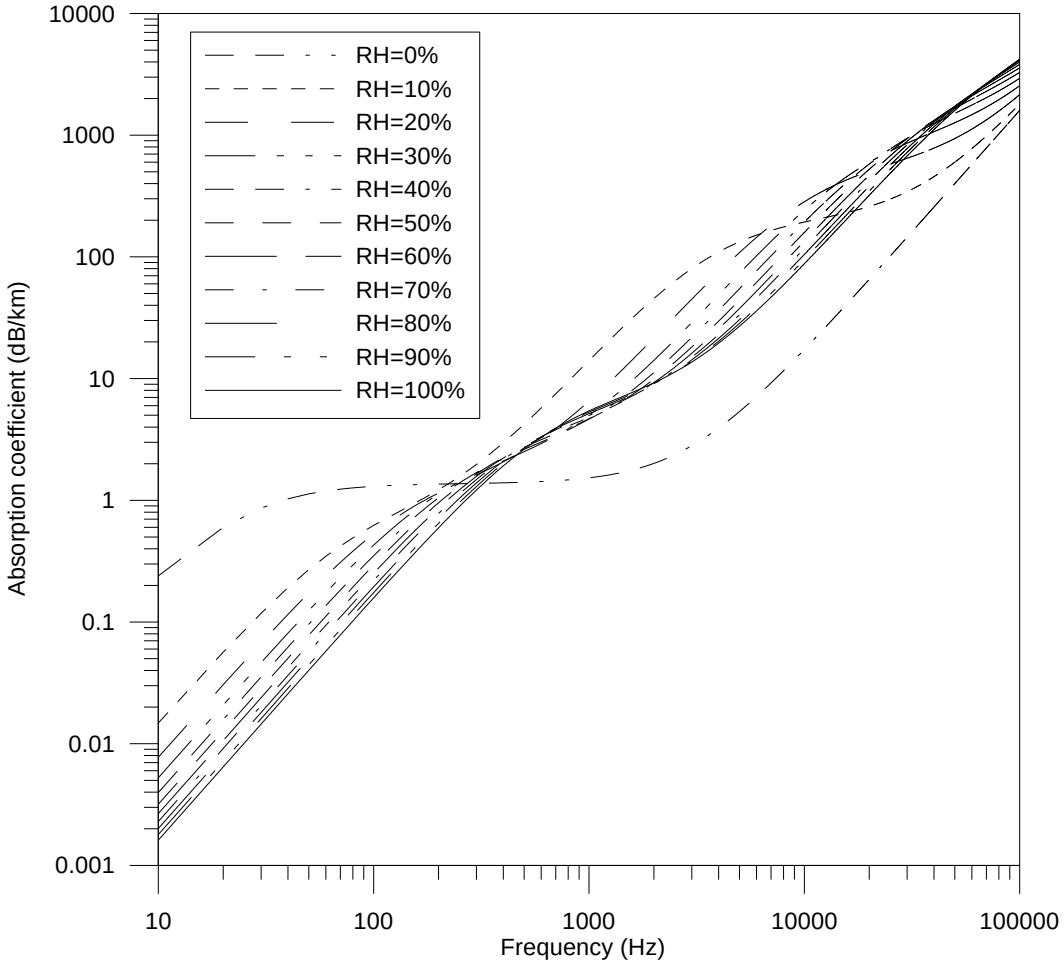

Figure 7.21: Air absorption coefficient is plotted as function of frequency at 20 ℃ and relative humidity for 0-100%.

From Figure 7.21 it is seen that the value of the absorption co-efficient for 10% RH and 400 Hz is 3 dB/km. This means that the sound pressure squared is reduced to half over one kilometer. When the absorption co-efficient is 10 dB/km at 1 kHz for 10% RH, the sound pressure squared becomes one tenth after travelling 1 km in the atmosphere.

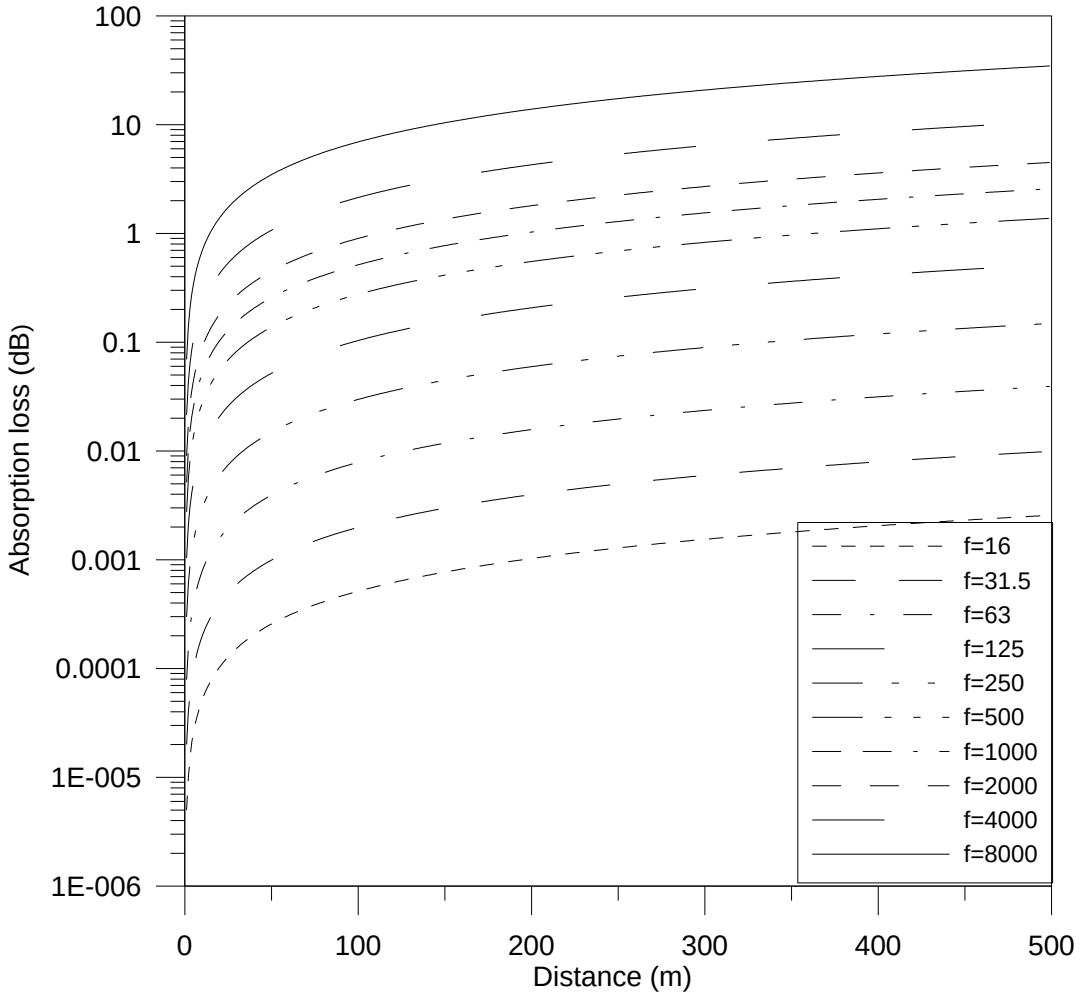

Figure 7.22: Air absorption loss with respect to distance from the source is shown for different frequencies (Hz). Octave band frequency is used for calculation. The relative humidity is 80%, air pressure is 1 atm and temperature is 20 ℃.

In Figure 7.22 air absorption loss is presented for distance from the source for different frequencies. Absorption loss is very low for low frequency and smaller distance and it gradually increases with both frequency and distance from the source.

7.8 Ground attenuation

The rays emitted from a source can reach the receiver directly. There are some rays that touch the ground and reach the receiver after one or multiple reflections from the ground surface. When a sound ray touches the ground, some energy gets absorbed, and the rest of the sound energy is reflected to the atmosphere (Long, 2014). This incident can be expressed by the following equation,

$$E_I = E_r + E_a \qquad (7.25)$$

Here, E_I = Energy of the incident sound wave

E_r = Energy of the reflected sound wave

E_a = Energy of the absorbed sound wave at the surface of material

If the above equation is divided by the incident energy it becomes,

$$1 = \frac{E_r}{E_I} + \frac{E_a}{E_I} \qquad (7.26)$$

Here, the second term on the right-hand side of the above equation is the reflection coefficient,

$$R_p = \frac{E_r}{E_I} \qquad (7.27)$$

The reflection co-efficient can be expressed in terms of ground impedance (Z) by the following equation. The ground impedance is the measure of resistance to the propagation of sound.

$$R_p = \frac{cos\varphi - {\rho c}/{Z}}{cos\varphi + {\rho c}/{Z}} \qquad (7.28)$$

Here φ is the incident angle of the sound ray and ρ is the air density (kgm^{-3}) and c is the speed of sound in the air (ms^{-1}). The incident angle is the angle between the ray and the ground surface

normal at the point of incidence. If it is zero ($\varphi = 0^o$), the incident ray will be reflected at the same angle and the ground attenuation will depend on the impedance of the surface. The amplitude and phase of the reflected wave get altered by the nature of the ground surface. To depict the effect of surface attenuation characteristics impedance is often used. There are several ground impedance models available to determine the ground attenuation. One of them is the model developed by Delaney and Bazley (1970). Their model was established based on experimental results. A large sample of commercial fibrous absorbent material were used. In this model impedance is dependent on the frequency and the flow resistance of the material. So, impedance data were collected for materials with wide range of flow resistivity and frequency. The impedance tube measurement method was used for the experiment. Flow resistance per unit thickness was measured directly across the sample material by sending a volume of air of known velocity through it. Impedance data recorded from the experiment were normalized with impedance of air (ρc) and plotted against frequency normalized by flow resistance. Equations to calculate impedance were derived by fitting a curve to those data. Normalized impedance calculated using the Delany and Bazley model is plotted in Figure 7.23. The real part (R) of the ground impedance decreases with frequency and the imaginary part(X) increases with frequency. The equations are given in Chapter Six.

Normalized impedance is plotted in Figure 7.24 and Figure 7.25 for different frequencies by varying flow resistance. Flow resistance only varies with the bulk density, the size of the fiber and the direction of the sound propagation through the material. In this model the sample material was considered isotropic so there was no variation with the direction of the flow. For wind turbine locations, the topography can be considered as land covered with short grass. A typical value of flow resistivity for this type of surface is 200 $kPa.s.m^{-2}$ (Salomons, 2001).

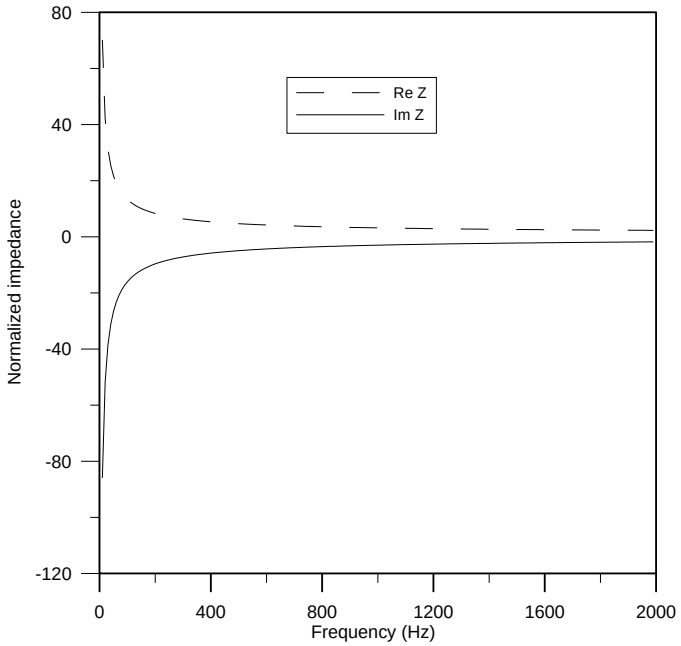

Figure 7.23: Normalized impedance is plotted for a range of frequencies. The flow resistance for this case is 150 kPa.s.m^{-2}, ρ is 1.2 kgm^{-3} and sound speed is 340 ms^{-1}.

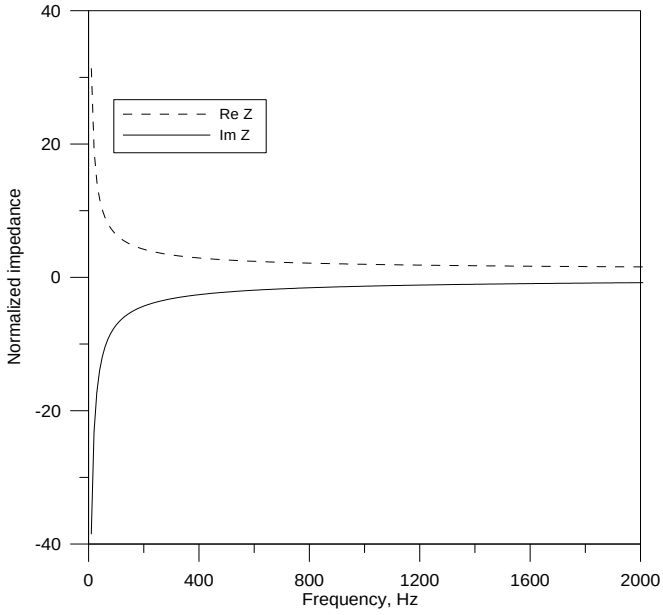

Figure 7.24: Normalized impedance is plotted for a range of frequencies. The flow resistance for this case is 50 kPa.s.m^{-2}, ρ is 1.2 kgm^{-3} and sound speed is 340 ms^{-1}.

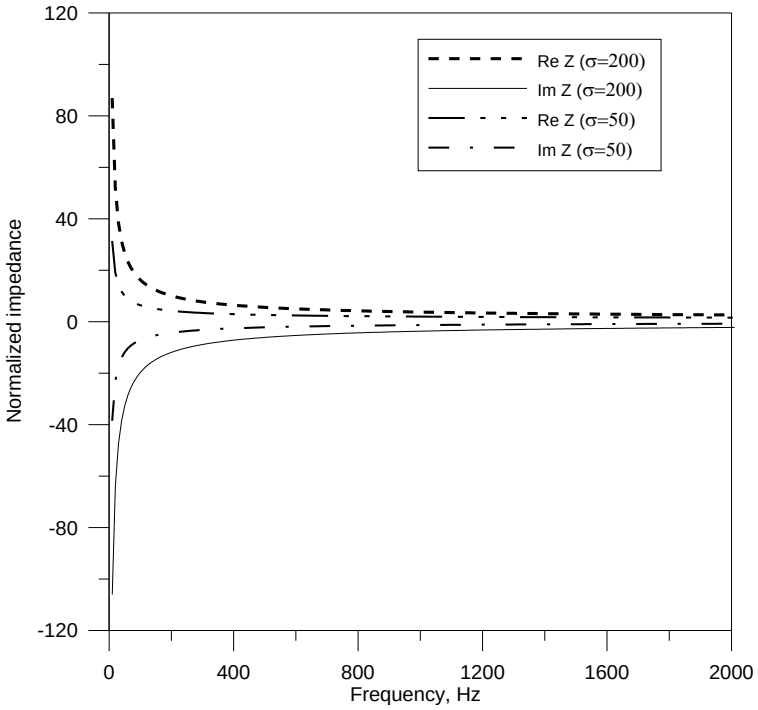

Figure 7.25: Normalized impedance is plotted for a range of frequencies. The flow resistances for this case are 200 kPa.sm^{-2} and 50 kPa.s.m^{-2}, ρ is 1.2 kgm^{-3} and sound speed is 340 ms^{-1}.

Loss due to ground attenuation during the reflection of a sound wave is calculated and presented in Figure 7.26. The loss is computed as a function of frequency for different values of angle of incidence. The high frequency sound is attenuated significantly, and the loss can be as high as 16 dB at high frequency. It also increases with the angle of incidence. From equation 7.28, it is evident that the reflection co-efficient decreases with increase in incident angle and the attenuation rises.

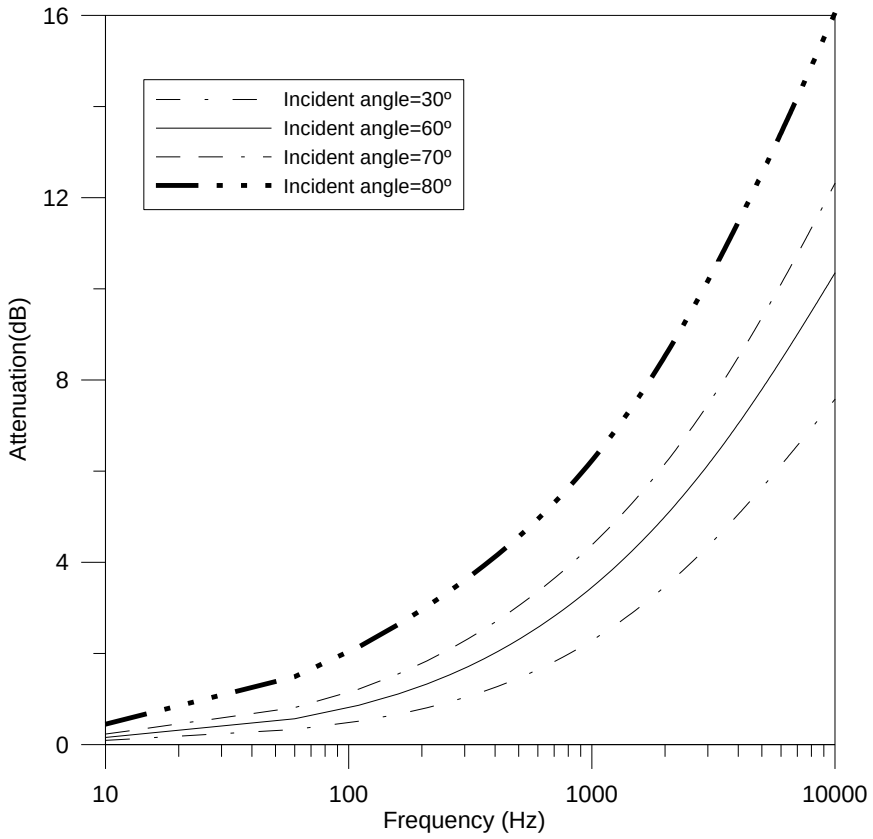

Figure 7.26: Loss due of interaction of sound wave with ground is calculated for a range of frequencies. The values of angle of incidence are 30º, 60º, 70º, 80º. The flow resistivity is 200 kPa.s.m^{-2}, ρ is 1.2 kgm^{-3} and sound speed is 340 ms^{-1}.

There are other models that are used to calculate ground impedance. Zwikker and Kosten (Salomons, 2001) developed a model based on the porosity, structure constant and the flow resistivity of the porous material. Due to the presence of pores the volume of air is less in a porous material than in air. Porosity in the volume fraction of air in the material. The structure constant is dependent on the shape of the pores and the frame of the material.

Attenborough (Salomons, 2001) developed a more refined four parameter model. In his model pore shape factor, grain shape factor, flow resistivity, porosity was adjusted to define different types of ground surface. The ground impedance measured from the model was compared with experimental data. A good agreement was found between them.

Reflection coefficient is calculated from the ground impedance and is used to determine the attenuation to the incident wave. Ground attenuation depends on the angle of incidence. In Figure 7.27 reflection coefficient is plotted for angle of incidence.

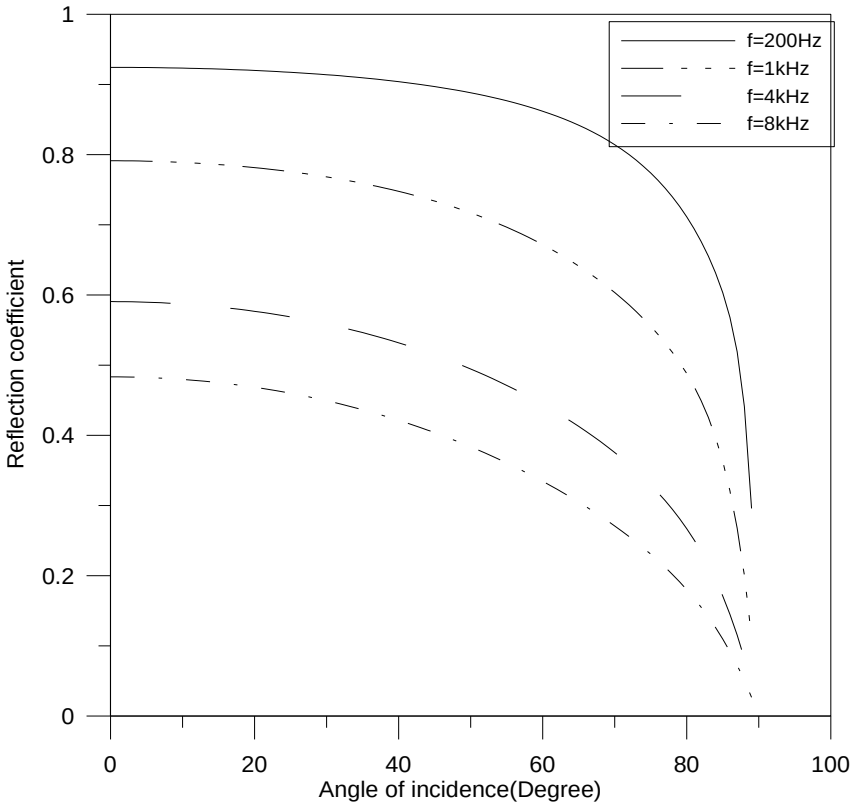

Figure 7.27: Reflection coefficient vs angle of incidence is shown in this figure. The flow resistance for this case is 200 kPa.s.m^{-2}, ρ is 1.2 kgm^{-3}, frequency is 1 kHz and sound speed is 340 ms^{-1}.

When the angle of incidence is zero the ray is perpendicular to the ground and the rays are reflected at zero reflection angle. The value of reflection coefficient is close to 1. As the angle of incidence increases the value of the reflection coefficient goes down. When the angle approaches 90º the reflection co-efficient is close to zero. It is also seen that the reflection coefficient decreases with increase in frequency. A lower vale of reflection coefficient means more sound energy will be absorbed by the ground and the ground attenuation will increase.

7.9 Total loss

The sound ray emitted from a source is modified by spherical spreading, refraction due to wind and temperature gradients, atmospheric absorption and interaction with ground. Among the losses, the maximum decrease in sound pressure level occurs due to spherical spreading. Refraction can cause losses or gains, sometimes represented as negative losses. The losses are shown in Figure 7.28 in a pie chart as a proportion of the total loss. For this figure a ray with zenith angle of 100º and zero azimuth angle is emitted from the source. The frequency of the ray is 2000 Hz, and the flow resistance is 200 kPa.s.m^{-2}. The wind speed is 15ms^{-1} at the hub height of 80m and surface roughness length is 0.01m. The receiver is set at 500m from the base of the turbine and the ray is reflected once before it reaches the receiver. The losses are presented as percentages. If the total loss is 100% (61.42 dB) then 87.64% (53.81 dB) of that loss occurs due to spherical spreading during propagation in the atmosphere. Atmospheric absorption covers 6.4% (3.95 dB), reflection loss is 5.1% (3.14 dB) and refraction loss is 0.81% (0.5 dB).

From Figure 7.28 it is apparent that loss due to distance travelled by the sound occupies the largest slice of the pie. The second highest portion is 6.4% of the total circle and it is the loss due to

atmospheric absorption. But this loss varies with frequency. In this situation with a low lapse rate, the least amount of loss takes place due to refraction (0.81 %). The combined value of atmospheric absorption loss, refraction loss and ground interaction loss is 7.61 dB which is significantly less than the propagation loss (53.81 dB).

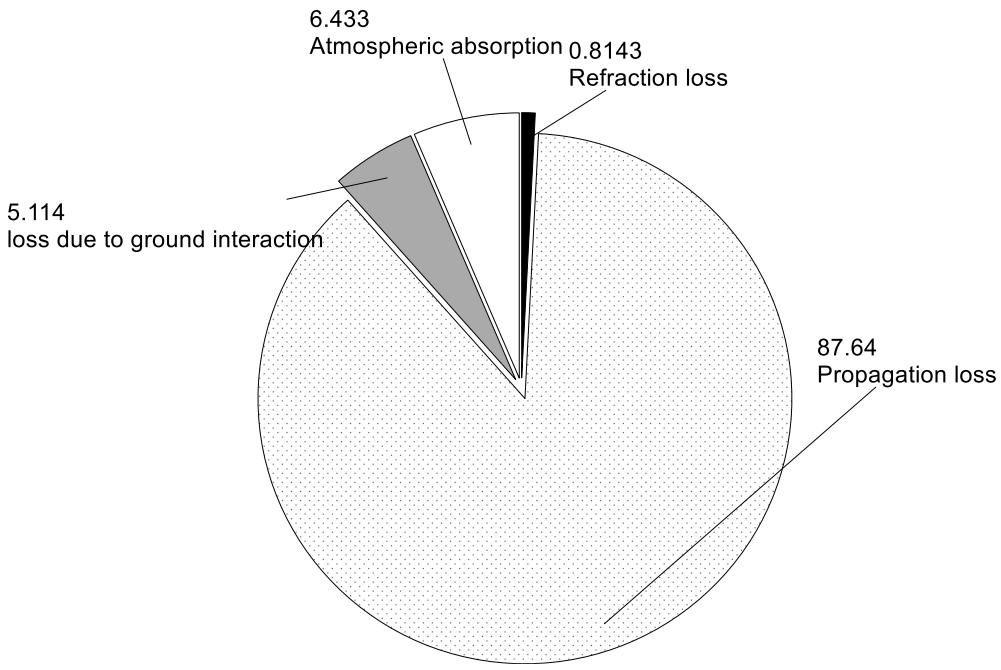

Figure 7.28: Loss at 500 m distance due to spherical spreading, atmospheric absorption, interaction with ground, and refraction is shown for a single ray emitted at 100º zenith angle and zero azimuth angle. The frequency of sound is 2 kHz and flow resistance for this case is 200 kPa.sm^{-2}. The wind speed at hub height of 80m is 15 ms^{-1}. The surface roughness length is 0.01 m. The lapse rate is 0.006 ºC/m.

7.10 Sound pressure level at the receptor location calculation

A large data set was created using the ray model by emitting 120×20 rays from the source location (0, 0, Hub height) over regular flat terrain. A receiver plane is set at a distance of 500 m downwind from the turbine base, X=500m and can be defined by varying values of y and z. When a ray intersects the receptor plane the azimuth, zenith angle, travel time, propagation direction, refraction loss, ground absorption loss, atmospheric absorption loss and the combined loss are calculated and recorded in a file.

A grid is specified by a range of values for y and z for interpolation onto single or multiple target points (YT, ZT). A triangle based linear interpolation technique using 3 surrounding points (in MATLAB) is used to find out the attenuation at the desired location. The unit of the total loss is dB.

In Figure 7.29 rays are emitted from zenith angles between 90º and 110º and at various azimuth angles in the downwind direction. The hub height is 80m and a logarithmic wind profile is used. The total loss presented in the graph includes loss due to spherical spreading, refraction loss and atmospheric absorption loss. The loss is computed for only direct rays and so no reflection loss is calculated. It is seen that the total loss increases as the distance in the crosswind direction increases from the turbine base. The reason is the loss due to spherical spreading is dependent on the distance travelled by the ray and hence the value is higher in both directions from the middle. It is also evident that the total loss has the same value at the same distance in both directions. For example, at 200 m on both direction the loss is 54.6 dB. The positions of the rays on the receiver plane are shown in Figure 7.30.

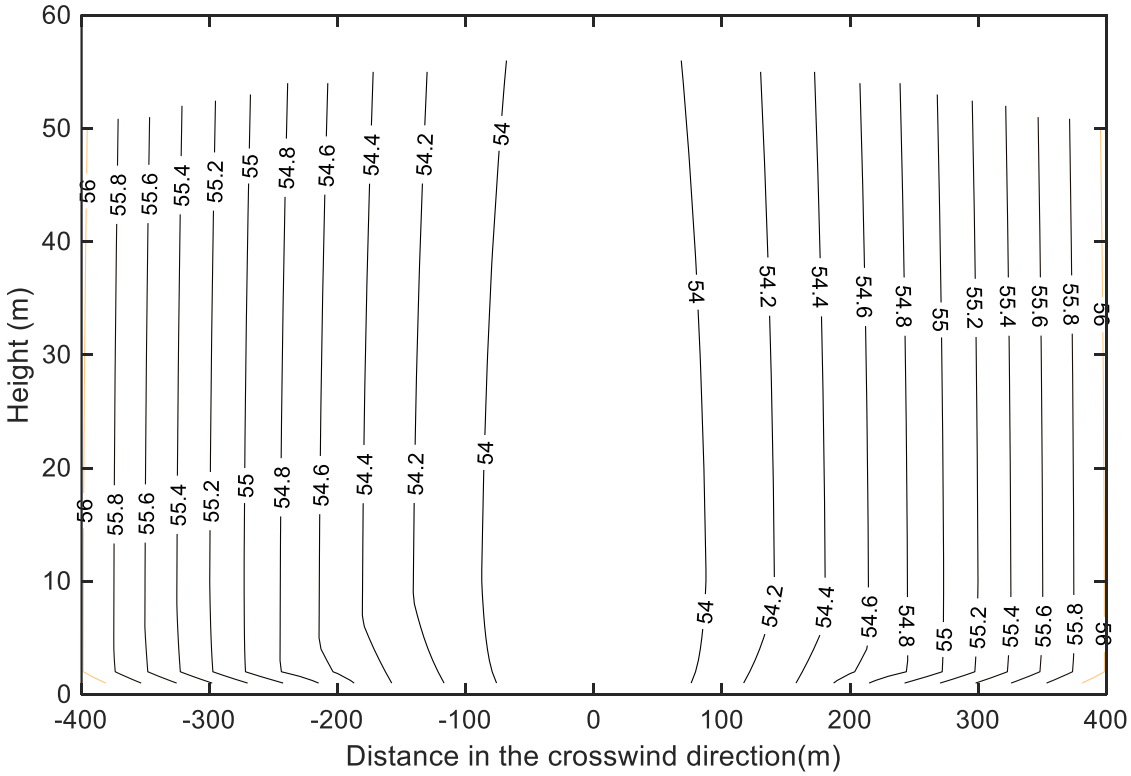

Figure 7.29: Contours of total loss for direct rays on a y, z grid at x=500 m. The azimuth angle, θ was varied from -60º to 60º and the zenith angle, ϕ was varied from 90º-110º to create the data set for interpolation. The temperature is 10 ºC and wind speed is 15 ms^{-1} at the hub height of 80 m. The wind speed varies logarithmically, and a temperature gradient of -0.006 ºC/m is used. Frequency is 1000 Hz for this calculation.

In Figure 7.31 rays with same range of zenith and azimuth angles have been used. But in this case losses are calculated for only rays that reached ground and had been reflected before hitting the receiver surface. As the contours are generated within 500 m from the turbine the rays are reflected only once from the ground.

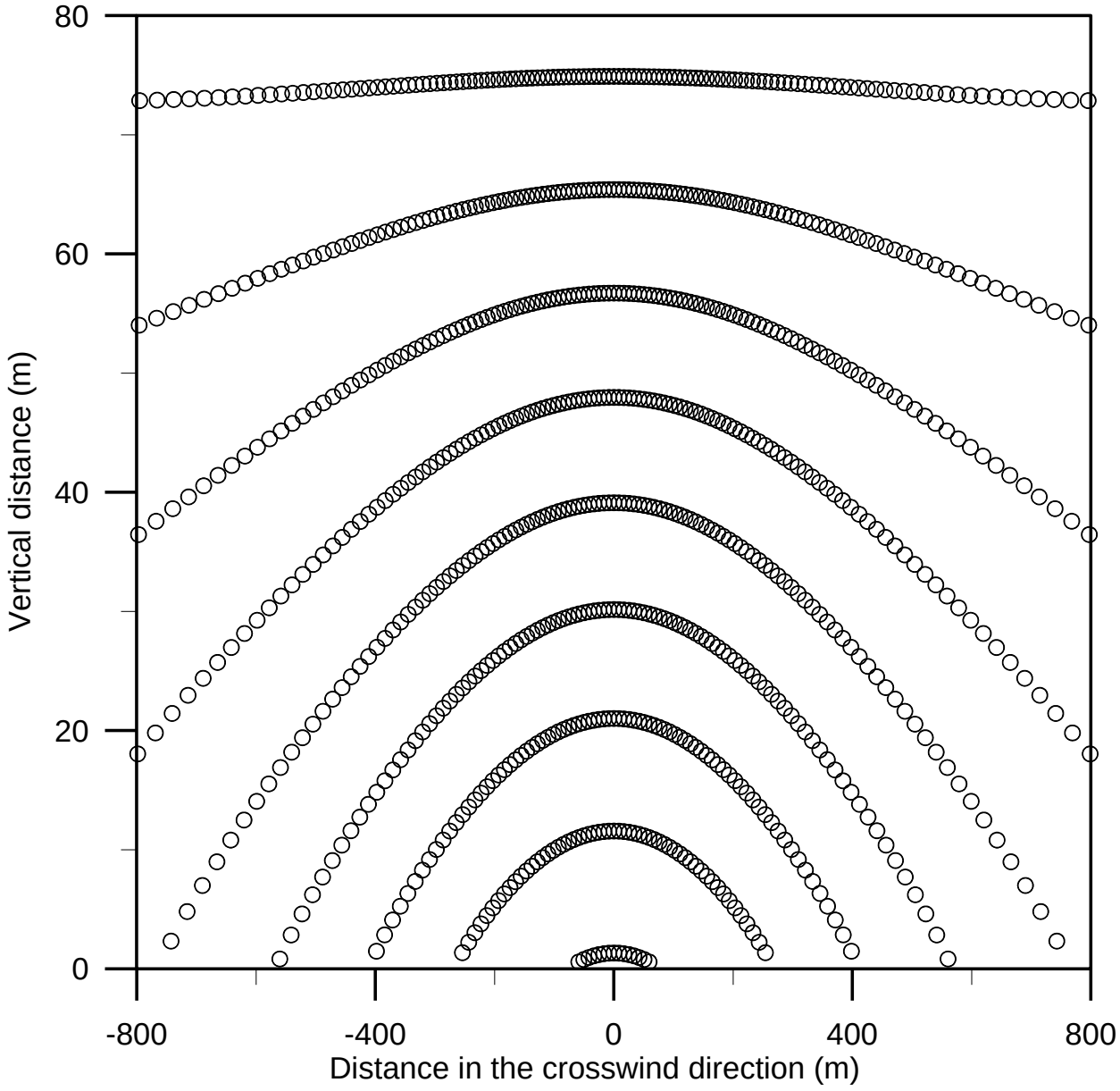

Figure 7.30: The position of the direct rays used in the previous figure to generate contours of total loss on the YZ plane. The azimuth angle, θ was varied from -60º to 60º and the zenith angle, ϕ was varied from 90º-110º to create the data set for interpolation.

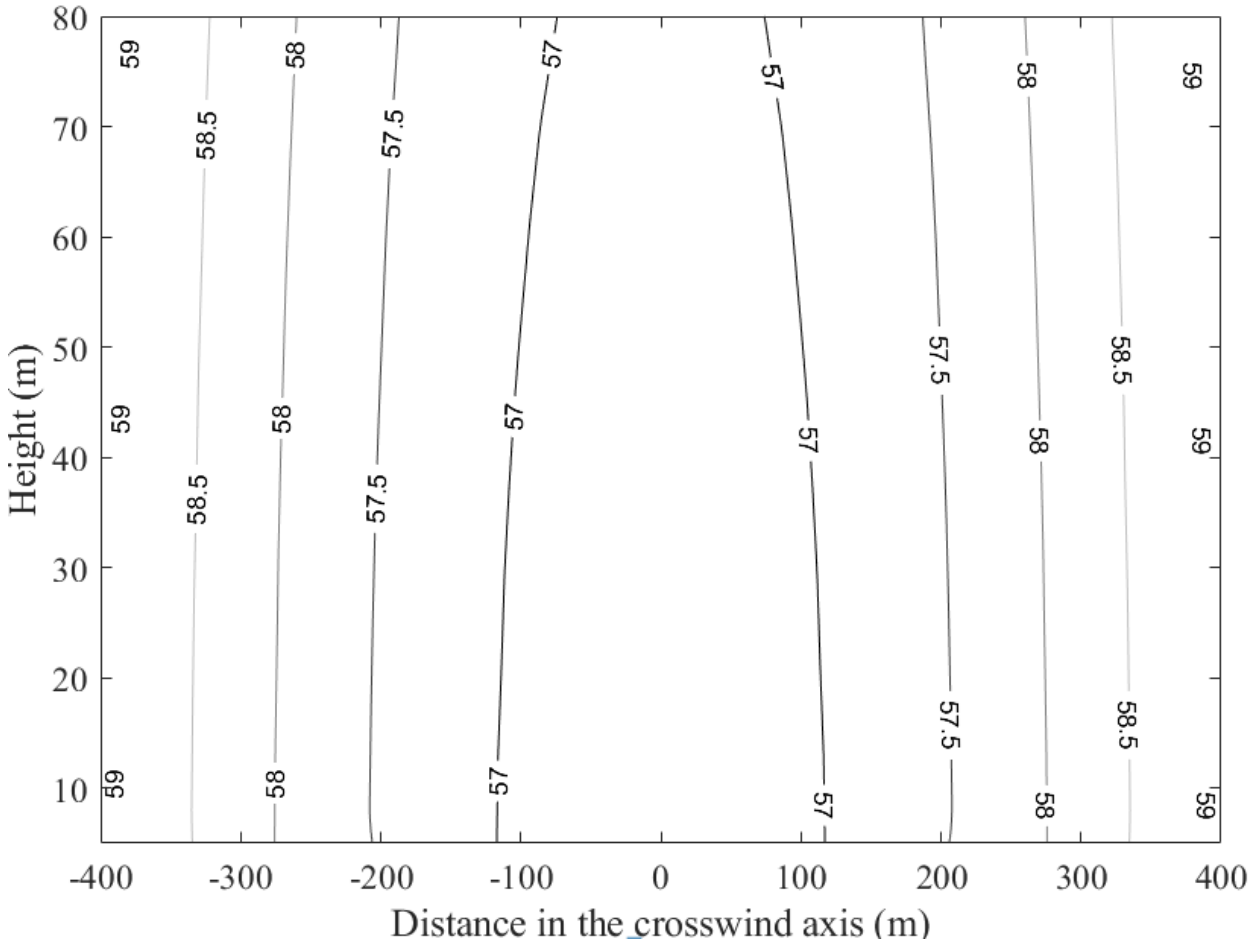

Figure 7.31: Contours of total loss for reflected rays on a grid for heights between 0 m to 80 m from the base of the turbine. The azimuth angle, θ was varied from -60º to 60º and the zenith angle, ϕ was varied from 90º-110º to create the data set for interpolation. The temperature is 10 ºC and wind speed is 15 ms^{-1} at the hub height of 80 m. The wind speed varies logarithmically, and a temperature gradient of -0.006 ºC/m is used.

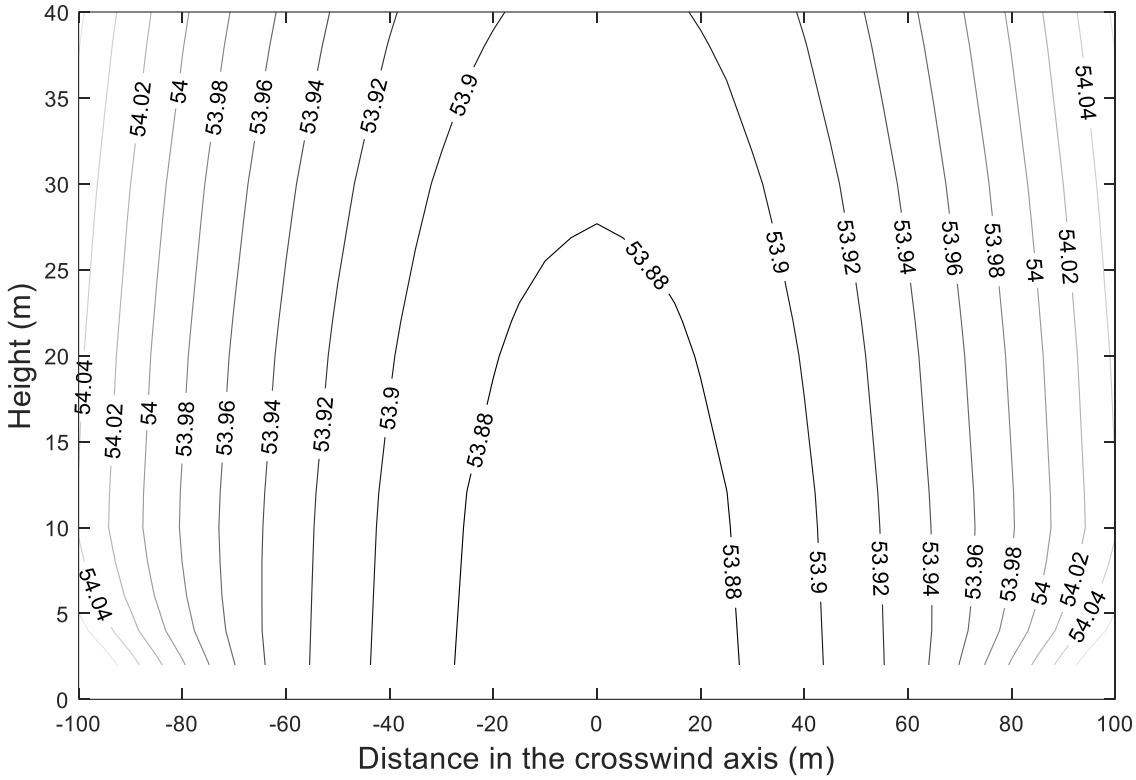

Figure 7.32: Contours of total loss for direct rays on a grid within 100 m from the base of the turbine in the crosswind direction. Loss is calculated at the receiver location, x = 500 m. However, the contours are shown only up to 100 m in crosswind direction on both sides of x axis. The azimuth angle, θ was varied from -60º to 60º and the zenith angle, ϕ was varied from 90º-110º to create the data set for interpolation. The temperature is 10 ºC and wind speed is 15 ms^{-1} at the hub height of 80 m. The wind speed varies logarithmically, and a temperature gradient of -0.006 ºC/m is used.

In Figure 7.32 the same set of rays are used to generate contours of loss within 100 m of the turbine base in the crosswind direction. The same wind and sound speed profile are used. It is seen that the value of loss is lower directly downwind of the turbine with less spherical spreading, and it increases with lateral distance. This graph also has same values of loss at the same distance at both sides of the turbine. Figure 7.33 shows contours of loss for only reflected rays, presented in a smaller region, and only extending up to 40m height.

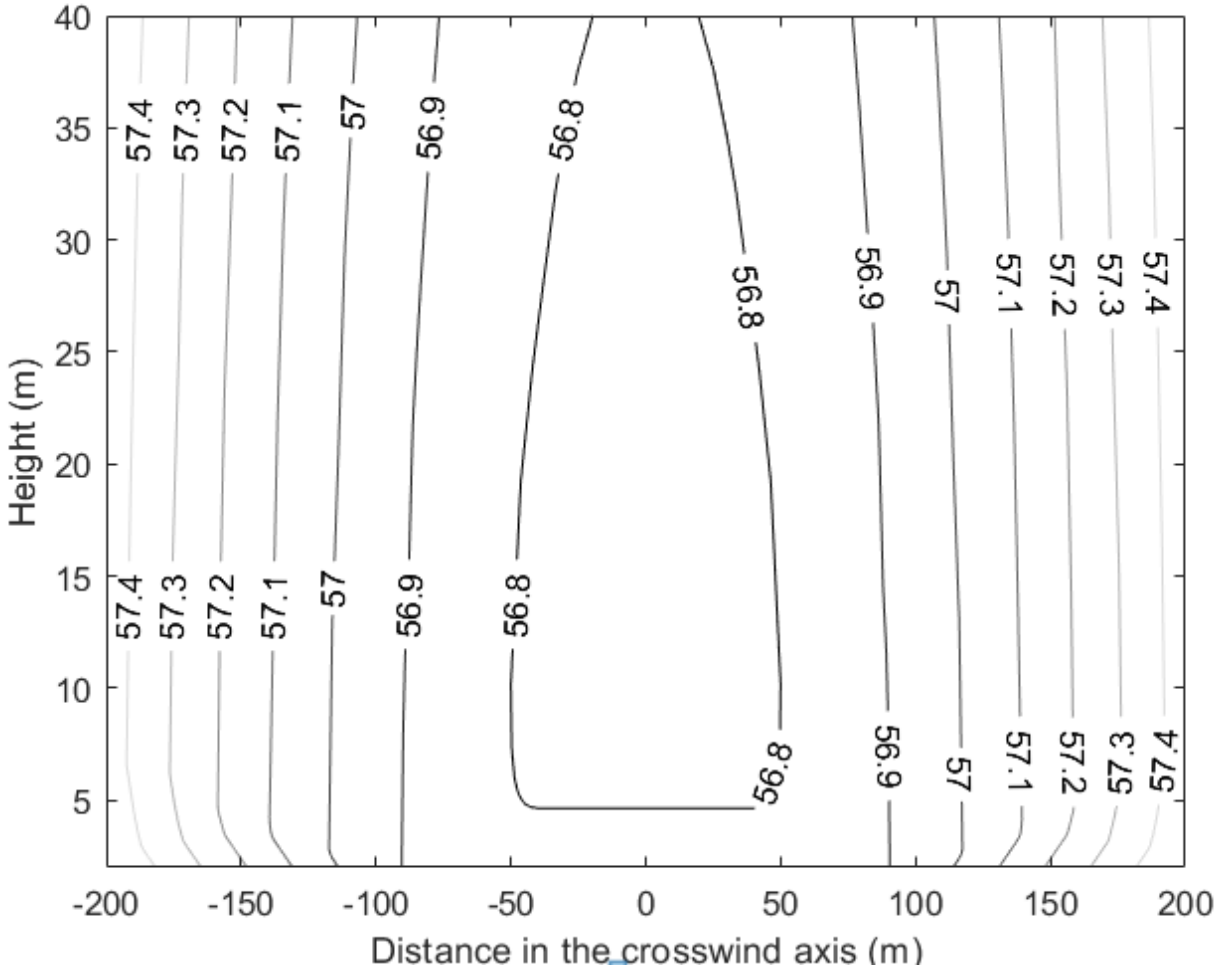

Figure 7.33: Contours of total loss for reflected rays on a grid at x=500 m from the base of the turbine and within 200 m in the crosswind direction. The azimuth angle, θ was varied from -60^o to 60^o and the zenith angle, ϕ was varied from 90^o-110^o to create the data set for interpolation.

The vertical distance is 40m.The wind and sound speed profiles are similar to the previous cases. The total loss does not change drastically with increase in lateral distance. The contours are evenly spaced in the entire region. The main contribution to total loss is from spherical spreading and increases in source-receptor distance account for most of the y variations.

7.11 Comparison of results

In this section some results from the ray model will be compared with similar cases presented in the book by E.M. Salomons (2001). In the book, sound pressure level has been computed at the receiver location by several different methods, including a ray model and a parabolic equation (PE) model. For comparison with our ray model, cases from the book have been selected that consider simple reflection from a hard ground surface. Comparison with some results showing the effects of refraction in the atmosphere will also be included.

When sound is emitted from a point source in an unbounded atmosphere the intensity decreases, as $1/s^2$, a result of wave front spreading with distance, s, and due to absorption in the air. Sound rays can reach the receiver location directly and/or after reflection from the ground. If the ground is hard, the sound ray is fully reflected. But if the ground is partially absorptive, a portion of sound is absorbed and the rest if reflected. When both direct and reflected sound rays reach the receiver location, the combined sound pressure level depends on their amplitudes and phase difference. In Figure 7.34 a case with no wind and no refraction and a simple single reflection from the ground is shown. In the figure the height of the point source and the receiver are z_s and z, respectively. In

this case a simple analytic solution is possible. The sound pressure level, L_p, at the receiver can be written, in decibels, as

$$L_p = L_{p,free} + \Delta L \qquad (7.29)$$

Here $L_{p,free}$ represents the sound pressure level (dB) at the receiver for the direct ray in the absence of any attenuation in the atmosphere. The term ΔL stands for relative sound pressure level. This term is a measure of the deviation of sound pressure level due to additional sound reflected from the ground, as well as absorption, refraction, turbulence etc. For our simple reflection case we have (as in Salomons, 2001, Eq 3.7)

$$\Delta L = 20log\left|1 + Q\frac{R_1}{R_2}exp(ikR_2 - ikR_1)\right| \qquad (7.30)$$

where, $R_1 = \sqrt{r^2 + (z - z_s)^2}$ and $R_2 = \sqrt{r^2 + (z + z_s)^2}$.

The symbol Q is the spherical wave reflection coefficient. It depends on the impedance of the ground surface, the wave number (k), the reflection angle and the distance between the source and the receiver. The horizontal distance between the source and the receiver is denoted as r.

The magnitude of the sound at the receptor can be computed from the amplitude and phase difference of the direct and reflected rays. The phase difference is related to the difference in their path length. If the phase difference is 180º then the rays will cancel each other out provided r >> z and z_s. It is called destructive interference. For destructive interference, the path difference between the direct and reflected rays should be equal to odd multiples of a half wavelength (λ/2).

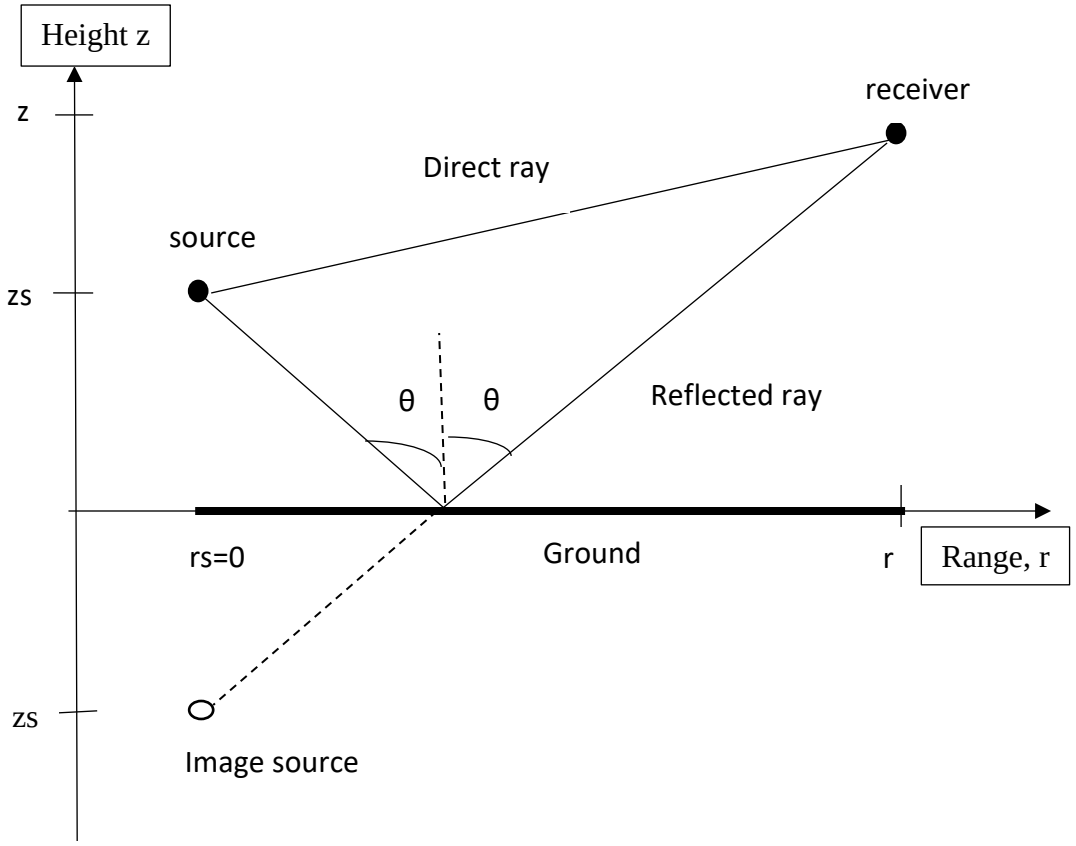

Figure 7.34: The source and receiver have been drawn above the ground to show a simple reflection case. An image source is also shown below the ground surface to represent the reflected ray.

The condition can be written as, path length difference, $R_2 - R_1 = \left(n + \frac{1}{2}\right)\lambda$ (7.31)

Where n=0,1,2…… Most turbine noise, associated with blade aerodynamics, occurs in the frequency range 500-2000 Hz (Baath, 2013) and so typical wavelengths are in the range c/f = 0.17 - 0.68 m. Talk of infrasound (< 20 Hz) and low frequency noise (LFN) is often about amplitude modulation as 3 blades rotate, at rates of around 15 rpm causing amplitude modulations or "swishing" at a frequency of about 0.75 Hz.

The height of source (z_s) and receiver (z) are sometimes very low compared to the horizontal distance (r) between them (although not necessarily for wind turbines). If this is the case then we can assume that $z_s << r$, $z << r$, and approximate $R_2 - R_1 \approx 2zz_s/r$. Then, using the relation between wavelength and frequency ($c = f\lambda$), equation 7.31 leads to

$$f_n = \left(n + \frac{1}{2}\right)\frac{rc}{2zz_s} \qquad (7.32)$$

The values of these frequencies are where the relative SPL (sound pressure level) will reach minimum values due to destructive interference (Salomons, 2001). They are directly proportional to the distance between the source and the receiver and inversely proportional to the height of the receiver. This relationship will be examined in the cases presented in this section.

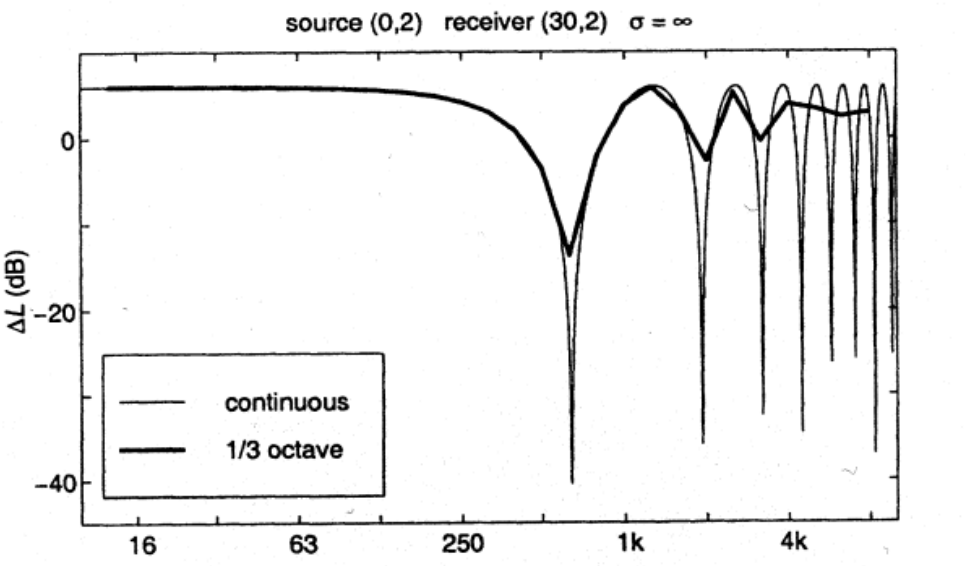

Figure 7.35: Continuous and one-third-octave band spectrum of the relative sound pressure level, for a rigid ground surface (Salomons, 2001).

In Figure 7.35 (Figure 3.6a from Salomons, 2001) relative sound pressure level is calculated at a 2 m receiver that is 30 m away from a source at a height of 2 m. The ground is rigid which means the flow resistivity is equal to infinity ($\sigma=\infty$) and no sound will be absorbed. The results (relative SPL) are based simply on Equation 7.30 since the rays are straight lines. The sound pressure is presented from both frequencies in the narrow band and in a smoothed, octave band spectrum. The wind speed is zero and there is no variation of sound speed with height. We have made similar computations using Equation 7.30 and with our Ray model under the same atmospheric conditions. These are shown in Figure 7.36 It is seen from both plots that there is general agreement between the two "continuous" spectra values and that the minimum values of relative SPL are lower from narrow band frequencies than the one-third octave band spectrum.

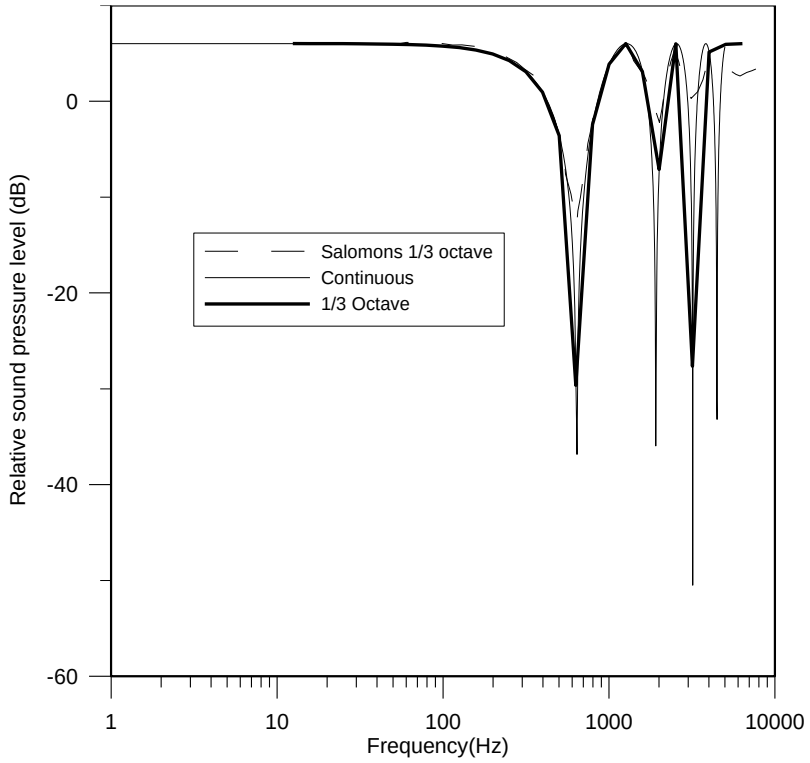

Figure 7.36: Continuous and one-third-octave band spectrum of the relative sound pressure level, for a rigid ground surface (Ray model).

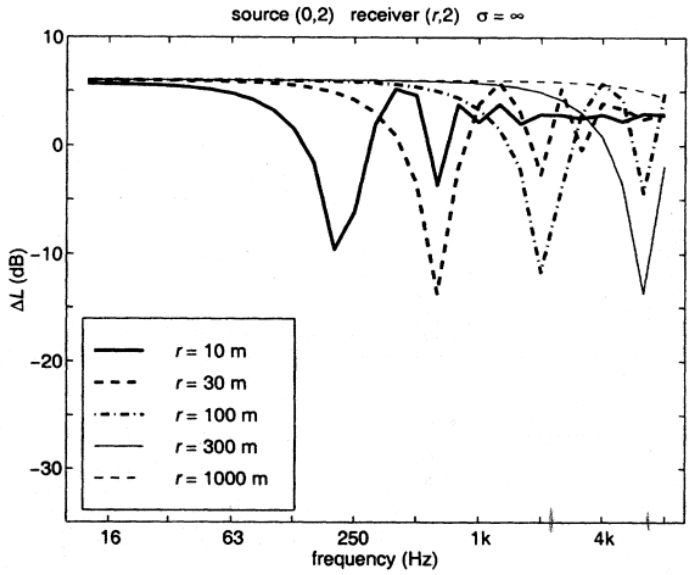

Figure 7.37: One-third octave spectrum of the relative sound pressure level, for five receivers and a rigid ground surface (Salomons, 2001).

Figure 7.37 (Figure 3.8 from Salomons, 2001) shows the effect of receiver range on the frequency spectrum. In this case again the ground is rigid and there is no variation of sound speed with height. It is seen that the frequency at which destructive interference occurs shift to higher value with increased distance. Similar results are obtained from the Ray model. Please note that, Figure 7.38 is drawn for narrow band frequency spectrum while one-third octave band spectrum of relative sound pressure level is shown in Figure 7.37. Therefore, the values of relative SPL at interference minima in Figure 7.38 are lower than the values shown in Figure 7.37. The relative sound pressure level computed with equation 7.30 (analytical solution) for receiver range 10 m is also included in Figure 7.38. The solution matches the output from the Ray model with some deviations in the SPL value for some frequencies. The minima are also lower than the minima calculated by the Ray model.

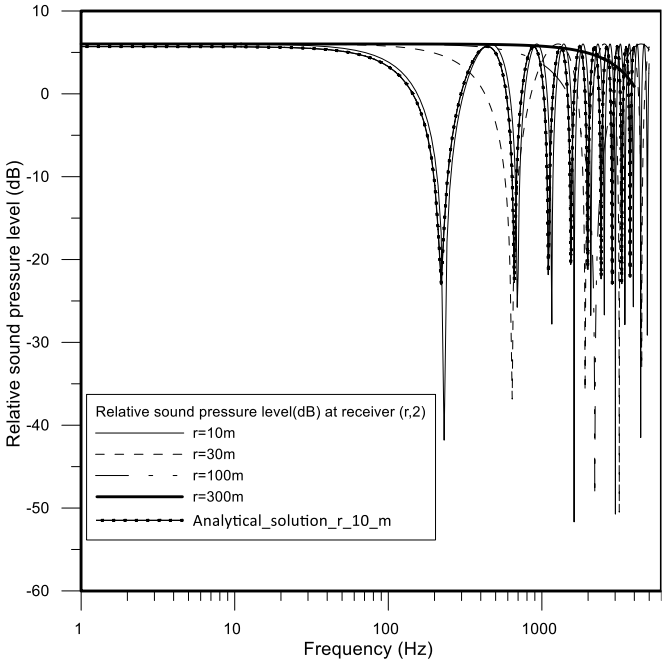

Figure 7.38: Relative sound pressure over narrow band spectrum for four receiver ranges and a rigid ground surface. The wind speed is zero. The sound speed gradient is zero. (Ray model)

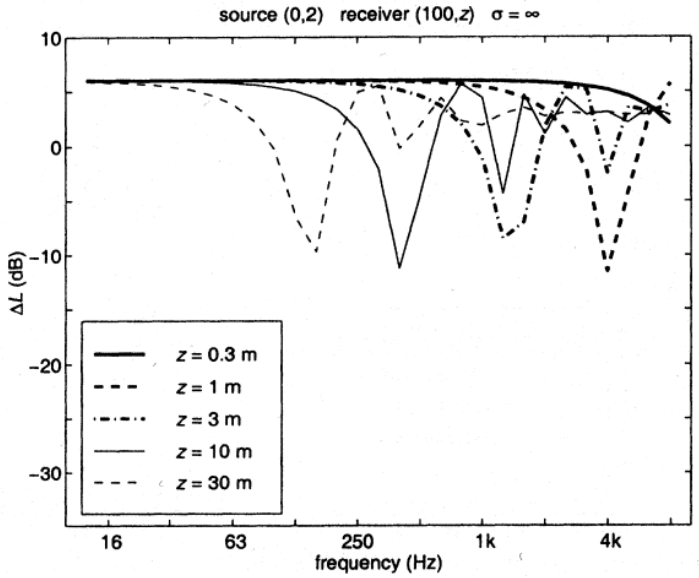

Figure 7.39 One-third octave spectrum of the relative sound pressure level, for five receiver height and a rigid ground surface (Salomons, 2001).

The influence of receiver height is shown in Figure 7.39 (from Salomons Fig 3.10) where relative SPLs over the one-third-octave spectrum are plotted for five receiver heights above a rigid ground surface. This case is also for simple reflection without any refraction in the atmosphere. The frequency at which destructive interference occurs is lower for greater receiver height. The narrow band spectrum results from the ray model also validates this relationship and is shown in Figure 7.40 but there are differences in SPL minima. The same result is shown in Figure 7.41 but just for center frequencies in the one-third-octave band spectrum.

It can be seen from all these figures that at low frequency (< 100 Hz) where wavelengths are long (> 3.4 m) and R_2-R_1 = 0.27 m the interference is almost fully constructive. In that case the sound pressure level of the direct + reflected rays should be doubled and the ΔL value (pressure squared) is $20\log_{10}(2)$ = 6.02 dB which it is, both in our ray model and in Salomons figures. The same 6.02 dB value is predicted at frequencies with constructive interference, $f_n = nrc/(2zz_s)$.

When there is exactly destructive interference the pressure can be reduced to near zero and the peak negative value of ΔL for complete destruction would be -∞ (Salomons, 2001). Very slight departures from exact frequencies, round off errors *etc*. leave the ray model, and Salomons, minimum ΔL values a little higher. Note that in Fig 7.35 and 7.36, the first ΔL minimum should be at

$f_c = rc/(4zz_s)$ = 637.5 Hz which the ray model achieves, as do Salomons results. The second minimum should be at 1912 Hz, also in agreement with the ray model. Similar agreement is found at different r values in Fig 7.38 and different receptor heights in Fig 7.40. Averaged over octave bands the reduction is reduced (Fig 7.41). These calculations are for specific frequencies. With a broad band of frequencies, at any point there will be some constructive and some destructive

interference and precise estimations of sound level become difficult. Assuming $\Delta L = 6.01$ dB could be used as an upper bound on the effect of reflection but it would generally be an overestimate.

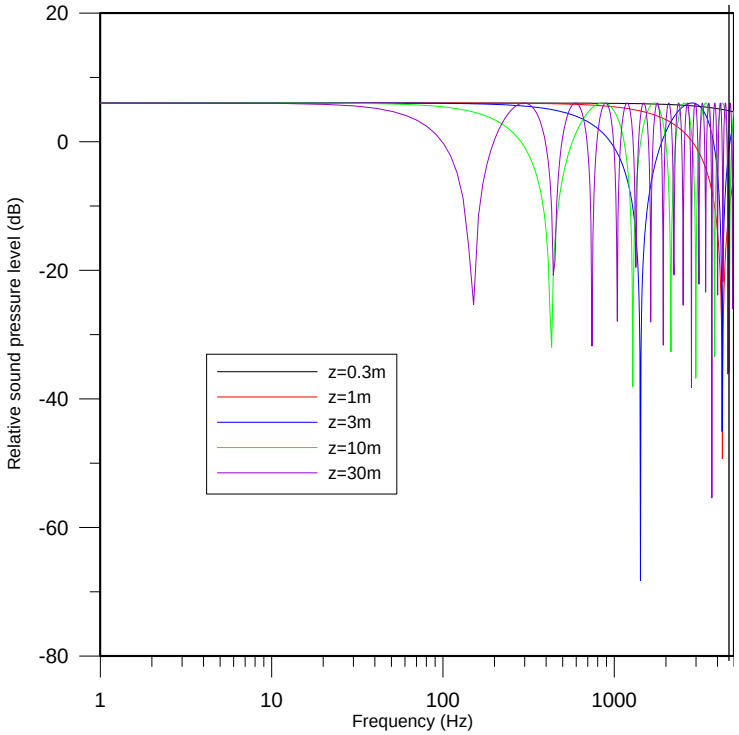

Figure 7.40: Relative sound pressure over narrow band spectrum for four receiver heights and a rigid ground surface. (Ray model).

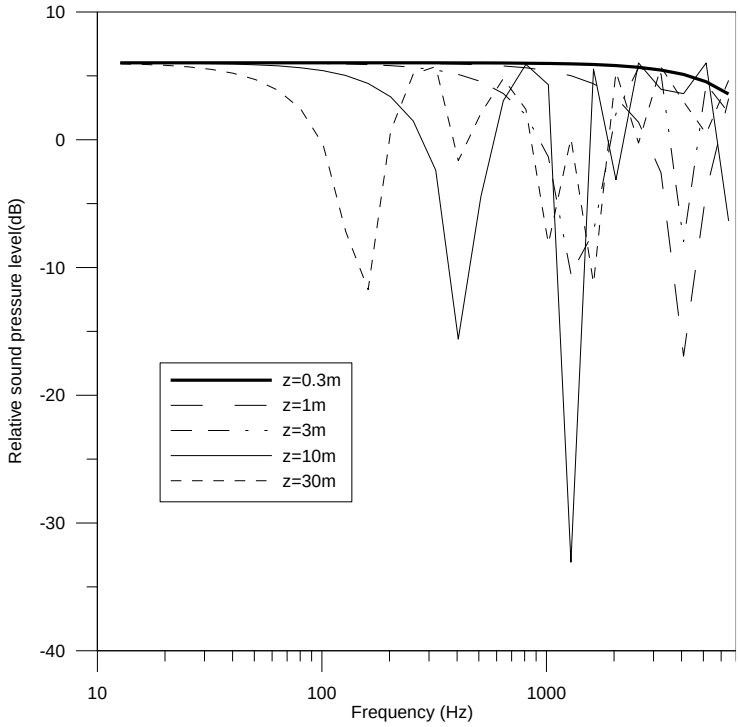

Figure7.41: Relative sound pressure over one-third-octave band spectrum for four receiver heights and a rigid ground surface. (Ray model).

The effect of reflection and refraction are shown in Figure 7.42 (from Salomons, 2001, Figure 4.24a). The sound speed profile in this case is,

$$c = c_o + bln\left(1 + \frac{z}{z_o}\right) \qquad (7.33)$$

Where, z is the height of the receiver and z_o is the surface roughness length of 0.1 m. The sound speed, c_o = 340 m/s. The value of b=1 ms^{-1} means the atmosphere is downward refracting while b = -1 ms^{-1} represents upward refraction. There is no variation of sound speed with height if b = 0.

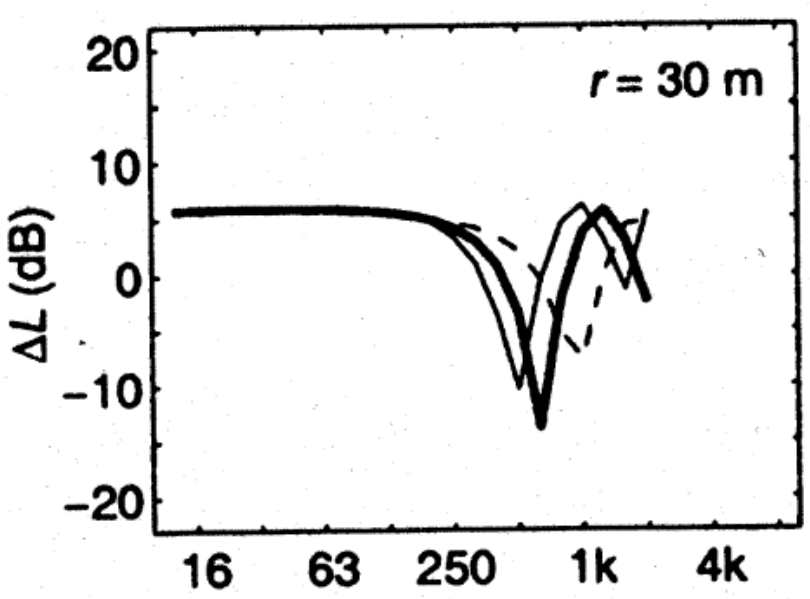

Figure 7.42: One third octave band spectra of the relative sound pressure level for a rigid ground surface, computed with CNPE method. In this figure the straight line is for b=1 ms^{-1}, the dotted line is for b=-1 ms^{-1} and the bold solid line is for b = 0 (Salomons, 2001).

In Salomons (2001) figure the Crank-Nicholson Parabolic equation method was used for this computation. It is seen from Figure 7.42 that the inference minima frequency is higher for the upward refracting atmosphere (b = -1). The same is true for the results from the Ray model that are shown in Figure 7.43. The one-third octave spectrum is shown in Figure 7.44 for the same case.

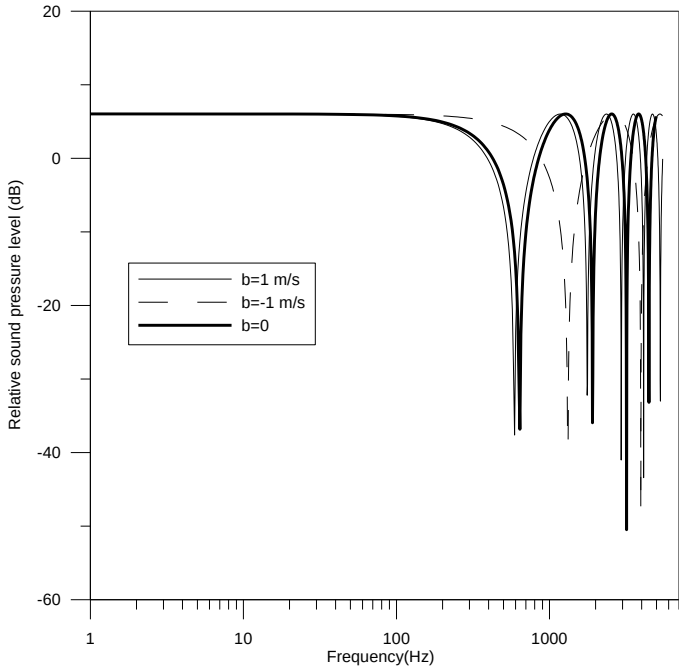

Figure 7.43: Narrow band spectra of the relative sound pressure level for a rigid ground surface computed with the ray model.

The relative sound pressure level was calculated using the Ray model and equation 7.30 for an elevated source such as a wind turbine and shown in Figure 7.45. The hub height was 100 m, and the receiver was at 300 m downwind. The receiver height was 2 m. There was no stratification in the atmosphere and the sound speed was 340 ms^{-1}.

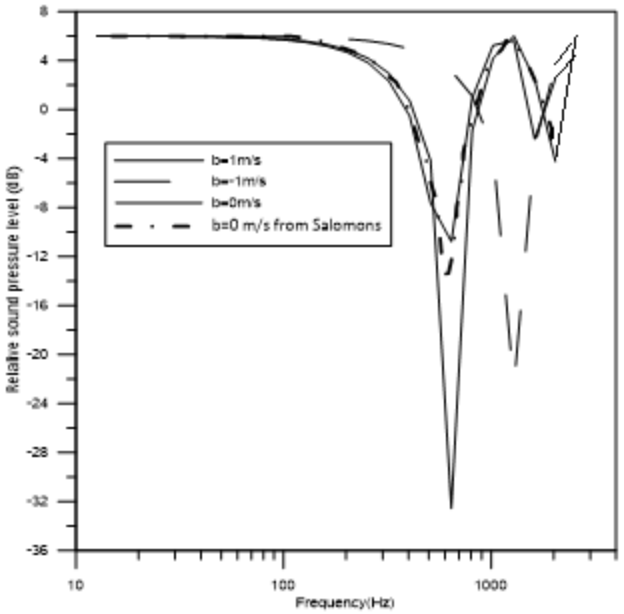

Figure 7.44: One third octave band spectra of the relative sound pressure level for a rigid ground surface, computed with the ray model.

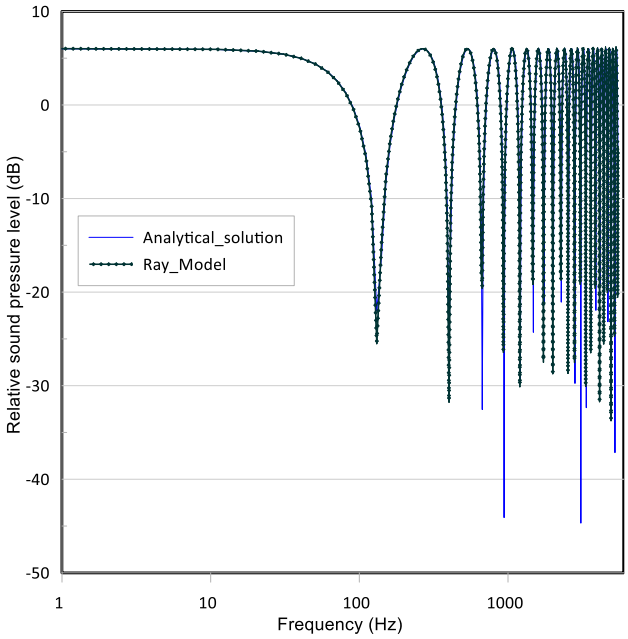

Figure 7.45: Relative sound pressure level from the ray model and the analytical solution by equation 7.30 for a rigid ground surface. The hub height was 100 m. The wind speed and the temperature gradient were zero, the sound speed was 340 ms^{-1}. (Ray model)

It is seen from Figure 7.45 that the results from both models' match. However, for some frequencies the analytical model gives lower value than the Ray model.

7.12 Comparison with the ISO-9613 method

In this section, results from the present model (the Ray Model) are compared with those from the ISO-9613 Standard model (ISO/DIS 9613-2: Attenuation of sound during propagation outdoors-Part 2: General method of calculation, 1996). The comparisons use similar source and receiver heights and environmental conditions.

In the ray model, the wind turbine is modelled as a point source. Turbine sound is emitted from the rotor center at 80 m above the ground. The sound power spectrum for center frequencies for eight octave bands are used with the source's sound power levels given in Table 7.2. The environmental parameters are listed in Table 7.3. There is no variation of wind speed and temperature with height. The topography around the turbine is flat without any barriers. The receiver is set at 4.5 m above the ground 550 m downwind from the turbine.

Table 7.2: Source sound power level (SWL) of a typical wind turbine source (dBA)

Wind turbine	Sound Power Level (dBA)								Sum (dBA)
	Octave Band Center Frequency (Hz)								
	63	125	250	500	1000	2000	4000	8000	
	86.0	91.6	97.5	98.3	99.9	97.2	93.5	77.9	105.0

Note that,

$$Sum = 10\ log_{10} \sum 10^{(0.1SWLj)} \qquad (7.39)$$

where SWL_j is the value in each octave band.

The losses included in the calculation are attenuation due to geometrical divergence (A_{div}), atmospheric absorption (A_{atm}), and ground interaction (A_{gr}). The equation to calculate the sound pressure level ($L_{p,j}$) of the *j*th eigen ray or a single ray can be written as (eq 6.16 in Chapter 6)

$$L_{P,j} = L_W - A_{div} - A_{atm} - A_{gr} \qquad (7.40)$$

$$A_{div} = 20lo\ g(r) + 11 \qquad (7.41)$$

Here, L_W = sound power level of the source

R = distance between source and receiver and 11 = 10 $\log_{10}(4\pi)$

Table 7.3: Environmental parameters used in both ISO-9613 method and Ray model.

Environmental Parameter	**Model Input**
Temperature	10 °C
Relative Humidity	70%
Wind Speed	5.0 ms^{-1} (No variation with height)
Wind direction	In the downwind direction from the facility to the receiver
Temperature gradient	None
Noise Propagation Standard	ISO 9613 and Ray model
Ground Conditions	Grassland
Topography	Flat
Receiver height	4.5 m above the ground

In the Ray model, rays are emitted and traced until one of them reaches the 4.5 m receiver height at 550 m downwind from the source. In this case, two direct rays emitted at zenith angle 97.9º and 98º reach respectively 4.79 m and 3.83 m height at 550 m distance. The travel time of these rays are recorded. The ray that hit the receiver height of 4.5 m and its travel time is determined by interpolating between these two rays. The same technique is applied for the reflected ray. The wind speed is 5 ms^{-1}, and the sound speed is 340 ms^{-1}. The attenuation for ground absorption is calculated using the Delaney and Bazley model (Delany & Bazley, 1970) described in detail in Chapter 6. In their impedance model different types of ground can be simulated by varying the flow resistance values (described in section 7.8). A smaller value of flow resistance (σ) of the ground means that the sound ray will penetrate easily into the ground and get absorbed. Examples of this type of surface can be dry fresh snow (σ = 10 to 30 $kPasm^{-2}$) (Salomons, 2001). On the other hand, a higher flow resistance resembles an acoustically hard surface which will reflect most of the sound energy. Ground made from asphalt and concrete has higher flow resistance ($\sigma > 2000$ $kPasm^{-2}$) (Salomons, 2001). For comparison, three different flow resistance values have been used to calculate loss due to ground absorption for the reflected ray and are shown in Table 7.4.

When the ray model is run, there are one direct ray and one reflected ray that reach the receiver height. The loss due to geometrical divergence, atmospheric absorption and ground interaction is calculated for each ray for each center frequency (63 Hz to 8 kHz) in the octave band and deducted from their corresponding sound power level to get receptor sound pressure level. The loss due to geometrical spreading is computed using the distance along the ray. The sound pressure level calculated (dBA) for both direct and reflected rays is presented in Table 7.4.

Now, the phase (φ_j) of the direct (j = 1) and reflected (j = 2,3 ...) rays can be computed for any specific frequency (in Hz) from their travel time (t_j). The equation for phase is (Prospathopoulos, 2007-03)

$$\varphi_j = 2\pi f t_j \qquad (7.42)$$

The sound pressure level is obtained by summing contributions from the rays (N=2 in this case) that intersect at the receiver using the equation below (in pressure units).

$$P = \sum_{j=1}^{N} |P_j| \left[cos\varphi_j + i(sin\varphi_j) \right] \qquad (7.43)$$

This can then be expressed in dB (10 $\log_{10}$P). The maximum sound pressures will occur if direct and reflected waves are in phase for the frequency involved. The sound pressure levels (dBA) calculated using the ISO-9613 method and the Ray model are listed in Table 7.4. Three ground factor values (G=0.5, 0, 1) have been used to simulate different type of surface. It is seen that the sound pressure levels (SPL) from the Ray model for reflected rays are lower than the SPL in the ISO-9613 method. The difference is significant in the case where the ground absorption is high.

Table 7.4: Comparison of result from the Ray model and the ISO-9613 method

Ground factor, G (0=Hard, 1=Soft)	Flow resistance, kPa.sm^{-2}	ISO-9613	Ray model		
		SPL, dBA	SPL, dBA (Reflected ray)	SPL, dBA (Direct ray)	SPL, dBA (Direct and Reflected ray)
0.5	200	38.4	36.38	37.8	40.2
0	200000	40.1	37.83	37.8	40.9
1	10	36.7	31.21	37.8	38.7

In the ray model the contribution of the direct and reflected ray at the same receiver height can be combined for a particular frequency using equations 7.42 and 7.43. If the direct and reflected ray are in phase, adding them will provide the highest combined sound pressure at the receiver. The combined SPL for direct and reflected ray at phase is calculated and presented in the last column of Table 7.4.

The ray model was run for two additional wind speeds: 10 ms^{-1} and 15 ms^{-1} with a flow resistance value of 200 $kPasm^{-2}$ for both cases. The sound pressure level for the reflected ray at wind speed, 10ms^{-1} was found to be 36.5 dBA. The SPL went up to 36.65 dBA when the wind speed was set to 15 ms^{-1}. The SPL for the direct ray at 10 ms^{-1} was 38 dBA and the combined (direct + reflected) SPL was 40.32 dBA. For a wind speed of 15ms^{-1}, the SPL of the direct and combined rays was 38.1 dBA and 40.45 dBA respectively. The difference in the SPL can arise from the fact that, the meteorological condition has an impact on which ray (elevation and azimuth angle) will reach the receiver distance. As the length of the ray is used to compute the loss for spherical spreading and atmospheric attenuation, it can cause the variation in the sound pressure level although the source to receiver distance does not change.

The prediction of attenuation due to ground is higher in Ray model. This estimates lower sound pressure level for reflected rays at the receiver than ISO model. Also, the variation in the SPL due to different values of flow resistance is higher in the Ray model. The reason of the variation is inherent in the computation method of ground impedance. The ISO method uses a parameterized method depending on the source height, receiver height and the distance between them to determine ground attenuation. In Ray model, the ground absorption depends on the incident angle while the ray hits the ground among other factors. The SPL for the direct ray does not include any attenuation due to ground and hence remains constant under same atmospheric condition. The

combined SPL (listed in the last column of Table 7.4) shows the highest SPL possible but can be lower depending on the phase difference of the direct and reflected ray. It can be concluded that results from both models are close match.

Chapter 8
Conclusion

To assess the impact of the issues related to ice throw and noise from wind turbines two independent mathematical models were developed. The first model involves solutions of the trajectory equations in a three-dimensional space to calculate the trajectory of an ice fragment thrown from a wind turbine. It has been assumed that the initial velocity of the ice fragment is equal to the initial velocity of the turbine blade. The aerodynamic drag and gravity determine the final trajectory and distance traveled by the ice fragment when it is treated as "compact debris" with drag but no lift forces. Sensitivity tests were carried out to see the impact of varying the mass of the ice fragment, the position of the ice fragment on the blade, the drag coefficient, the rotor speed and the wind speed.

It was found that all the parameters mentioned above affect the total distance the ice fragment will travel and the impact location of the ice fragment on the ground. However, the speed of the rotor and wind speed have greater influence on the distance an ice fragment will travel in both downwind and crosswind direction. The drag co-efficient has more control over the distance the ice piece will go in the crosswind direction. A combination of drag co-efficient, area and mass of the ice fragment (C_DA/M) is proposed to be the governing factor to determine the trajectory based on the

results of simulation. The greatest distance an ice fragment of 1 kg (rotor speed 14.5 rpm) could travel was roughly 200 m.

In the case of non-spherical, plate-like substances, lift can also be a significant component of the force balance and therefore the model was modified to include lift. The lift force was computed at different positions during the flight of the ice trajectory until it reached the ground. With the effect of lift, the ice fragment could travel a larger distance. The results from the model are significant in terms of finding the possible distribution of the ice impact locations on the ground.

The second mathematical model is for the propagation of sound waves in a three-dimensional medium, with potential application for wind farms. The model is based on ray theory and calculates the trajectories of rays emitted from a source (*e.g.*, a wind turbine) and the evaluation of sound pressures along them. Once a ray is emitted from the source its trajectory is determined by various mechanisms in the atmosphere. Refraction can occur due to the presence of wind shear, temperature gradient and sound speed variation. As a result of refraction, the rays can change the direction of propagation. Sound speed, wind speed and temperature profiles can be specified in the model. The rays are emitted under different scenarios by varying these profiles to see which has the most impact on the sound path. The cases examined included, a) constant temperature and various wind profiles, and b) different values of temperature gradient with a logarithmic wind profile. Sensitivity analyses show that, rays generally bend the most when the temperature gradient is positive.

Different types of losses have been calculated in the model including those due to refraction and spherical propagation. The propagation loss or geometrical attenuation ($10\log(4\pi r^2)$ in dB) was calculated from the distance traveled by the rays. The refraction loss was calculated from the change in intensity due to differential bending of rays when propagating through a refracting

medium. For a positive lapse rate, the refraction loss was negative which can be referred as gain. The value of the gain was between 0.02-0.2 dB within 700 m from the turbine base. The refraction loss/gain was calculated for various azimuth angles under the same meteorological condition at several receiver locations.

Loss due to atmospheric absorption is included in the model. The absorption coefficient is calculated from the absolute temperature, the relative humidity, and the atmospheric pressure. Loss due to atmospheric absorption is also frequency dependent and increases with increase in frequency. It is also range dependent with absorption increasing with distance. Sound loss due to absorption can be as high as 57 dB at 8 kHz at 500 m from the source. For typical circumstances this is a significant amount of attenuation.

Reflection from the ground is also treated and the loss due to ground interaction is calculated using the impedance of the local ground surface. Phase change due to ground interaction is ignored in calculating the reflected ray trajectory. It is assumed that reflection of rays only occurs in the same plane. The reflected angle is taken to be equal to the incident angle. Ground impedance is calculated using the empirical formula of Delany and Bazley (1970). The ground impedance was calculated for several values of flow resistivity for a range of frequency. The impedance decreases with higher frequency for all values of flow resistivity. That means sound rays with higher frequency will be more absorbed by the ground. The loss due to reflection increases with frequency.

The nature of terrain surrounding the sound source can have a significant effect on the sound propagation. Small hills and terrain surface curvature can influence the wind profile which then affects the sound propagation and noise pressure level at the receptor. This change in the sound wave propagation due to terrain effects is also considered in the model. Several uneven

topographies such as a downward slope and small hills are used to observe the impact on the ray trajectory. In the case of a downward slope between the source and the receptor, rays can converge at a certain height which may result in an increase in the sound pressure level at that point. In case of small hills, sound can be blocked by the hill creating a noise shadow zone.

Contour plots showing the combined loss due to spherical spreading, refraction loss, atmospheric absorption, and reflection around turbine source sound are also presented. The loss increases with distance from the source, resulting in a decrease of the sound pressure level at a receiver located far from the turbine. A relative comparison among all the losses shows that the loss due to spherical spreading is usually the highest.

The results from the ray model were compared with similar cases presented by Salomons (2001). Relative sound pressure level (ΔL), which accounts for the attenuation in excess of spherical spreading and atmospheric absorption was computed. Calculation of ΔL requires consideration of the phase of the direct ray and reflected ray at the receptor point. The phase difference was determined from the difference in the travel time of the direct and reflected ray upon reaching the receiver. The ΔL values were evaluated for non-refracting and refracting media. In both cases a rigid ground surface was assumed which means all the incident rays will be reflected. When ΔL was plotted against frequency the locations of minima were found to be dependent on the receiver height and distance. The result from the ray model was in good agreement with the analytical solution provided by Salomons (2001). For a refracting atmosphere, ΔL, computed using the Crank-Nicholson parabolic equation method was presented by Salomons (2001). The ray model produced similar results for similar meteorological conditions.

Results from the Ray model are also compared with results from sound propagation calculations using the methodology of the ISO-9613-2 Standard (ISO/DIS 9613-2: Attenuation of sound during

propagation outdoors- Part 2: General method of calculation, 1996). Results from both models show good agreement.

Future work to improve the ice throw and ray-based noise prediction model could involve the following initiatives.

- There is some limited information available on ice fragment mass, size, and location on the ground gathered from field studies. However, the researchers mention some limitations such as the possibility of an ice fragment melting before it is found, difficulty in locating ice slab in winter snow *etc*. Therefore, more reliable field study data will be useful to enrich the current database.

The ray model currently considers single point source for noise but can be extended to study a distributed source or multiple sources.

- The model can evaluate sound propagation for onshore wind turbines over different acoustic surface types. Sound propagation over an acoustically hard water surface can be included in the model for offshore turbines.
- A simple, vertically displaced, logarithmic wind profile has been used to calculate ray trajectories and sound pressure levels over irregular terrain. The ray model could, in principle. be adapted to work with wind fields generated by models of boundary-layer flow in complex terrain to study the impact of complex horizontal and vertical wind regimes on the propagation of wind turbine noise in the local environment.

References

Aballea, F. D. (2004). Sound propagation over irregular terrain with complex Meteorological effects using the parabolic equation model. *Inter noise 2004.* The 33rd International Congress and Exposition on Noise control Engineering.

Aballea, F., & Defrance, J. (2006). Outdoor Sound Propagation : Comparisons between calculations performed with ATMOS, A pre-based model, and wind tunnel experiment. *Euro Noise.* Tampere, Finland.

Andreas, K. (2018). *Available Technologies for Wind Energy in Cold Climates-report-2nd edition.* IEA Wind TCP Task 19.

(2014). *ANSI S1.26-2014, "Method for the calculation of the absorption of sound by the atmosphere.* New York: American National Standards Institute.

Anthony L. Rogers, P. J. (n.d.). Wind Turbine Acoustic Noise. 2006. Renewable Energy Research Laboratory.University of Massachusetts Amherst, MA.

Attenborough, K. (1995-01). Benchmark Cases for outdoor sound propagation modelsnuary 1995, 174-190. *Journal of Acoustical Society of America. Vol. 97(1),* 174-190.

Baath, L. (2013). Noise spectra from wind turbines. *Renewable Energy. Vol.57,* 512-519.

Baker, C. (2007). The debris flight equations. *Journal of wind energy Ind. Aerodyn. Vol.95,* 329-353.

Barlas, E., Zhu, W., Shen, W., Dag, K., & Moriarty , P. (2017-11). Consistent modelling of wind turbine noise propagation from source to receiver. *The journal of Acoustical Society of America, Vol.142 (5),* 3297-3310.

Barone, M. (2011). *Survey of Techniques for Reduction of Wind Turbine Blade Trailing Edge Noise.* Albuquerque (NM): Sandia National Laboratories, operated for the United States Department of Energy by Sandia Corporation.

Batchelor, G. (1967). *An introduction to fluid dynamics.* Cambirdge: Cambirdge University Press.

Bateman, H. (1914-05). The influence of meteorological conditions on the propagation of sound. *Monthly Weather Review*, 258-265.

Battisti L., F. R. (2006). Sea ice and icing risk for offshore wind turbines. Citavecchia, Italy.

Bies, D. A. (2018). *Engineering Noise control (5th Edition).* Boca Raton, London, New York: CRC press, Taylor and Francis Group.

Biswas, S., Taylor, P.A., & Salmon, J. (2011). A Model of Ice Throw Trajectories from Wind Turbines. *Wind Energy journal*, 15:889-901.doi:10.1002/we.519

Blokhintzev, D. (1946-10). The propagation of sound in an inhomogeneous and moving medium I. *The journal of Acoustical Society of America, Vol.18(2),* 322-328.

Bolin K., A. M. (2014). Long term estimations of low frequency noise levels over water from an off-shore wind farm. *The Journal of the Acoustical Society of America, 135*, 1106-1114.

Boorsma, K., & Schepers, J. (n.d.). Enhanced wind turbine noise prediction tool SILANT. *Fourth International Meeting on Wind turbine noise* (p. 2011). Rome, Italy: Energy research centre of Netherlands.

Brooks, T. P. (1989). Airfoil Self Noise and prediction. *NASA Reference Publication 1218*.

Bullmore, A. (2011). Chapter 3. Sound Propagation from Wind Turbines. In D. Bowdler, & G. Leventhall, *Wind Turbine Noise*. Essex: United Kingdom: Multi-Science Pulishing Company, Ltd.

Cattin, R., Kunz, S., Heimo, A., Russi, G., Russi, M., & Tiefgraber, M. (2007). Wind turbine ice thrw studies in the Swiss Alps. *EWEC.*

Cavar, D., & Réthoré, P. E. (2016-01-01). Comparison of OpenFOAM and EllipSys3D for neutral atmospheric flow over complex terrain. *Wind energy Science, Vol.1(1),* 55-70.

Chessell, C. (1977). Propagation of noise along a finite impedance boundary. *Journal of acoustical society of America*, 825-834.

Chiles, D. S. (2010). A new wind farm noise standard for New Zealand NZS6808:2010. *Proceedings of 20th International Congress on Acoustics, ICA 2010* . Sydney.

Crocker, M. (2007). *Handbook of Noise and Vibration Control.* Hoboken(NJ): John Wiley and Sons.

Daigle, G. (1979). Effects of atmospheric turbulence in the interference of sound waves above finite impedance boundary. *Journal of acoustical society of America. Vol. 65*, 45-49.

Delany, M., & Bazley, E. (1970). Acoustical properties of fibrous absorbent materials. *Applied Acoustics*, 105-116.

Directive 038(2007): Noise control. Energy resources conservation board.

Evans, L., & Bass, H. S. (1971-09). Atmospheric absorption of Sound: Theoretical Predictions. *The journal of Acoustical Society of America*, 1565-1575.

Evans, T., & Cooper , J. (2012). Comparison of predicted and measured wind farm noise levels and implications for assessment of new wind farms. *Acoustics Australia. Vol.40, No.1*, 28-36.

Expert Group study on recommended practices for W/Ts and evaluation(1994). 4. Acoustic measurement of noise emission from W/Ts (3rd edn). The Executive Committee of the International Energy Agency Programme for Research and Development on Wind Energy Conversion Systems.

Ffowcs Williams J.E., Hall, L.H. (1970). Aerodynamic Sound generation by Turbulent Flow in the vicinity of a Scattering Half-Plane. *J.Fluid Mech., 40*, 657-670.

Findeis, H. P. (2004). Disturbing effects of low frequency sound Immissions and vibrations in residential buildings. *Noise and Health. Vol 6(23)*, 29-35.

Foreman, T. (1983). *Ray modelling methods for range dependent ocean environments.* The University of Texas, Austin,(ADA-137202): Apllied Research Laboratories Technical Report No. 83-41 (ARL-TR-83-41).

Georges, T., Jones, R., Riley, J. (1986). Simulating ocean acoustic tomography measurements with Hamiltonian ray tracing. *IEEE J. Oceanic Eng, OE-11(1)*, 58-71.

Georges, T. Jones, R., Riley, J. (1990). A PC version of the HARPO ocean-acoustic ray-tracing program . *NOAA Tech Memo ERL WPL-180*, 18.

GoC. (2004). *Radiation Emitting Devices Act (R.S.C., 1985, c. R-1).* (Government of Canada).

Hansen, C., & Hansen , K. (2020). Recent advances in wind turbine noise research. *Multidisciplinary Digital Publishing Institute (Acoustics)*, 171-206.

Haugen, K. (2011). *International Review of Policies and Recommendations for Wind Turbine Setbacks from Residences: Setbacks, Noise, Shadow Flicker and Other Concerns.* Saint Paul (MN): Minnesota Departmnet of Commerce:Energy facility permitting.

Hawkins, J. (1987). *Application of ray theory to the propagation of low frequency noise from wind turbines.* Hampton: NASA, Langley research center.

Holmes, J., & Letchford, C. N. (2006). Investigations of plate-type windborne debris-Part II: Computed trajectories. *Journal of wind energy. Ind. Aerodyn. Vol.94*, 21-39.

Holmes, J., Baker, C., & Tamura, Y. (2006). Tachikawa number: A Proposal. *Wind energy jounal,Aerodyn., Vol.94, 94*(Aerodynamics), 41-47.

Hubbard, H. H. (1990). Wind turbine Acoustics. *Langley reserch center. NASA technical report.*

ISO 266(1976): Acoustics Preferred frequencies for measurements. International Organization for Standardization.

ISO/DIS 9613-2 (1996): Attenuation of sound during propagation outdoors- Part 2: General method of calculation. Geneva, Switzerland.: International Organization for standardization.

Jacobsen , F., & Juhl, P. (2013). *Fundamental of general linear acoustics.* Chichester: West Sussex: John Wiley and Sons Inc.ISBN-13:978-1118346419.

Keith, S. E., & Feder, K., Voicescu, S.A., Soukhovtsev, V. (2016b). Wind turbine sound power measurements. *Journal of Acoustical society of America. Vol.139(3),* 1431-1435.

Keith, S. E., & Feder, K., Voicescu, S.A., Soukhovtsev, V. (2016a). Wind turbine sound pressure level calculation at dwellings. *Journal of Acoustical Society of America. Vol 139(3),* 1436-1442.

Keith, S. E., Daigle, G. A., & Stinson, M. R. (2018-08). Wind turbine low frequency and infrasound propagation and sound pressure level calculatios at dwellings. *The Journal of the Acoustical Society of America. Vol. 144(2),* 981-996.

Kinsler, L. F. (1982). *Fundamentals of acoustics.* Newyork: John Wiley and Sons.

Kordi, B., & Kopp, G. (2009-07). Evaluation of Quasi-Steady Theory Applied to Windborne Flat Plates in Uniform Flow. *Journal of engineering mechanics. Vol.135(7),* 657-668.

Krenn, A., Alexander, S.,Nina, W., Sten, B., Weidl, T.,Bredesen, R.E., Lannic, M., Müller S., Stoffels, N., Hahm, T., Storck, F., Lautenschlager, F. (2018). *International recommendation for ice fall and ice throw risk assessments.* The International Energy Agency Wind Technology Collaboration Programme (IEA Wind Task 19).

Lacroix, A., & Manwell, D. J. (2000). *Wind energy: Cold weather issues.* Renewable energy research laboratory, University of Massachusetts at Amherst.

Lamancusa, J.S., Daroux, P.A. (1993). Ray tracing in a moving medium with two-dimensional soundspeed variation and application to sound propagation over terrain discontinuties. *Journal of acoustical society of America. Vol.93(4),* 1716-1726.

Leblanc, M. (2007). *Recommendations for Risk Assessments of Ice Throw and Blade Failure in Ontario.* Report from Garrad Hassan & Partners to the Canadian Wind Energy Association.

Lennie, M., Dominin, S., Marten, D., & Pechlivanoglou, G. (2019). Development of Ice throw model for wind turbine simulation software QBlade. *AIAA Scitech* .

Lighthill, M. (1978). *Waves in fluids.* Cambridge Eng.; New York: Cambridge University Press.

Long, M. (2014). *Architechtural acoustics.* Boston: Elsevier/Academic Press .

Lundén, J. (2017). ICETHROWER Mapping and tool for risk analysis. *Winterwind. Skellefteå.*

Manning , C. (1981). *The propagation of noise from petroleum and petrochemical complexes to neighbouring communities.* Acoustic technology limited. Report no.4/81.

Manwell, J.F., McGowan, J.G., Rogers, A.L. (2010). *Wind energy explained:Theory, design and application.* Chichester: United Kingdom: John Wiley & Sons Ltd.

Marsh, K. (1982). The CONCAWE model for calculating the propagation of noise from open-air industrial plants. *Applied Acoustic. Vol.15*, 411-428.

Morgan, C., & Bossanyi, E.(1996). Wind turbine icing and public safety – a quantifiable risk. *Proceedings of Boreas III conference.* Sariselka, Finland.

Morgan, C., Bossanyi, E., & Seifert, H. (1998). Assessment of safety risks arising from wind turbine icing. *Proc BOREAS IV, Hetta, Finland, and EWEC'97, Proceedings of the International Conference,* (pp. 113-121). Hetta, Finland: Finnish Meteorological Institute.

Nicolas, J., Berry, J., & Daigle, G. (1985). Propagation of sound above a finite layer of snow. *Acoustical society of America*, 67-73.

Noise guidelines for Wind Farms. (2008). Ministry of the Environment Conservation and Parks.

(Delta). *Nord2000:Comprehensive outdoor sound propagation model. Part 2: propagation in an atmosphere with refraction.* Delta.

Oerlemans, S. (2011). Chapter 2. Primary Noise Sources. In D. Bowdler, & G. Leventhall, *Wind Turbine Noise.* Essex: United Kingdon: Multi-Science Publishing Company, Ltd.

Ontario Regulation. (2012). *Environmental Protection Act* . Ontario: Ontario regulation 359/09.

Parry, G. (2008). A review of the use of different noise prediction models for windfarms and the effects of meteorology. *Acoustics 08 Paris.* Paris.

Pedersen, S. M. (2007b). Indoor Measurements of Noise at Low Frequencies- Problems and Solutions. *Journal of Low Frequency Noise, Vibration and Active Control. Vol26(4)*, 249-270.

Pierce, A. D. (1989). *Acoustics: an introduction to its physical principles and applications.* Acoustical society of America, 678pp.

Press, W. S. (2007). *Numerical Recipes: The Art of Scientific Computing* (3rd ed.). New York: Cambridge University Press. Retrieved from http://apps.nrbook.com/fortran/index.html

Prospathopoulos, J. M. (2007-03). Application of a Ray Theory Model to the Prediction of Noise Emissions from Isolated Wind Turbines and Wind Parks. *Wind energy. Vol 10(2)*, 103-119.

Ramani, R. (2007). *Wind turbine facilities noise issues:acoustic consulting report.* toronto: The ministry of environment of Ontario.

Renewable UK. (2013). *Wind Turbine Amplitude Modulation: Research to Improve Understanding as to its Cause and Effect.* London, United Kingdom: Renewable UK.

Richards, P. W. (2008). Numerical calculations of the three-dimensional motion of wind-borne debris. *Journal of wind energy. Ind. Aerodyn. Vol.96*, 2188-2202.

Rudnik, I. (1957). *Propagation of sound in air. In Handbook of Noise Control, pp. 3-1 to 3-17.* New york: edited by C.H. Harris , McGraw-Hill Book Co.

Sack, R.A., West, M. (1995). A parabolic equation for sound propagation in two dimensions over any smooth terrain profile: The generalised terrain parabolic equation (GT-PE)". *Applied Acoustics, 45*, 113-129.

Salomons, E. M. (2001). *Computational atmospheric acoustics.* 335pp, Kluwer Academic publishers.

Seifert, H. W. (2003). Risk analysis of ice throw from wind turbines. *Proc BOREAS 6*, (p. 9). Pyha, Finland.

Sen, S. N. (1990). *Acoustics waves and oscillations.* New Delhi: New Age international limited. ISBN: 81-224-0266-6.

Shen, W. Z., Zhu, W., Barlas, E., Ye, L. (2019). Advanced flow and noise simulation method for wind farm assessment in complex terrain. *Renewable energy . Vol.143*, 1812-1825.

Søndergaard, B., & Plovsing, B. (2009). *Validation of the Nord2000 propagation model for use on wind turbine noise.* Denmark: Delta.

Stephanie, L., Heath, G. L. (2006). Propagation Effects of wind and temperature on acoustic ground contour levels.

Szász , R.-Z., Leroyer, A., & Revstedt, J. (2019). Numercal modelling of the ice throw from wind turbines. *International Journal of Turbomachinery Propulsion and Power*.

Tammelin, B. C. (2000). *Wind Energy in Cold Climate.* Helsinki, Finland: Final Report WECO (JOR3-CT95-0014) ISBN 951-679-518-6, Finnish Meteorological Institute.

Taylor, P., & Teunissen, H. (1987-04). The Askervein Hill project: Overview and backgrounf data. *Boundary-layer meteorology. Vol.39 91-2)*, 15-39.

The expert panel on Wind Turbine, and Human Health. (2015). *Understanding the evidence:Wind turbine noise.* Ottawa: THE COUNCIL OF CANADIAN ACADEMIES.

The parabolic approximation method (Chapter 5). (1977). In F. Tappert, J. Keller, & J. Papadakis, *Wave propagation and under water acoustics* (pp. 224-287). New-York: Springer-Verlag.

Tom Evans, J. C. (2012). Comparison of predicted and measured wind farm noise levels and implications for assessments of new wind farms. *Acoustics Australia*, 28-36.

Tonin, R. (1985). Estimating noise levels from petrochemical plants, mines and industrial complexes. *Acoustics Australia. Vol. 13(2)*, 59-67.

van den Berg, F., & Bowdler, D. (2011). Chapter 5. Amplitude Modulation. In D. Bowdler, & G. Leventhall, *Wind turbine Noise.* Essex, United Kingdom: Multi-Science Publishing Company, Ltd.

Weiner, R. F., & Aarne., M. R. (2003). *Environmnetal engineering.* Amsterdam: Amsterdam; Boston: Butterworth_Heinemann (4th Edition).

Weng, W., & Taylor, P. (2011). A non-linear mixed spectral finite-differnce 3_D model for planetary boundary-layer flow over complex terrain. *Advances in Science and Research, Vol.6(1),* 75-78.

WillShire, W. (1985). Long-range downwind propagation of low-frequency noise. *Journal of Acoustical Society of America. Vol. 7,S1 (A).*